Development of Legged, Wheeled, and Hybrid Rover Mobility Models to Facilitate Planetary Surface Exploration Mission Analysis

by

Scott H. McCloskey

B.S., Aerospace Engineering
University of Arizona, 2005

Submitted to the Department of Aeronautics and Astronautics
in Partial Fulfillment of the Requirements for the Degree of

Masters of Science in Aeronautics and Astronautics

at the

Massachusetts Institute of Technology

June 2007

Signature of Author……
Department of Aeronautics and Astronautics
June 8, 2007

Certified by……
David W. Miller
Professor
Thesis Supervisor

Accepted by……...
Jaime Peraire
Chairman, Department Committee on Graduate Students

Development of Legged, Wheeled, and Hybrid Rover Mobility Models to Facilitate Planetary Surface Exploration Mission Analysis

by

Scott H. McCloskey

Submitted to the Department of Aeronautics and Astronautics
on June 8, 2007 in Partial Fulfillment of the
Requirements for the Degree of

Masters of Science in Aeronautics and Astronautics
at the Massachusetts Institute of Technology

Abstract

This work discusses the Mars Surface Exploration (MSE) tool and its adaptation to model rovers featuring legged, wheeled, and hybrid mobility. MSE is a MATLAB based systems engineering tool that is capable of rapidly designing a large trade space of rovers to fulfill a user defined science mission. This allows mission planners to make well informed design decisions in the earliest stages of a rover mission. The original version of MSE models exclusively six-wheeled rovers. This wheeled mobility model is refined, validated, and applied to an analysis of a Mars Sample Return fetch rover. The trade off between using a larger, more capable rover or a highly accurate landing system to retrieve a sample is examined. The results indicate that highly accurate landing systems are only needed if the fetch rover has a short period of time to retrieve the sample.

After the wheeled mobility model and its application are presented, the motivation to model legged and hybrid mobility is explained. Many scientifically interesting locations cannot be reached by traditional wheeled mobility systems, thus new forms of mobility should be considered for future Mars rovers. A survey of different forms of mobility is presented, with particular emphasis on the Modular Rover for Extreme Terrain Access (MoRETA) developed at MIT. The detailed implementation of four-wheeled, eight-wheeled, legged, and hybrid mobility models and their integration into MSE is discussed. The enhanced MSE tool is benchmarked against other simulations and existing robots. Finally, initially application of the tool reveals that wheeled mobility is best suited for flat and level terrain, and legged mobility is best suited for rocky or steep terrain.

Thesis Supervisor: David W. Miller
Title: Professor

Acknowledgements

First and foremost, I would like to thank Professor David Miller for giving me the opportunity to be part of the Space Systems Lab at MIT. His support and understanding has made my experience here more educational, both academically and personally, than it would have been otherwise. His advice has been very instrumental to the completion of this research. I am also extremely grateful that I had the opportunity to serve as a teaching assistant for the MoRETA class. I would also like to thank Julien-Alexandre Lamamy for his guidance and patience in helping me get up to speed with the MSE tool and completing this research.

The efforts of a handful of other MIT students have been valuable in completing this research. Adam Wahab and Christine Edwards deserve credit for the walking robot model they developed. I would also like to acknowledge all of the MoRETA students for devoting so much effort to their project. Terrence McKenna provided data from leg testing that was used for validation. Cristina Wilcox also provided torque outputs from her simulation that were useful for validation. Fred Gay assembled the full CAD drawing of the MoRETA rover.

I would also like to thank JPL for continually funding this research. I appreciate the efforts JPL has made to reach out to undergraduates and graduates and enrich their educations. On a related note, I would like to express my gratitude to the Space Grant program at the University of Arizona. Looking back, I now realize how much those experiences shaped me and how unique of an opportunity I given as an undergraduate.

Finally, I would like to acknowledge my friends and family for their support.

Table of Contents

List of Figures

List of Tables

Chapter 1

Introduction

Robotically exploring our solar system is an exciting endeavor that enlightens and inspires our civilization. Most recently, Mars has been the planet of choice for exploration missions. Roving vehicles like Sojourner and the Mars Exploration Rovers (MER) act as robotic geologists that can study the surface of Mars and communicate their findings back to Earth. Both the Sojourner and MER rovers have been very successful, as demonstrated by the fact that both MER rovers are operating years past their design lifetime. Despite recent successes by the Jet Propulsion Laboratory (JPL), robotically exploring the surfaces of other planets in our solar system is an exceedingly challenging task. Future rover missions will push the envelope and expand beyond the limitations of current rover designs. A systems engineering tool is needed to help rover designers prepare for the next generation of robotic explorers.

1.1 Motivation

One of the most critical systems on future Mars surface explorers will be the mobility system. The mobility system is the difference between a lander like Viking, which can only explore its immediate surroundings, and a rover like MER, which can drive across the surface, into and out of craters, and up hills. The mobility system is responsible for getting the science instruments to their targets, so if the rover is unable to drive to its target, then measurements of some potentially very valuable samples cannot be obtained. Mobility systems discussed in this thesis will include wheeled, legged, and hybrid (both wheeled and legged) mobility. Modeling these forms of mobility within a broader rover modeling framework allows rover designers to gain a better understanding of how the trade-offs associated with mobility design affect a rover mission architecture. It is very

important that tools are available to perform trade space exploration early in the lifecycle of a project, because design changes made later in a project cost more.

Wheeled mobility, as demonstrated by Sojourner and MER, is a very simple form of mobility that will continue to have value even as new forms of mobility are explored. Developing and refining models of wheeled mobility is important to be able to predict what future wheeled rovers will look like. Chapter 4 presents a specific example of why it is important to model wheeled mobility: a future Mars Sample Return (MSR) mission could potentially use a wheeled robot to retrieve a sample and return it to a lander to launch back to Earth.

Legged, hybrid, and other forms of mobility are useful to pick up where the capabilities of wheeled mobility stop. As will be discussed in more detail in Chapter 5, wheeled rovers do not perform as well on steep terrain or very soft sand. Rover designers are looking to new mobility technologies to allow the next generation of Mars rovers to reach samples that traditional six-wheeled rovers cannot reach. Creating a tool to model legged and hybrid mobility will allow comparisons to be made between mission architectures with varying types of mobility. Ultimately, the question is whether the benefits offered by new forms of mobility outweigh the risks of sending a more complicated and non flight proven technology to explore Mars. This work aims to establish a modeling capability to help rover designers evaluate this trade-off and determine the form of future Mars rovers.

1.2 Thesis Overview

The Mars Surface Exploration (MSE) tool is a rover modeling tool that allows systems engineers to make educated decisions about mission architecture in the earliest phases of design. A brief overview of the tool and why it can be modified to model alternative forms of mobility is presented in Chapter 2. Chapter 3 discusses the wheeled mobility model in MSE, and how it has been refined and validated using data from JPL missions. Chapter 4 then provides an example application of the wheeled mobility version of MSE to the MSR mission.

Chapter 5 through Chapter 8 focus on modeling new forms of mobility in MSE, specifically legged and hybrid mobility. Chapter 5 provides an overview of mobility

forms, discusses currently existing robotic systems, and explains the motivation to model legged and hybrid mobility. Chapter 6 takes a closer look at one hybrid robot developed at MIT, the Modular Rover for Extreme Terrain Access (MoRETA). A system overview of MoRETA is given, and then the rover's relevance to developing legged and hybrid mobility models in MSE is discussed. Chapter 7 describes in detail how wheeled, legged, and hybrid mobility are modeled. Chapter 8 compares the model outputs to other simulations and real world data to judge the accuracy of the models. Initial analysis is done with the tool to begin to study the terrain types on which wheeled and legged rovers perform well. Finally, Chapter 9 provides a summary of this work and emphasizes key contributions and future work.

1.3 Research Context

The mobility systems discussed as new technologies for Mars have obviously been implemented on Earth to various degrees. A survey of these vehicles is presented in Chapter 5. Many of the legged and hybrid rovers built to date are research robots. The hardware specifications of these robots, when available, are helpful in developing parametric models and providing data to validate against. The research focus of these robots, however, tends to concentrate on the control and software systems.

In addition to considering existing robots on Earth, it is important to understand the underlying theory of various types of locomotion. Much of the theory of land locomotion was formalized by Bekker, whose work was partially motivated by World War II [Bekker 56]. Many of the design principles he set forth are still relevant today, even for Mars rovers. Researchers at the Surrey Space Centre have since adapted Bekker's theories to robotic explorers [Patel 2004]. Another very relevant body of knowledge to mobility modeling is first hand experience gained by engineers who have designed and operated Mars rovers. Whenever possible, MSE incorporates the lessons learned and advice from these experts.

The MSE tool is unique in its ability to rapidly create a large trade space of rover designs. Other modeling tools are capable of modeling select subsystems in more depth, but sacrifice some of the breadth of MSE. The Rover Mobility Performance Evaluation Tool (RMPET) provides detailed mobility modeling and analysis capabilities, but lacks

the full rover design framework of MSE [Patel 2004]. JPL uses a modeling tool called Automatic Dynamic Analysis of Mechanical Systems (ADAMS) to evaluate their rover mobility systems, but this is more of a dynamic model of a design's ability to withstand a load [Lindemann 2006]. MSE's purpose is similar to that of JPL's Team X, a group that analyzes mission concepts, but differs in that MSE specializes in rover modeling and can be run by one user. MSE is also better suited to compare many different designs. Applying research in the robotics field and bringing together relevant theory regarding mobility will enhance MSE's utility and provide a unique modeling capability.

Chapter 2

The Mars Surface Exploration Tool

The Mars Surface Exploration (MSE) tool is a systems engineering tool to facilitate rover mission design in its earliest stages. MSE allows the rover designer to quickly explore a large trade space of design options to determine the best rover architecture for a given mission. The tool, written in MATLAB, was originally developed by the 16.89 Space Systems Engineering course at MIT in 2003 [16.89 2003]. Since then, graduate students of the Space Systems Laboratory at MIT have continued to develop and refine the tool. This chapter will provide a brief overview of the MSE tool and discuss why the tool is suited to model multiple forms of mobility.

2.1 Rover Design using MSE

The MSE tool has several Graphical User Interfaces (GUI) that help the user run the tool, input parameters that define the rover trade space to be explored, and analyze the resulting designs. The design structure matrix of MSE, shown in Figure 2-1, illustrates the major modules of MSE and the flow of information between them. To run the tool, the user firsts defines which acquisition tools, science instruments, and navigation instruments the rover will carry along with a few key environmental parameters. These parameters are represented by the science vector in Figure 2-1. Next, the user defines ranges for parameters describing the rover designs to be explored in the design vector. These parameters include mission duration, computing power, level of autonomy, wheel diameter, and type of power system.

The user specified science vector and design vector inputs then flow to the modeling segment of MSE, which is enclosed by a dashed line in Figure 2-1. The modeling segment is composed of modules of code representing the various rover

subsystems. The subsystem modules are executed in an order that minimizes the amount of feedback between modules. Feedback loops could not be avoided between avionics, power, and rover hardware. These loops result in design iterations that must converge before analysis can proceed. The details pertaining to each subsystem module are described in more depth in the literature [16.89 2003] [Lamamy 2004]. Outputs from the modeling segment that describe the design of each rover and its exploration capability are saved in data structures and outputted to the MATLAB workspace. The user can browse through the rover designs and use various analysis tools to explore the trade space of rovers created.

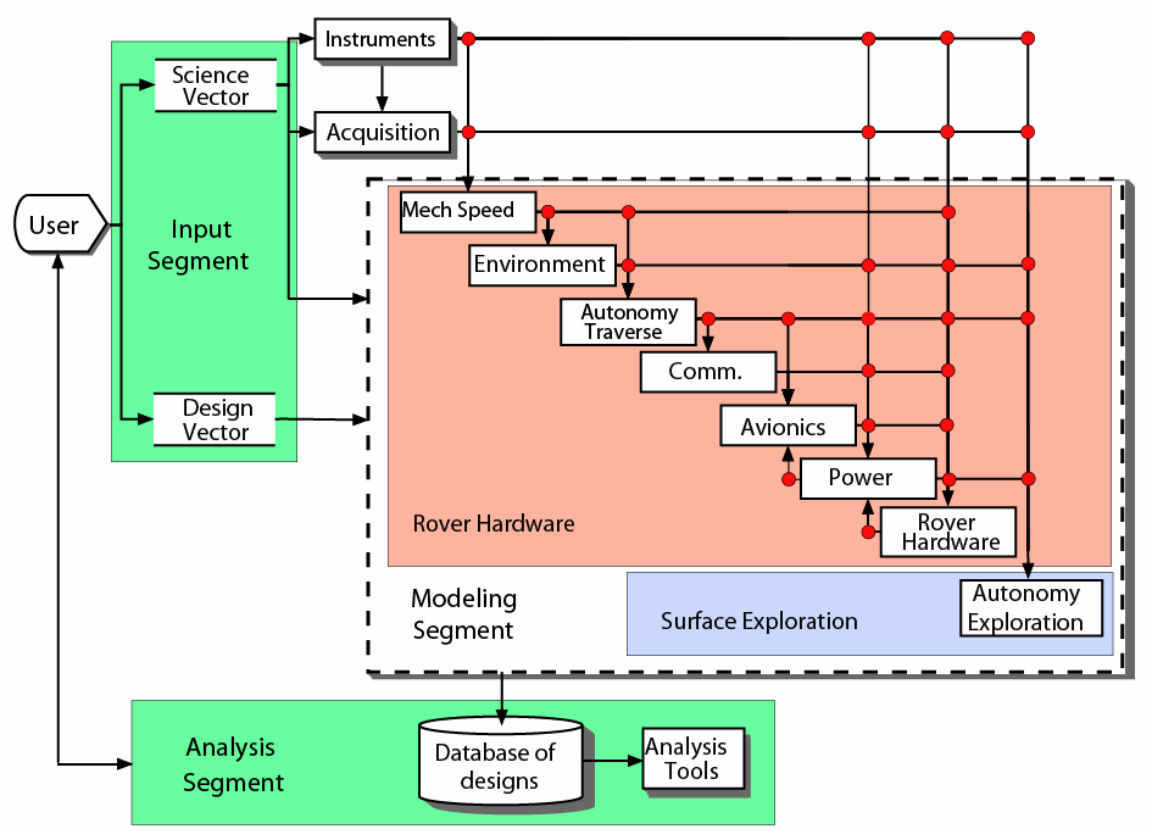

Figure 2-1: Design Structure Matrix of MSE

2.2 Application of MSE to Mobility Modeling

The modular organization of code in MSE depicted in Figure 2-1 allows for modules of code to be swapped out, modified, or tested independently without the need to significantly modify other code. This feature has made the modeling work presented in

this thesis possible. The mobility code is a sub-module of the rover hardware module. Modeling additional forms of mobility primarily involved only changing the code in the mobility sub-module. These additions, as well as the other minor modifications made to the rest of the code are described in more detail in Chapter 7. Before additional forms of mobility are discussed, refinement of the original wheeled mobility model and its application to a trade study will be presented in Chapter 3 and Chapter 4.

Chapter 3

Wheeled Mobility Hardware and Exploration Model Validation

Validation is an important part of the modeling process. Benchmarking MSE with information from existing rovers allows models to be refined and the tool's overall accuracy to be improved. MSE is validated by simulating actual rover missions and comparing the modeled output to existing rover data. Two types of validation will be discussed in this chapter: validation of the rover hardware models and validation of the rover exploration model. The rover exploration model includes the autonomy software on the rover that is used to navigate as the rover drives.

The rover hardware models are validated by inputting design parameters representative of the Sojourner, MER, and Mars Science Laboratory (MSL) rovers. For example, the design vector used to simulate MER includes a 90 sol lifetime, solar power, and 0.25 m diameter wheels. The modeled mass of the mobility, WEB, arm, mast, communication, power source, battery, and avionics systems are compared to actual masses to determine if the models are sufficiently accurate. The most recent results of this type of validation show that MSE estimates the mass of JPL's rovers within 14% of their actual values [Lamamy 2007]. This accuracy is sufficient for the intended use of MSE as a preliminary architecture trade tool. The discussion of hardware validation in this chapter will focus specifically on the mobility model.

The rover exploration model is validated by studying the number of sols it takes to travel a distance and collect a number of samples representative of actual Sojourner and MER operations. Validating both the hardware and exploration models of MSE

provides confidence in the models and gives credibility to the results of analyses performed using the models.

3.1 Wheeled Mobility Model

The MSE tool is validated both as a whole and in pieces. Comparing modeled rover designs to actual rover designs on both system and subsystem levels allows the overall accuracy of the tool to be checked along with the accuracy of more detailed models of select subsystems. In this section, the mobility subsystem of the wheeled version of MSE is examined.

3.1.1 Description of Wheeled Mobility Model

When the wheeled mobility code is run, like every module of code in MSE, inputs from previously executed modules are used as inputs (see Figure 2-1). This includes environmental parameters describing the gravitational acceleration and the soil bearing strength. Constants describing the relationships used to determine wheel size, rover size, and defining the number of driving and steering wheels are also inputs to the mobility model. Finally, the raw velocity of the rover and mass that the suspension system must support are inputted.

The portion of the code that calculates the size and mass of the wheels and size of the rover has remained essentially unchanged from the original model [16.89 03] [Lamamy 04]. After the rover dimensions are determined, the suspension system is designed. The suspension system used in the wheeled mobility model is based on the rocker bogie suspension systems used by JPL on the Sojourner, MER, and MSL rovers. Figure 3-1 shows the rocker bogie suspension system used on MER. Two horizontal beams are used to represent the bogie portion of the suspension system and two beams at 30 degree angles are used to represent the rocker portion. The beams are assumed to be made of titanium, like the MER suspension system, and of constant hollow square cross section [Lindemann 06]. Parameters defining the cross section of the beams are adjustable within the mobility code. The dimensions, orientation, and material properties of the beams are used to assemble a global stiffness matrix that relates the forces and displacements of the suspension system. If the maximum stress, with a factor of safety,

in any of the beams exceeds the ultimate stress, then the dimensions of the beam cross section are iteratively grown until the beam is strong enough. The mass of the suspension system is then determined by multiplying the total volume of material by its density.

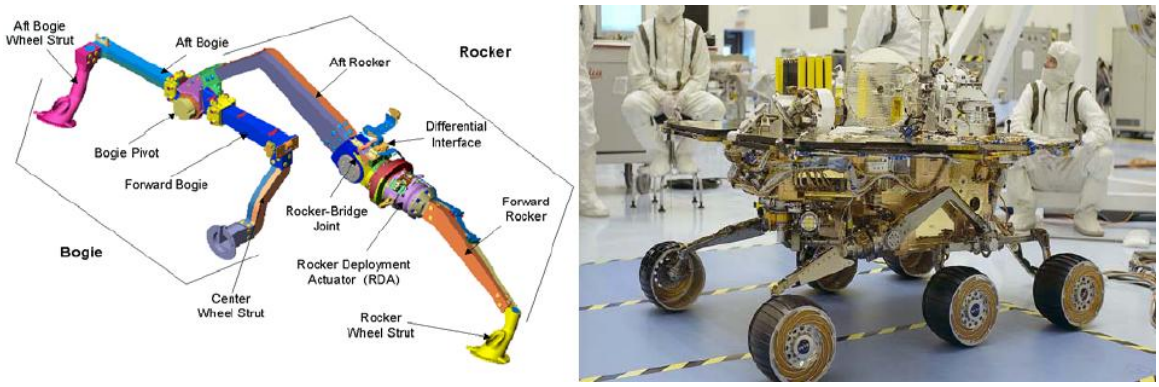

Figure 3-1: One Side of MER's Rocker Bogie Assembly (left) and Spirit Featuring its Rocker Bogie Suspension System (right) [Lindemann 06]

In addition to the mass of the wheels and suspension system, the mobility model accounts for the mass of motors, a differential, cabling, and miscellaneous actuation components. The motor mass in kilograms is determined as a function of power rating in Watts using Equation 3-1, which is a curve fitted to the Maxon RE series data sheets [Maxon 07].

$$mass = 0.0147 \times power^{0.8745} \qquad 3\text{-}1$$

This function is plotted with data from the Maxon catalog in Figure 3-2. Note that most of the motors used for this curve fit have low power ratings, and that the error of the fit increases for higher power motors. In the future, other sources of motor data could be added to the curve fit to improve its accuracy.

The differential and cable masses are modeled as fractions of the total mobility mass, equivalent to the differential and cable mass fractions on the ExoMars rover [Lamamy 04]. Lastly, miscellaneous actuation component mass is included to eliminate the discrepancy between estimated motor mass and the actuation mass actually on Sojourner, MER and MSL. Gears and encoders, for example, would be considered miscellaneous actuation components. Once the mobility component masses are estimated, the mobility module simply sums up the total mass of the mobility system.

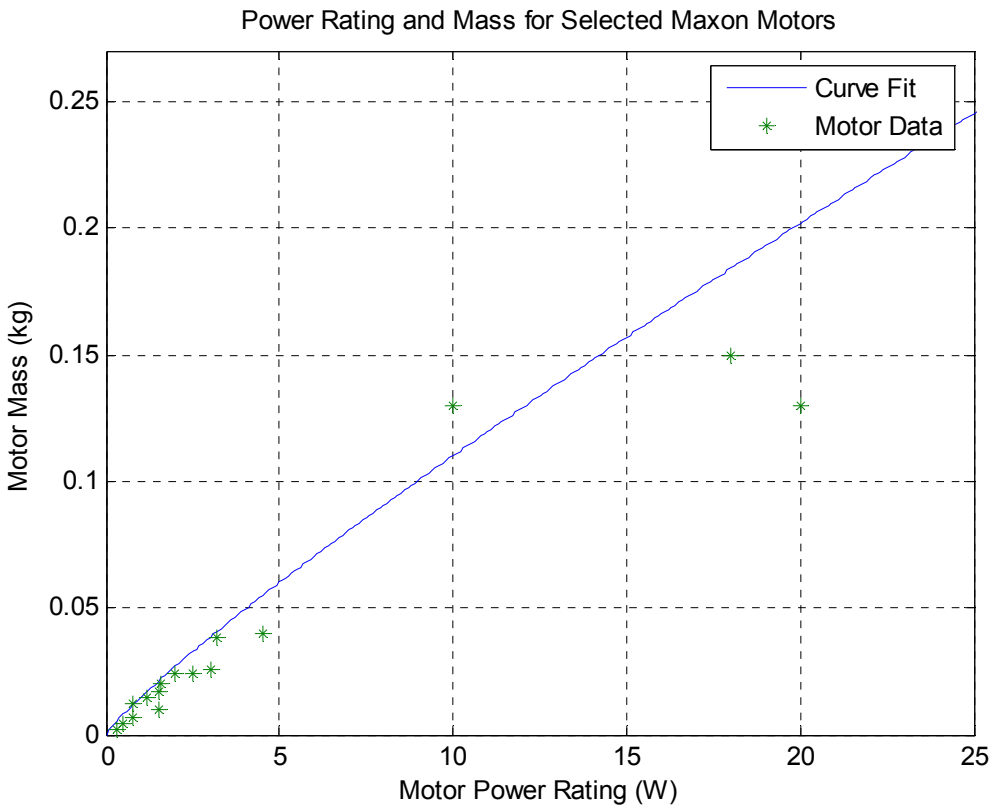

Figure 3-2: Plot of Motor Mass and Power

3.1.2 Benchmarking with Sojourner, MER, and MSL

The wheeled mobility model described above was tested with input parameters to simulate Sojourner, MER, and MSL rovers. Wheel diameters of 13 cm, 25 cm, and 50 cm and supported masses of 7 kg, 148 kg, and 536 kg were used to model Sojourner, MER, and MSL, respectively. Figure 3-3 shows the mobility system mass breakdown for each of these three rovers, as well as the actual mass breakdowns for each rover. These results show that the MSE wheeled mobility model outputs match actual hardware designs reasonably well. MER and MSL mobility masses are underestimated by about three percent, while Sojourner's mobility mass is underestimated by about 30 percent. The largest source of the discrepancy is in the wheel mass, but since the wheel mass model doesn't consistently under or overestimate mass, it was left unchanged. The accuracy of these results is acceptable because, while the percentage error for Sojourner is large, the actual error is still less than a kilogram. Additionally, a majority of the rovers modeled with MSE are between the size of MER and MSL, where the mobility

model is most accurate. These results give confidence that rovers similar to MER and MSL can be modeled, but it should be noted that since Sojourner, MER, and MSL data was used to create the model, data from new and varied rovers should be used to validate the wheeled mobility model should it become available.

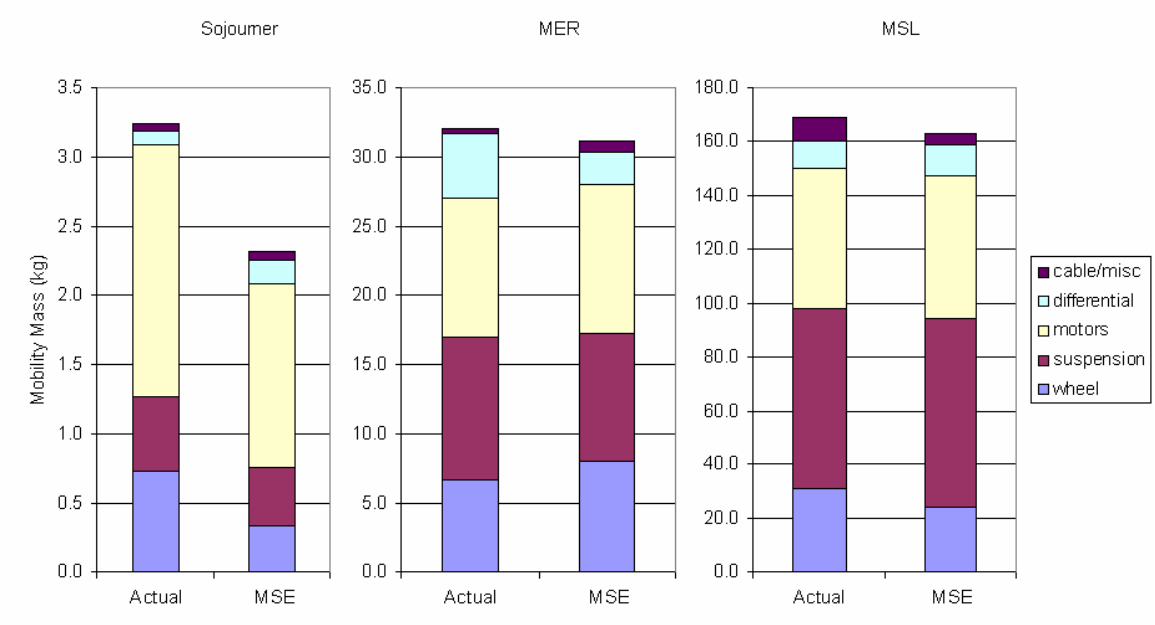

Figure 3-3: Comparison of Actual and Modeled Mass Breakdowns for Mobility Systems

3.2 Exploration Model Validation

Modeling wheeled mobility hardware is an important part of rover modeling, but the full utility of MSE also depends on modeling the performance or exploration capabilities of a wheeled rover. This section will describe how MSE models a wheeled rover's traverse as well as how data from the MER rovers has been used to refine and validate the exploration model.

3.2.1 Description of Exploration Model

The function of the exploration model is to predict the distance the rover travels, the number of sites visited, and the number of measurements taken during the mission lifetime specified by the user in the design vector. The exploration model carries out a repeating pattern of rover actions until the mission lifetime is exceeded. Two sols are allotted for the rover to egress from the lander and 33% of the mission duration is held as

margin. The rover begins by performing reconnaissance when it arrives at a science site. The rover then proceeds to examine the user defined number of samples within the user defined site diameter. It is assumed that every instrument is used on each sample. The amount of time it takes the rover to get to each sample within the site depends on the type of communication system and level of autonomy, among other things. After a site is fully explored and if there is time remaining, then the rover travels to the next science site. The site-to-site distance is a user defined input in the science vector. The rover performs reconnaissance at the new site and so on until the mission lifetime is used up. The higher the user defined terrain rock density, the greater the distances traveled by the rover, since the rover must navigate around rocks on the way to samples and sites.

The average speed of the rover during inter-site and intra-site traverses is the primary driver of exploration capability. The average speed of the rover depends on whether it is in auto-navigation mode or blind drive mode. As in the original version of MSE, the average velocity in auto-navigation mode is determined by the raw velocity and the computation time required before making each movement. The average speed in meters per second is determined over this think-move cycle using

$$v_{avg} = \frac{d_{cycle}}{d_{cycle} / v_{raw} + t_{think}} \qquad 3\text{-}2$$

where v_{raw} is the raw velocity of the rover in m/s. The distance traveled during each think-move cycle is half the length of the rover in meters (d_{cycle}), and the time required to think between movements (t_{think}) is dependent on the computational power selected by the user in the design vector.

The second driving mode used by the MER rovers, blind drive, was added to MSE after comparison to MER operations data. Blind drive mode involves no path planning, as the rover is supplied with a predetermined route. The MER rovers are capable of a faster average speed when in blind drive mode, but their range is limited to the few tens of meters previously imaged and sent to Earth [Biesiadecki 05]. Figure 3-4 shows the distance covered by Spirit in blind drive mode compared to auto-navigation mode for part of its traverse. This data is from the mission manager's reports, which

only occasionally differentiate between the two driving modes [MER 07]. No drive distance was entered for sols on which no distinction was made.

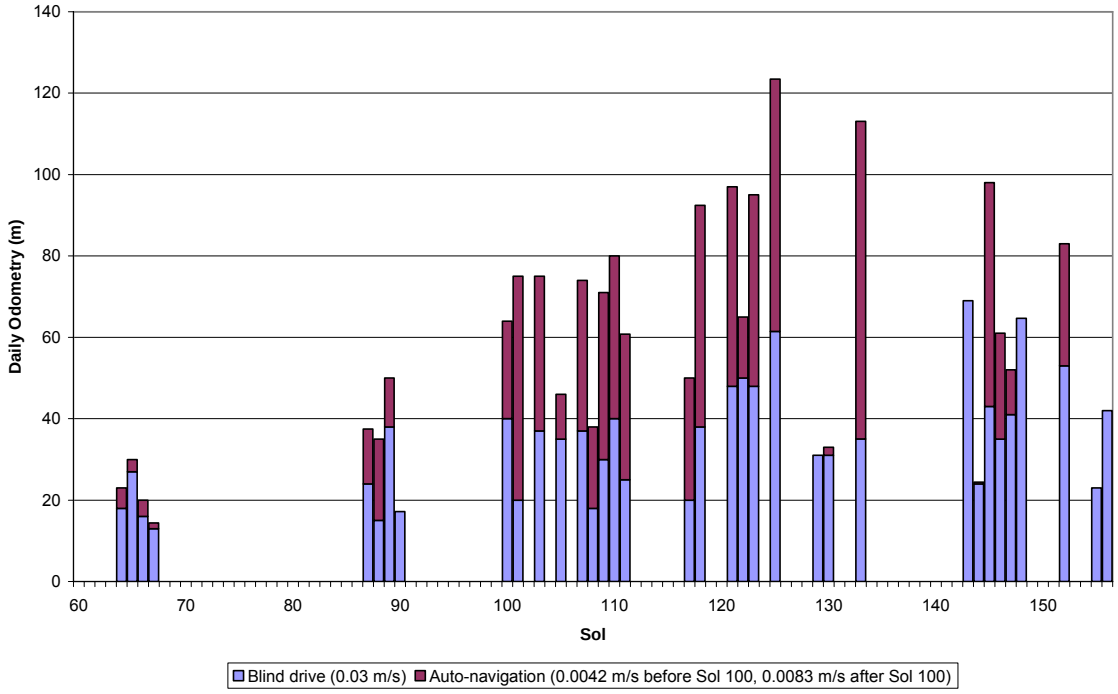

Figure 3-4: Drive Mode Used on Spirit to Navigate to the Colombia Hills

The accuracy of the exploration model in MSE was greatly improved with the addition of blind drive mode, since a significant portion of driving is done in this mode. Like the MER rovers, MSE simulates each sol's traverse by driving as far as possible in blind drive mode, then operating in auto-navigation mode while there is enough power.

3.2.2 Validation using MER

The MSE tool was originally created before MER operations data was available. Now that such data exists, the MSE models can be benchmarked to the actual performance of Spirit and Opportunity. MER data was obtained from the MER Analyst's Notebook produced by the PDS Geosciences Node at Washington University in St. Louis [MERAN 06]. Rover Motion Counter (RMC) data were used to reconstruct a profile of drive start and end locations within and between sites (see blue line in Figure 3-5 and black line in Figure 3-6) as well as an approximate estimate of instrument usage [Deen 04]. Sol summaries were used to obtain the total odometry traveled by each of the rovers over

time (see green boxes in Figure 3-5 and Figure 3-6). The total odometry exceeds the straight line distance because odometry includes wheel slippage and maneuvering to avoid rocks and other obstacles. The difference between RMC data (blue and black lines) and actual odometry (green boxes) depends on the rock density of the landing site.

The MSE exploration model is validated by inputting a mission scenario consisting of distances between sites and the desired number of measurements to be taken at each site. A mission scenario must be used because the actual commands sent to the rovers are very irregular, as opposed to the MSE assumption of identically sized sites all equally spaced. The rover abundance and rover parameters, such as clearance and raw velocity, are also provided. The MSE exploration model then creates a model of the MER rover and determines the time it takes to complete the mission scenario. The output of the MSE model is shown as the red dashed line in Figure 3-5 and Figure 3-6. This MSE output approximately equivalent to actual profile of odometry over time (green boxes), indicating that the MSE model is able to correctly assess how much time it takes for the rover to complete a site-to-site command traverse, which combines blind and autonomous drives, and to correctly assess the extra odometry due to terrain roughness. The modeled Spirit exploration took about 60 sols less than it actually did, but this is in large part due to the fact that MSE does not model spacecraft anomalies and failures such as the two week flash memory problem at the beginning of the mission.

3.2.3 Validation using Sojourner

Validating the exploration model using MER data shows the robustness of the model to different operating environments and science itineraries. Validation using Sojourner is also important because it shows robustness across different rover platforms. The Sojourner traverse was validated using the same approach as the MER traverse. A science itinerary representative of the targets that Sojourner visited was inputted into the MSE model [MPF 99]. The actual Sojourner traverse is shown in blue in Figure 3-7, and the modeled traverse is shown in orange in Figure 3-7. The actual and modeled odometry match very well for the first 21 sols, until Sojourner began to drive further each sol. The discrepancy could be explained by the fact that the sensor data Sojourner used to perform drives was simpler and required less time to process than the visual data used by the

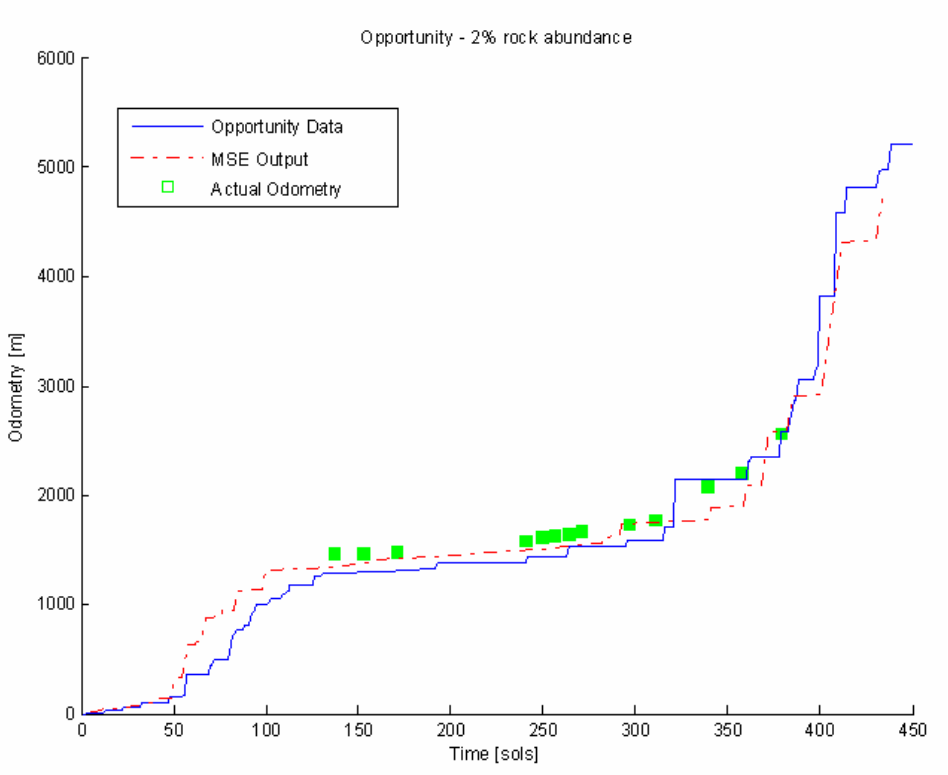

Figure 3-5: Actual and Modeled Opportunity Odometry

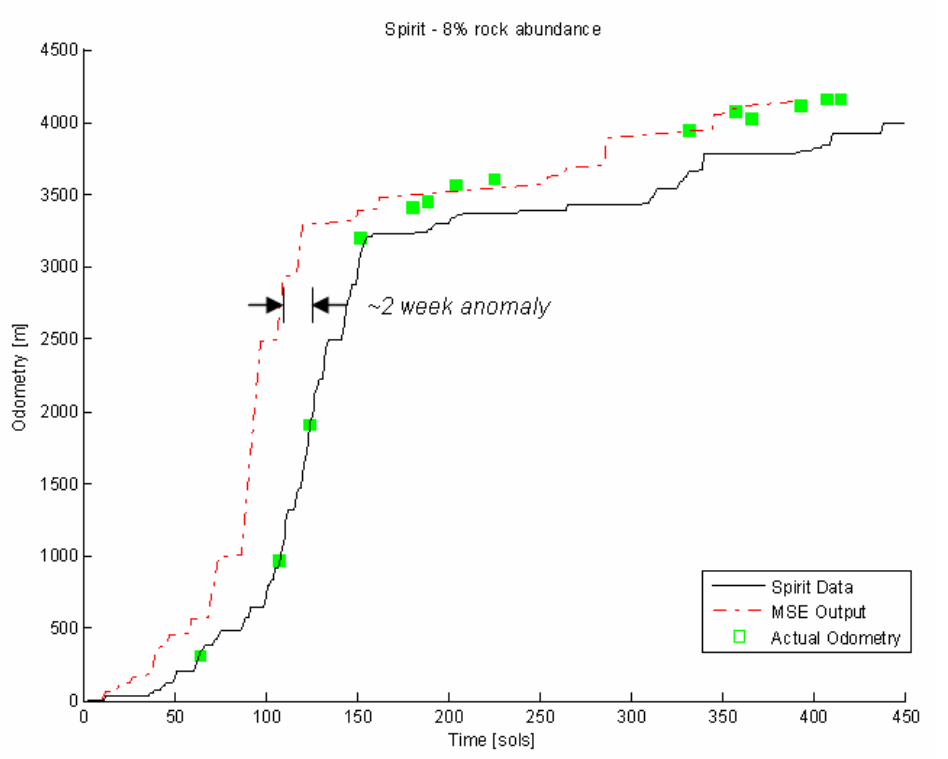

Figure 3-6: Actual and Modeled Spirit Odometry

MER rovers. Also, safety parameters may have been adjusted in the rover software that allowed it to drive more aggressively. Overall, the results show good validation against the Sojourner mission.

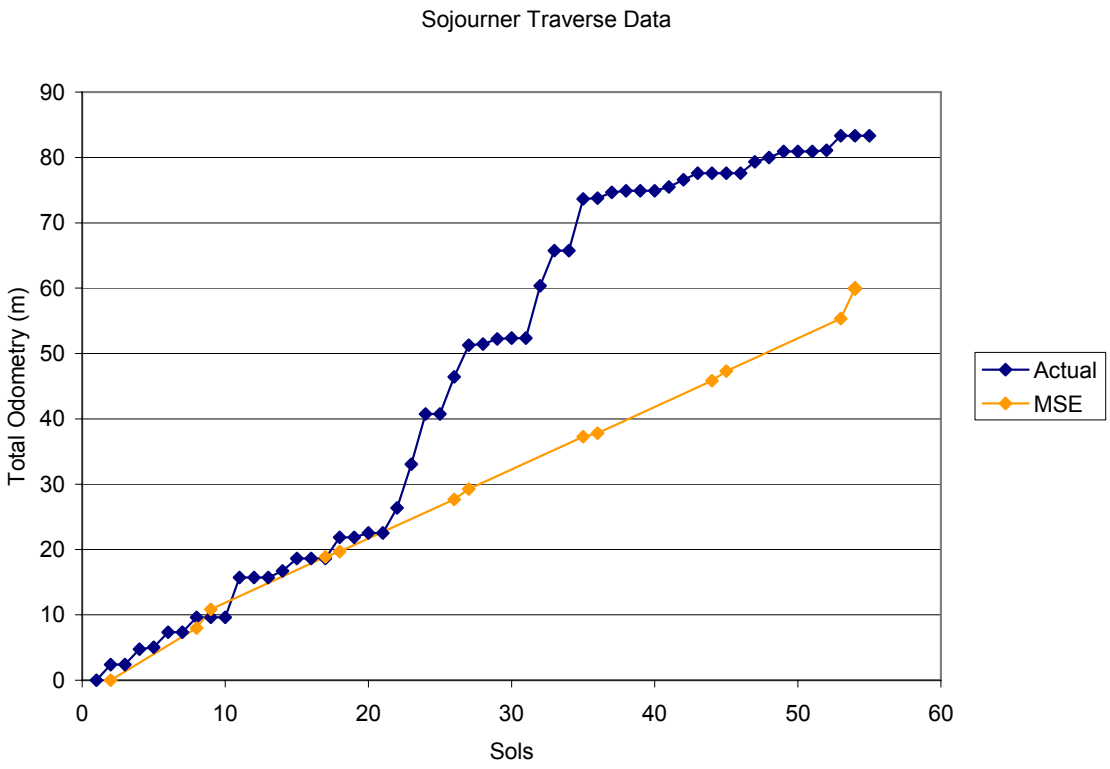

Figure 3-7: Actual and Modeled Sojourner Odometry

3.2.4 Conclusions

Validating the MSE exploration model with both Spirit and Opportunity mission profiles indicates that the exploration model is robust to different environments and commanded drives. A similar validation was carried out using a mission profile for Sojourner to validate the model across engineering platforms. The MSE exploration model was close to the actual Sojourner odometry, but underestimated the distance that Sojourner could drive primarily due to the fact that sensor data Sojourner used to perform drives was simpler and required less time to process than the visual data used by the MER rovers. This discrepancy is acceptable, since the future rovers that MSE is used to model implement autonomous navigation techniques similar to the MER mission.

Chapter 4

Application of the Wheeled Rover Model to Mars Sample Return

The validated wheeled mobility version of MSE can and has been used to perform a number of trades for various rover missions. To illustrate the tool's utility and provide an example of the trades for which it can be used, an application to the Mars Sample Return (MSR) mission will be discussed. This application combines the MSE tool's rover modeling capability with an Entry, Descent, and Landing (EDL) model to examine the trade-off between landing accuracy and rover size for a sample fetch rover.

4.1 Motivation

The MSE tool has been used to analyze a MSR scenario in which a fetch rover is sent out from a lander to retrieve an existing cache of samples and return it to a Mars Ascent Vehicle (MAV) at the lander. Determining the minimal size of the fetch rover is of interest to help minimize the cost of the rover and reduce the entry mass of a MSR mission. The traverse capabilities, and therefore the size, of the fetch rover are dependent on the worst case distance between the landing site and the sample cache. The worst case distance the fetch rover will have to traverse is twice the semi-major axis of the landing ellipse. The size of the landing ellipse can be reduced by a number of techniques, including the use of a powered descent stage that can actively correct for other sources of error in the EDL system. A trade-off exists between using larger, more capable rovers with relatively inaccurate EDL systems and using smaller rovers with more complex and accurate EDL systems. A graphical representation of these two extremes is illustrated in Figure 4-1. The need to be at these extremes is driven by the limited amount of time

available to fetch the sample. The MAV must launch the sample back to Earth while Mars and Earth are at favorable positions in their orbits. Both of these extremes reduce the time required to retrieve the sample, since large rovers can drive faster and more accurate EDL systems reduce the required traverse distance.

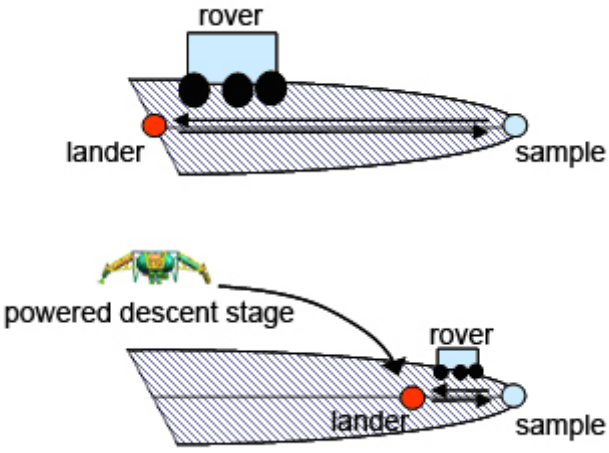

Figure 4-1: A Large Rover (top) or a Small Rover with a more Accurate EDL System (bottom) are Two Possible Methods for Retrieving a Cache of Samples Quickly

4.2 Approach

To answer these questions about MSR fetch rovers and landing accuracy, the typical rover modeling capabilities of MSE were supplemented with an EDL system model. Figure 4-2 shows a block diagram of the approach used to model a MSR mission. The MSE tool is used to create a database of fetch rovers which span many possible variations of mission duration, power source, and wheel diameter. Each of these rovers is analyzed to check to see that it can retrieve the sample in the allotted time as well as carry the required weight (the cache is assumed to have a 5 kg mass). This is done for a range of different sized landing ellipses, so some rovers are valid only for small landing ellipses.

By the time a MSR mission flies, it is assumed that EDL accuracy capabilities will have matched and exceeded the planned capabilities of the MSL mission. It is reasonable to expect that improvements in approach navigation and the use of guided hypersonic entry can reduce errors at chute deploy to 3 – 4 km [Wolf 06]. Assuming

conservatively that the lander will drift on its chute for 90 seconds at a horizontal velocity of 25 m/s (1σ wind velocity), there will be an additional 2.25 km of error in landing accuracy. Combining these gives a landing ellipse of roughly 12 km major axis as shown in Table 4-1 (assuming no correction is done during powered descent).

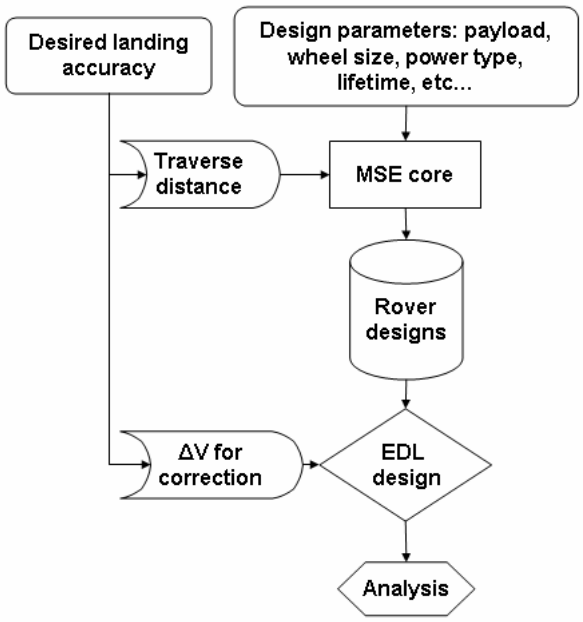

Figure 4-2: Block Diagram of MSR Modeling Approach

Table 4-1: Landing Error without Correction during Powered Descent Stage

error chute deploy	3.75 km
wind drift on chute for 90 s at 25 m/s (1σ wind velocity)	2.25 km
error at powered descent start	**± 6 km**

For the purpose of this analysis, 12 km is assumed to be the default landing ellipse major axis, meaning that it can be achieved without expending any extra propellant to travel horizontally. To achieve pin-point landing using the EDL system that is modeled, additional propellant must be added to allow the lander to fly (roughly) horizontal from its position at the start of the powered descent phase to the location of the sample cache. The amount of propellant needed to perform this correction depends on the amount of error that needs to be corrected and the mass of the rover and lander.

To approximate the overall penalty of performing correction during powered descent and thereby increasing landing accuracy, entry mass is compared for a wide range of rovers and landers. Entry mass must be modeled as a function of rover mass and desired landing accuracy (EDL Design diamond in Figure 4-2). This was previously done by assuming a constant ratio between propellant mass and lander mass, then also between lander mass and total entry mass [Lamamy 04]. This has been replaced by a much higher fidelity model of the EDL system that includes a heatshield, mass balance, backshell, chute, thermal system, and descent stage [Wolf 06]. The descent stage is similar to the skycrane planed for use on MSL, shown in Figure 4-3. Given the payload mass (mass of fetch rover designed by MSE plus the MAV mass of 280 kg) and the ΔV required, a set of scaling rules derived from MSL determines the total entry mass of the system, including the heatshield, mass balance, backshell, chute, thermal system, and structure.

Figure 4-3: The Descent Stage is similar to the MSL Skycrane [Wolf 06]

The scaling rules used to model entry mass are based on the diameter of the aeroshell. Since MSE does not estimate aeroshell size, a curve fit to Viking, Mars Pathfinder, MER, Phoenix, and MSL data is used to estimate aeroshell diameter in meters [Braun 05].

$$D_{aeroshell} = 1.0271 \times \ln\left(M_{rover}\right) - 2.3245 \qquad 4\text{-}1$$

where M_{rover} is the mass of the fetch rover in kg as determined by MSE. Equations 4-2 through 4-12 are from the published MSL derived scaling rules [Wolf 06]. All masses are in kg. The mass of the descent stage is found using

$$M_{descent} = M_{structure} + M_{prop\_system} + M_{thermal} + M_{other} + M_{propellant} + M_{rover} \qquad 4\text{-}2$$

where

$$M_{structure} = 295 \times \left(\frac{M_{rover}}{600} \right) \quad 4\text{-}3$$

$$M_{prop\_system} = 194 \times \left(\frac{M_{rover} + pmf \times M_{descent}}{600} \right) \quad 4\text{-}4$$

where *pmf* is the mass fraction of the propellant on the descent stage

$$M_{thermal} = 18 \times \left(\frac{D_{aeroshell}}{3.75} \right) \quad 4\text{-}5$$

$$M_{other} = 59 \quad 4\text{-}6$$

$$M_{propellant} = M_{descent} \times pmf \quad 4\text{-}7$$

After the mass of the descent stage is calculated, the entry mass can be found using

$$M_{entry} = M_{descent} + M_{heatshield} + M_{balance} + M_{backshell} + M_{chute} \quad 4\text{-}8$$

where $M_{descent}$ is found using Equation 4-2 and

$$M_{chute} = 40 \quad 4\text{-}9$$

$$M_{backshell} = 250 \times \left(\frac{D_{aeroshell}}{3.75} \right)^{2.4} \quad 4\text{-}10$$

$$M_{balance} = 75 \times \left(\frac{D_{aeroshell}}{3.75} \right) \quad 4\text{-}11$$

$$M_{heatshield} = 285 \times \left(\frac{D_{aeroshell}}{3.75} \right)^{2.2} \quad 4\text{-}12$$

These calculations are done for each combination of rover size and landing accuracy, and then the calculated entry mass is used to compare designs. In the future, it would be interesting to use total cost, rather than entry mass, as a metric by which designs are compared, but modeling the cost of EDL systems is a feature that has not been implemented into MSE.

4.3 Results

The modeling approach described above was applied to a trade space of both solar power and radioisotope power (RPS) rovers with wheel diameters between 0.15 m and 0.42 m. Landing accuracy was varied between +/- 100 m to 6 km and mission duration was varied

between 30 and 210 sols. First, the results for 90 sol duration missions are presented to give an example of the model output. These results are then compared to the full range of mission durations.

4.3.1 90 Sol Mission Duration

The trade space first considered includes only missions with 90 sol durations. The results are shown in Figure 4-4. The x-axis represents the metric, entry mass, and the y-axis represents the landing accuracy achieved by a given architecture. Each arc of points of the same symbol and color represents one fetch rover design that is used in conjunction with EDL systems of varying degrees of accuracy. As one moves down an arc of constant color and symbol (increasing landing accuracy), the entry mass increases. To provide a relative sense of entry mass, the MER rovers each had an entry mass of about 830 kg and MSL plans to have an entry mass of about 2800 kg (2.8 MT) [Braun 05].

Note that the RPS fetch rovers can all achieve the 12 km roundtrip traverse within 90 sols, so no additional EDL accuracy is necessary. The solar powered fetch rovers, on the other hand, are unable to complete a 12 km traverse within 90 sols, as indicated on the figure by the lack of points in the pink shaded region. It can therefore be concluded that if solar powered rovers are to be used to fetch a cache within 90 days, additional propellant must be expended to improve landing accuracy. The lowest mass system for a 90 sol mission utilizes a rover with 19 cm diameter wheels and solar power (label A in Figure 4-4). Using the smallest possible solar rover with propellant for roughly 4 km of correction proved to have a lower entry mass than using the smallest possible RPS fetch rover (27 cm diameter wheels) with no additional propellant for correction (label B in Figure 4-4). Note that four km of correction corresponds to an eight km reduction in landing ellipse major axis.

One last worthwhile observation about this scenario is that the entry mass is not reduced by decreasing the major axis of the landing ellipse to smaller than roughly 4 km. This is because a rover that is large enough to carry the samples will be able to traverse the required distance in less than 90 sols. Not having to reduce the landing ellipse major axis below 4 km reduces the need to add more sensors to track and identify landmarks on the surface.

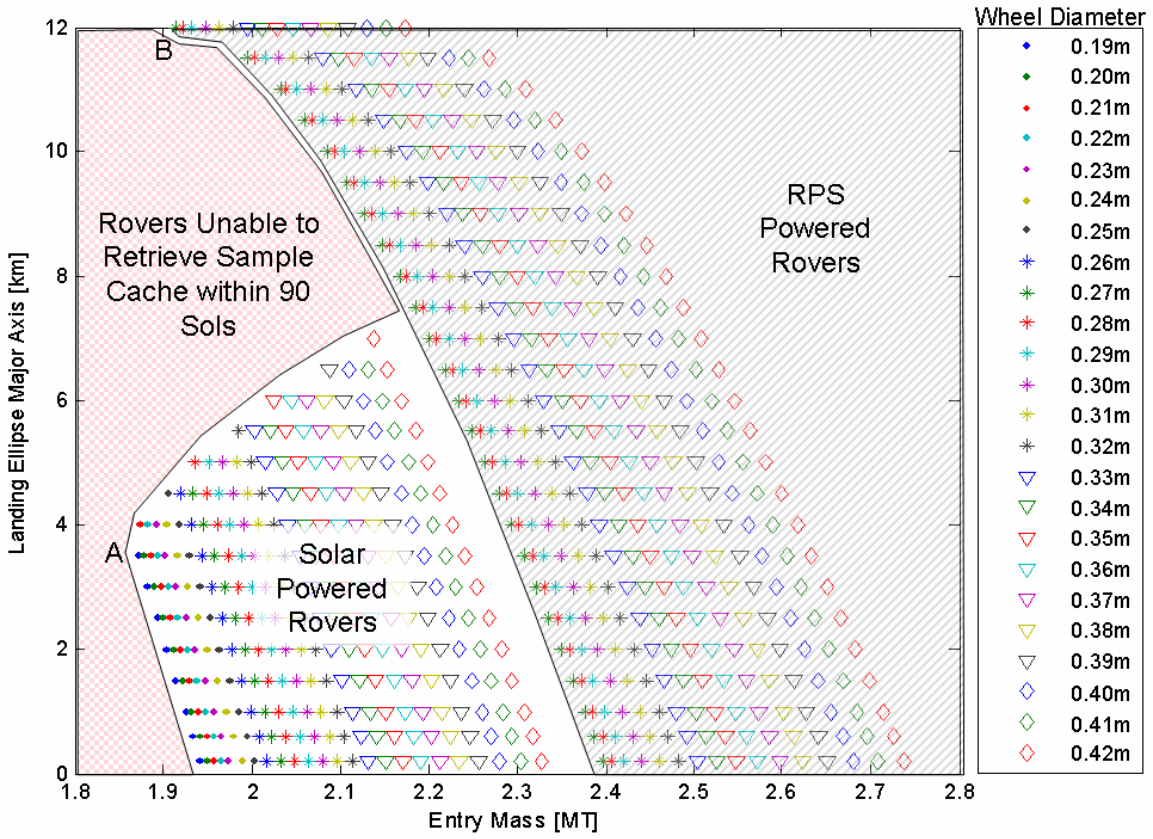

Figure 4-4: Valid Combinations of Rover and EDL System Designs for 90 Sol Duration Fetch Rover Missions

4.3.2 Varying Mission Duration

While 90 sols is a reasonable mission duration for a fetch rover mission, it is interesting to study the sensitivity of entry mass and the need for precision landing to the time allotted to the rover to fetch the sample. Figure 4-5 shows the contours of capability for mission durations ranging between 30 and 210 sols for both solar and RPS rovers. Labels A and B in Figure 4-4 correspond to labels A and B in Figure 4-5. The black lines in Figure 4-4 that bound the regions of solar powered and RPS powered rovers correspond to the solid and dashed red lines, respectively, in Figure 4-5. Regions to the right of the contours are feasible entry masses for the desired landing accuracy. It can be seen that even 30 sols is enough for a fetch rover to retrieve the samples; however, it must be landed within 100 m of the cache if it is a solar powered rover (label C in Figure 4-5), or within 500 m if it is RPS powered (label D in Figure 4-5). These solutions require a large

EDL system and have a significantly higher entry mass than systems with less landing accuracy and more time given to the rover to fetch the sample.

For solar powered rovers and mission durations greater than 150 sols, spending the extra propellant to land more accurately is not worthwhile. This can be concluded from the fact that the left most (lowest mass) points on the black, yellow, and purple curves all lie along the top of the plot where no propellant is spent to improve landing accuracy (labels E in Figure 4-5). For solar powered rovers mission durations of 120 sols or less, the lowest mass point lies somewhere in the middle of the plot. In the case of 120 sols the lowest mass point is at a landing ellipse of roughly 5.5 km major axis (label F in Figure 4-5). This indicates that adding propellant for correction will allow a smaller fetch rover to be used such that overall entry mass is reduced.

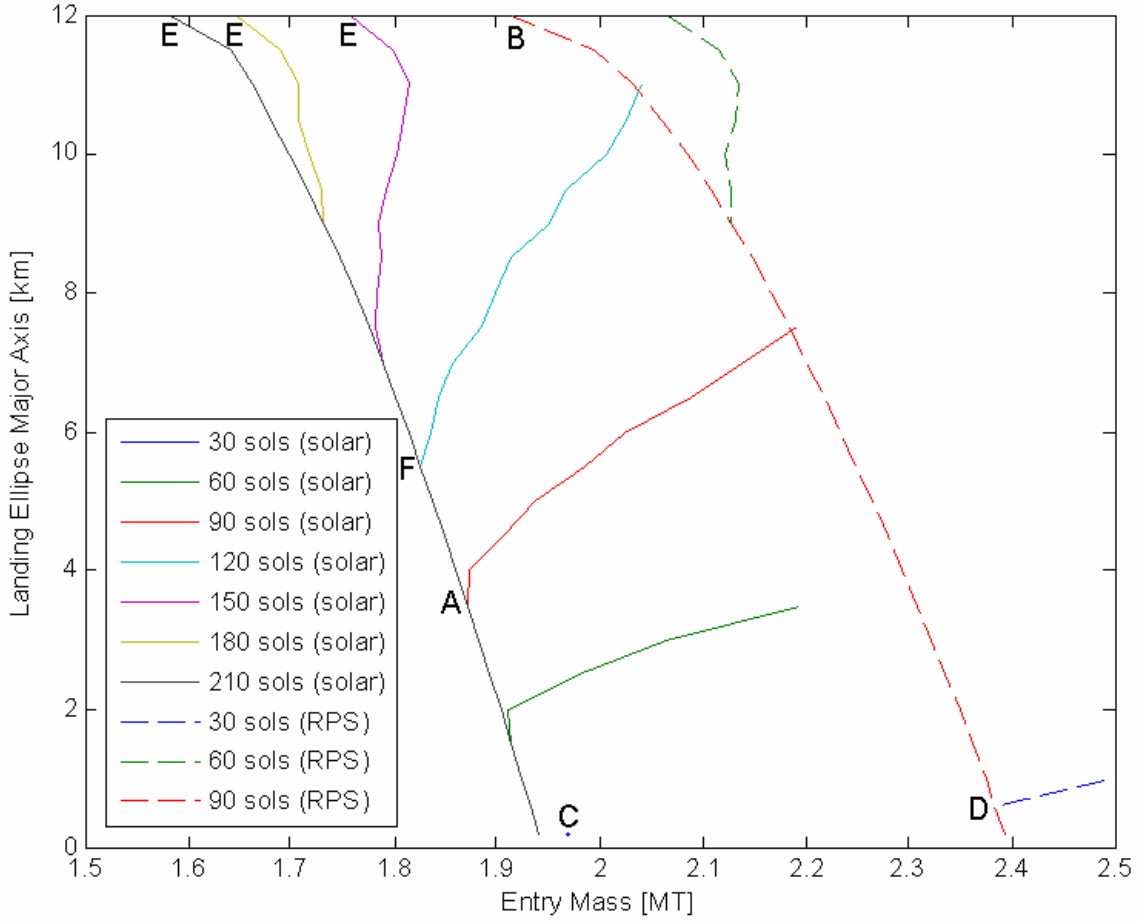

Figure 4-5: Contours of Achievable Traverses for Fetch Rovers of Varying Lifetime

Interpolating between these minimal entry mass points for each mission duration gives a sense of the relationship between mission duration and entry mass, as shown in Figure 4-6. The entry mass for a RPS powered rover does not decrease when the fetch rover lifetime is extended beyond 90 sols, since the need for a powered descent stage is eliminated for long mission durations. Similarly, the entry mass for a solar powered rover cannot be reduced by extending the lifetime beyond 210 sols. The bottom line is that the lowest mass system that can retrieve a 5 kg cache of samples includes a solar powered fetch rover with 19 cm diameter wheels, allows 210 sols for the fetch rover to retrieve the sample, and does not perform any correction during powered descent.

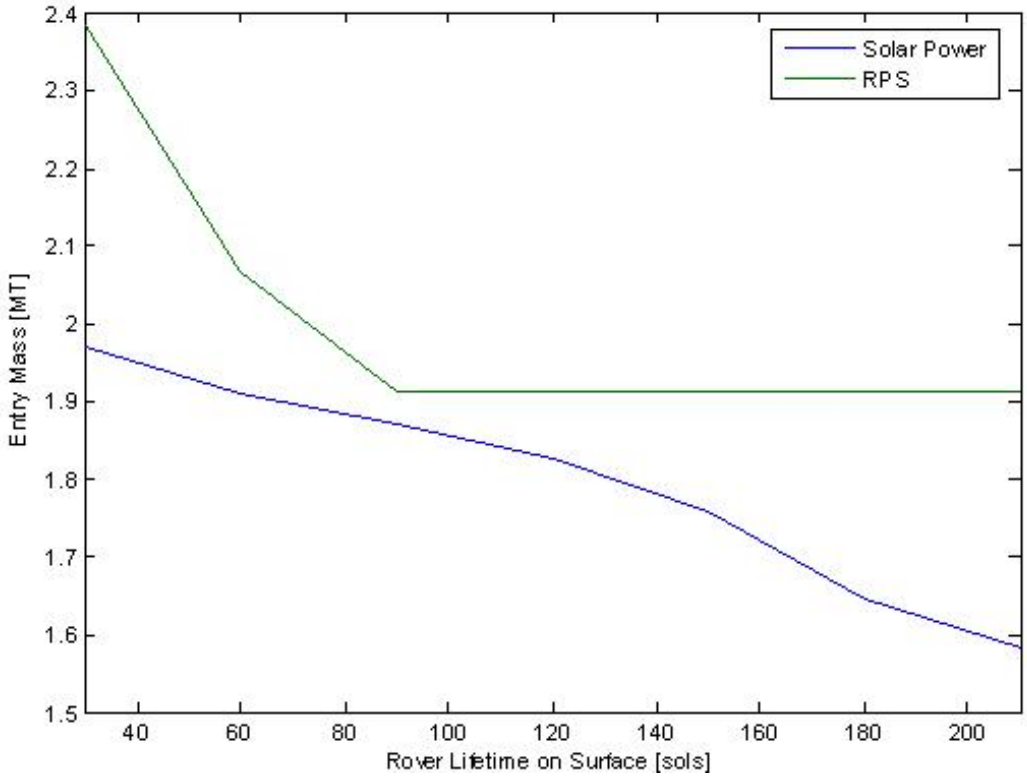

Figure 4-6: Entry Mass as a Function of Fetch Rover Lifetime for RPS and Solar Powered Rovers

4.4 Conclusions

A model has been implemented into MSE that is capable of rapidly sizing the EDL system for a variety of rovers and landing accuracies. This model is used to compare the entry mass of a large trade space of rover designs and degrees of landing accuracies. The

results indicate that solar powered rovers, although they are not as capable as RPS rovers in general, always allow for a lower overall entry mass. The smallest feasible fetch rover design found by the MSE tool had wheels of 19 cm diameter. The degree to which landing accuracy needs to be improved is dependent upon the time allotted to the fetch rover to retrieve the sample, but generally becomes important if four months or less are given to fetch the sample.

Chapter 5

Overview of Alternative Forms of Mobility

While the wheeled form of MSE has many uses, it is limited to modeling traditional six-wheeled rovers. The limitations of these traditional six-wheeled systems will be discussed in the context of motivating rover designers to consider new, alternative forms of mobility. A variety of mobility types will be discussed with an emphasis on the types added to the MSE tool: wheeled, legged, and hybrid mobility.

5.1 Limitations of Traditional Mobility Systems

Successful Mars rovers have featured exclusively six-wheeled rocker bogie suspension mobility systems. There are many advantages to these traditional designs, but there are also weaknesses that motivate rover designers to look to new mobility systems for future Mars rover missions. The six-wheeled rocker bogie suspension system features three wheels on each side of the rover; two connected to a bogie and one connected to the rocker. The bogie and rocker are both free to pivot, allowing the front, rear and middle wheels to maintain contact with the ground, even on rough terrain. The two sides of the suspension system are connected by a differential, allowing each set of three wheels to be oriented differently and equilibrating the average pressure on the ground for each wheel [Lindemann 06]. The rocker bogie suspension system allows the rover to traverse over obstacles up to a wheel diameter in height. The most well known implementation of this design was on the MER rovers, shown in Figure 5-1 [Lindemann 06].

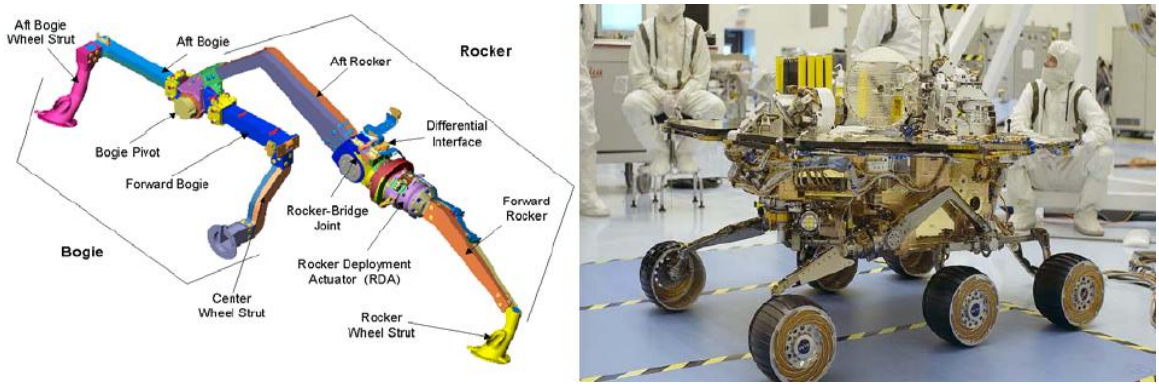

Figure 5-1: One Side of MER's Rocker Bogie Assembly (left) and Spirit Featuring its Rocker Bogie Suspension System (right) [Lindemann 06]

Two major drawbacks of the rocker bogie suspension system, as demonstrated by the MER rovers, are its inability to climb steep slopes and the risk of getting stuck in soft soils. The MER rovers are limited to 30 degree slopes because of wheel slippage at high inclinations. Figure 5-2 shows wheel slippage on a test slope covered in dry, loose sand as a function of the slope angle [Lindemann 06]. At a 20 degree inclination, the percentage of wheel slippage exceeds 90%, indicating that wheels are a very ineffective form of mobility under these conditions. Wheels can do better on slopes if the surface is hard or if they don't drive directly up the slope, but wheel slippage still ultimately limits the steepness of terrain that can be traversed.

Another drawback of the rocker bogie suspension system is the potential to get stuck in soft sand. The robustness of a wheeled vehicle to sinking into the sand and becoming stuck is determined by its ground pressure, which is a function of wheel size and vehicle mass. Heavier vehicles and vehicles with smaller wheels have higher ground pressure and more wheel sinkage. High ground pressure was a problem in particular for MER, whose ground pressure was 2.5 times that of Sojourner [Lindemann 06]. Opportunity demonstrated this weakness when it got temporarily stuck is sand dunes. Figure 5-3 shows two of Opportunity's wheels significantly submerged in sand.

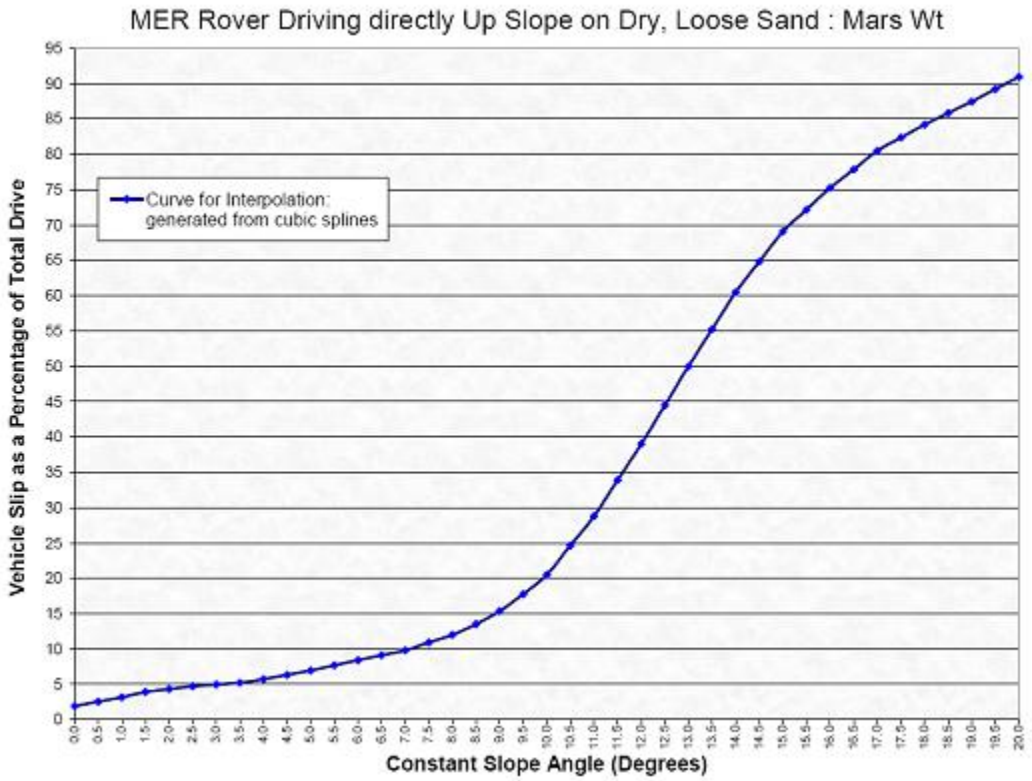

Figure 5-2: MER Wheel Slippage as a Function of Inclination on a Dry, Loose Sand Test Surface [Lindemann 06]

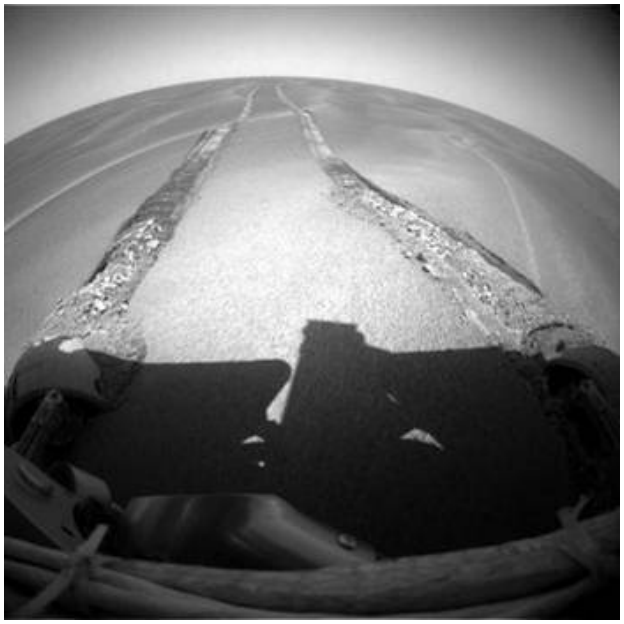

Figure 5-3: Opportunity Stuck in Sand [MER 07]

Despite its disadvantages, the rocker bogie has performed very well on the surface of Mars. It also has the major benefit of being proven to work on the surface of Mars. A specific need must be identified to shift designers away from traditional, proven designs. As knowledge of Mars improves, it is becoming apparent that many high value science targets are in locations inaccessible to rocker bogie mobility systems. One example encountered by the MER rovers is steep crater walls, as seen in Endurance crater. Steep crater walls and other cliffs often expose interesting layers of terrain that would otherwise be buried. Gullies are another interesting but difficult to reach terrain type, because they are potentially formed by water. New mobility systems must be conceived to allow scientist to study these features and get the most from future Mars missions.

5.2 Alternative Forms of Mobility

Many forms of mobility have been proposed for future Mars exploration missions. More radical ideas include aerial forms of mobility and tumbleweed concepts [Lamamy 07]. When selecting which forms of mobility to model with MSE, it is important to consider the underlying assumptions built into MSE and how compatible they are with new forms of mobility. An aircraft, for example, would have drastically different design requirements and operating parameters than a rover. Modeling more radical forms of mobility would require significant reworking of the MSE tool or the creation of an independent modeling tool. MSE is better suited to model forms of mobility that retain some of the same basic constraints on rover form. This generic rover form includes a rectangular prismatic body to house the rover electronics and mount instruments, communication equipment, and potentially solar panels on the top surface. MSE is also better suited to model forms of mobility with operational constraints similar to MER and MSL. Operational constraints involve the repeating pattern of communicating, collecting information, charging batteries, driving, and thinking that the rover carries out to move across the surface.

Forms of mobility that fall into this classification of being compatible with the core assumptions of MSE include wheels, legs, tracks, and hybrid mobility. Another interesting form of mobility that could be modeled is a rover with a repelling section. This would require more modification to MSE, but would be worth modeling in the

future since it is a candidate form of mobility for future missions. JPL has developed the Cliffbot testbed to demonstrate the repelling rover concept [Volpe 07]. Of these forms of mobility, four-wheeled, eight-wheeled, legged, and legged plus wheeled hybrid rovers have been selected to be modeled with MSE.

5.2.1 Wheeled Mobility

The advantages of wheeled mobility are numerous, including the flight heritage from previous Mars rovers and the relative simplicity of controlling wheels. The disadvantages of wheels include their tendency to sink into soil, which leads to high soil resistance as the wheels must compact and push the surface [Bekker 56]. Six-wheeled mobility has already been modeled in MSE, but four and eight-wheeled systems are new additions. Changing the number of wheels can help mitigate some of these disadvantages. An eight-wheeled rover would have two extra wheels to spread its weight between, and therefore lower ground pressure, resulting in less wheel sinkage. A four-wheeled rover sacrifices mobility performance to save mass, since a good portion of the suspension system and two wheels can be removed.

5.2.2 Legged Mobility

Legged rovers have some advantages over wheeled rovers. One is that legs do not have to compact sand as they walk, since the feet can be lifted up and moved through the air. Another advantage is that legs can step over rocks and other rough terrain. Legs also allow a rover to shift the support base to maintain static stability on steeper inclines. A big disadvantage of legged mobility is its complexity; in particular the control complexity. Walking algorithms are still an area of research on terrestrial vehicles, so it would be necessary to prove that the software to run a legged rover on Mars is mature and robust enough before flight. This increased complexity could also place burdens on a rover's computational power. Another drawback of legged mobility is that energy is lost moving the mass of the rover vertically up and down with each step, whereas wheeled mobility in theory could avoid such losses.

There are many examples of legged robots on Earth. At JPL, the Limbed Excursion Mechanical Utility Robots (LEMUR) series of legged robots have

demonstrated both walking and climbing mobility. The LEMUR robots also feature interchangeable manipulators at the end of limbs that could be used for assembly, inspection, or maintenance of space vehicles [Kennedy 05]. Boston Dynamics Inc. has developed both the LittleDog and BigDog four-legged robots. BigDog is a larger, cargo carrying legged robot that has a dynamic gait. LittleDog is a smaller, three kg robot that walks with a static gait [BDI 06]. Each of these robots can be seen in Figure 5-4. Other examples of all types of legged robots are prevalent in the literature.

Figure 5-4: Examples of Legged Robots from Left to Right: LEMUR, LittleDog, and BigDog [Volpe 07] [BDI 07]

5.2.3 Hybrid Mobility

Hybrid mobility refers to a vehicle with more than one form of mobility, in this case legs and wheels. By combining multiple forms of mobility on one vehicle, the benefits of multiple forms of mobility can be exploited. Wheels would be used when they are more efficient, to travel over flatter and less rugged terrain. Legs would be used either when they are more efficient because the terrain is too rocky or if the slope is too great for a wheeled vehicle to avoid slippage. In addition to just walking or regular rolling, hybrid rovers can be designed to roll on their wheels, but use their legs as an active suspension system. Such an active suspension system would allow the rover to equilibrate the ground pressure on each of its wheels and improve mobility performance.

The adaptability and flexibility of hybrid vehicles comes at a price. Carrying two mobility systems adds a significant amount of mass to a vehicle. While some integration can be done, for example a hybrid rover's legs can double as a suspension system; there is ultimately a lot of additional hardware that must be added. Because a hybrid vehicle is

heavier, it is less efficient at driving than a purely wheeled rover and less efficient at walking than a purely legged rover. There is also increased software and control complexity on a hybrid robot because the rover must transition between modes of locomotion depending on the terrain.

Several examples of legged and wheeled hybrid rovers can be found in the literature (see Figure 5-5). JPL has developed the All-Terrain Hex-Legged Extra-Terrestrial Explorer (ATHLETE) vehicle, which moves using six wheels on the ends of six legs. Each leg has six degrees of freedom and can be used to roll or even manipulate specially designed tools. ATHLETE is designed to carry a payload of up to 450 kg and support human exploration of the lunar surface [Volpe 07]. ATHLETE's primary mode of locomotion is rolling on six wheels while using the legs as an active suspension system. Implementation of a statically stable walking gait is underway [Wilcox 06]. Another example of hybrid mobility can be seen on the HyLoS robot developed by the Laboratoire de Robotique de Paris. HyLoS, like ATHLETE has wheels on the ends on each of its legs, but differs from ATHLETE in that it is smaller and has only four legs [Besseron 05]. Finally, the Modular Rover for Extreme Terrain Access (MoRETA) is a four-wheeled, four-legged robot being developed at MIT [Coso 07]. A picture of MoRETA without its wheels is shown in Figure 5-6, and a full CAD drawing is shown in Figure 6-1. MoRETA differs from ATHLETE and HyLoS in that its wheels are on the bottom of the rover body, as opposed to on the ends of the legs. This is beneficial because the legs do not have to move the mass of the wheels as they step, but prevents the rover from using the legs as an active suspension system when rolling. However, the MoRETA legs can perform other manipulation tasks while the rover is rolling, including pushing the rover along. MoRETA and its relation to this modeling work will be described in Chapter 6.

5.3 Summary

A survey of existing legged, wheeled, and hybrid rover systems was done to establish background for the models described in Chapter 7. First, a closer look at the MoRETA hybrid rover that was used to help develop mobility models will be described in more detail in Chapter 6.

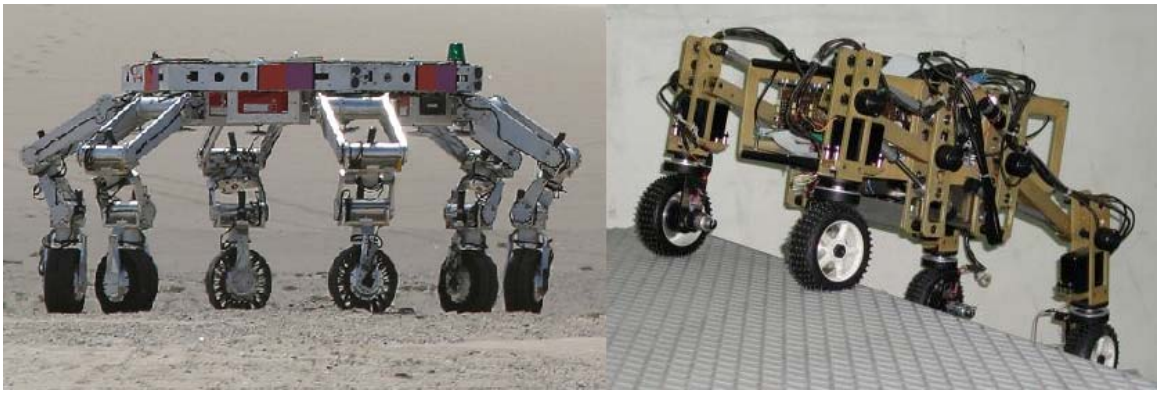

Figure 5-5: Examples of Hybrid Robots from Left to Right: ATHLETE and HyLoS [Volpe 07] [Besseron 05]

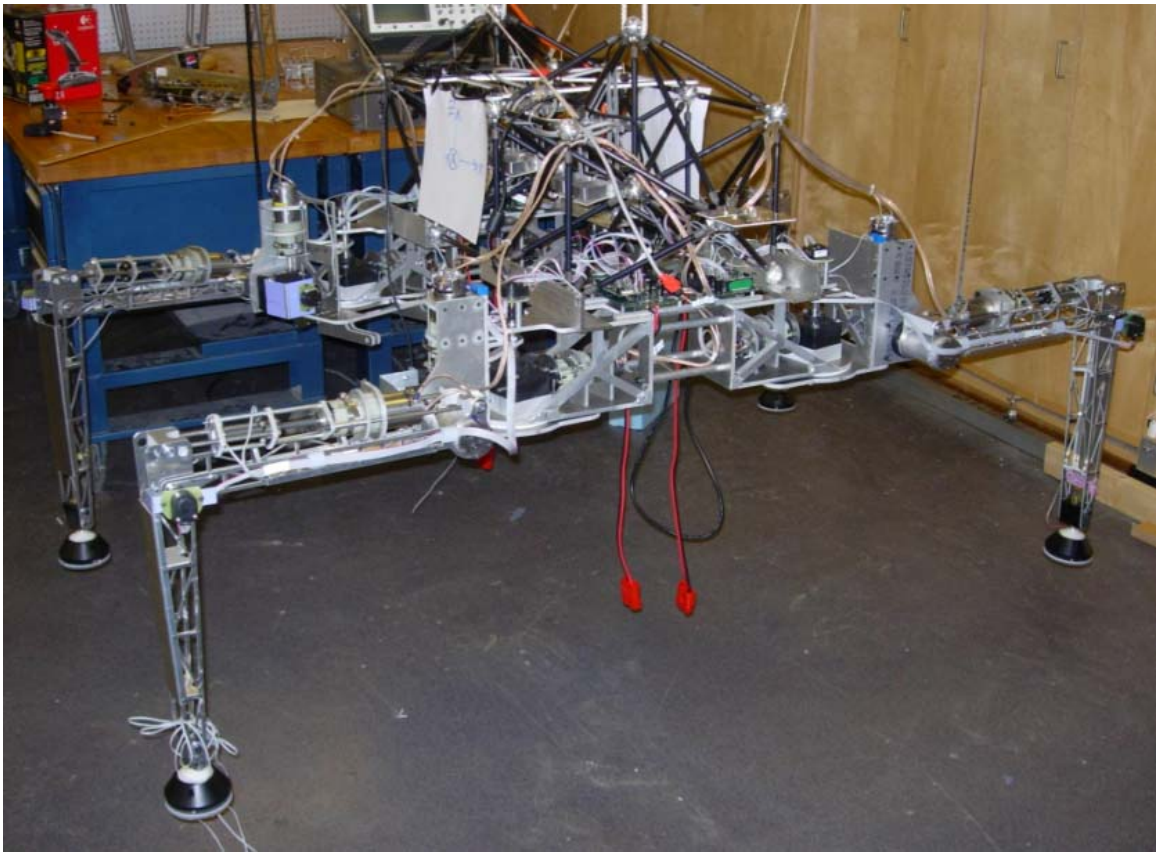

Figure 5-6: MoRETA without Wheels Attached

Chapter 6

The MoRETA Rover and its Relevance to Mobility Modeling

Experience and familiarity with rover hardware is very valuable when creating models of alternative forms of mobility. The Modular Rover for Extreme Terrain Access (MoRETA) rover, with its hybrid wheeled and legged locomotion system, has provided an opportunity to gain insight into the challenges of developing a hybrid rover [Coso 07]. MoRETA was designed and built by undergraduates during the three semester Space Systems Product Development capstone course at MIT. This chapter will provide a system description of the MoRETA rover, then discuss the design parameters and lessons learned that aid in mobility modeling and how they were integrated into the model.

6.1 System Description

The objective of the MoRETA project is to develop and validate a modular rover testbed capable of operating in extreme terrains by making use of both wheeled and legged mobility. Achieving this objective is significant because many of the most scientifically interesting targets on planetary surfaces are in difficult to reach areas. Utilizing hybrid mobility allows the rover to reach these targets with legs, while still allowing for more efficient long range traverses on benign terrain with wheels. The system created to meet this high level requirement is shown in Figure 6-1 and described in the literature [Massie 07]. The rover weighs roughly 70 kg and is 0.75 m long, 0.70 m wide, and 0.65 m tall when resting on its wheels. Each of the 0.80 m legs extends beyond this footprint and can lift the rover so that the wheels are up to 0.45 m off the ground. It is estimated that the rover can roll on its wheels at a speed of roughly 1 m/s and walk with its legs at

roughly 0.05 m/s, but testing to confirm these estimates has not been carried out as of this writing. The development of the MoRETA rover can be divided into the mechanical, avionics, and autonomy subsystems, which are described in more depth below. The high level flow of information within and between MoRETA's subsystems is shown in Figure 6-2.

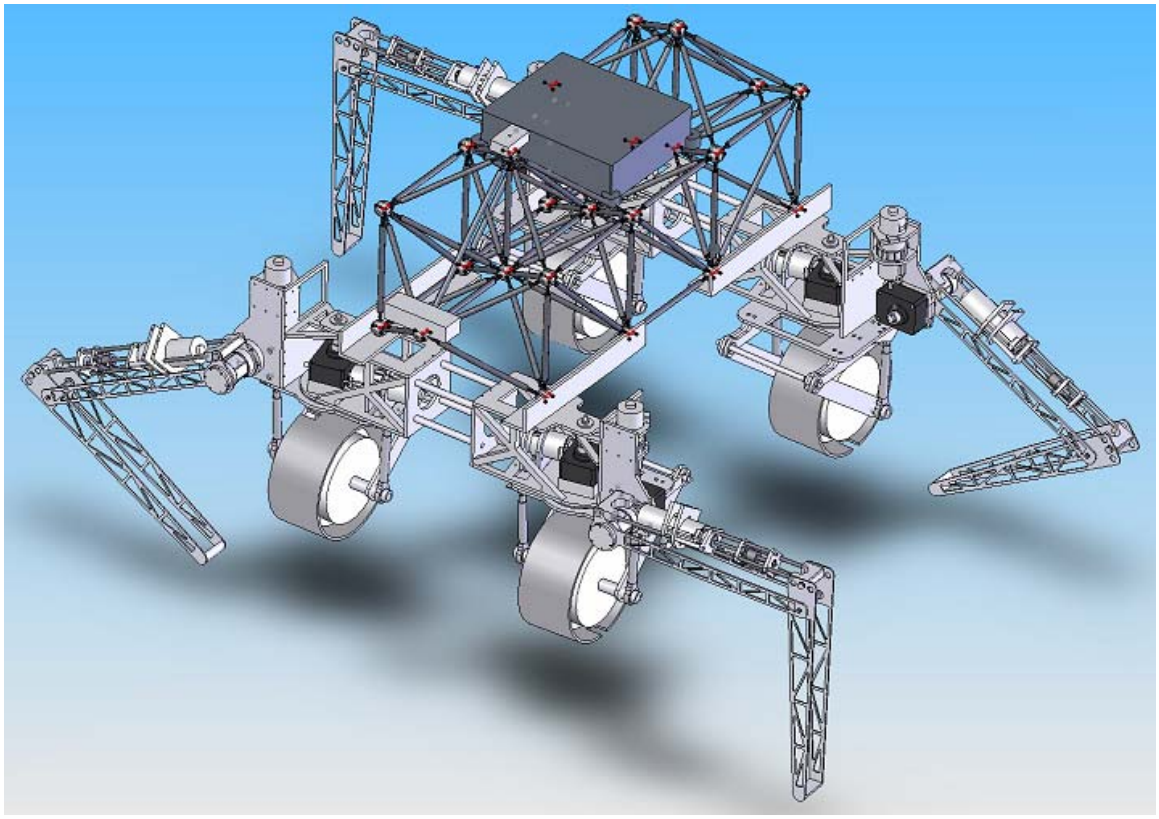

Figure 6-1: Integrated CAD Model of MoRETA

6.1.1 Mechanical

The mechanical design of the MoRETA rover can be further broken down into the chassis, leg, and wheel components. The chassis is a trust structure assembled from aluminum rods and balls, and provides structural rigidity despite its low mass. Aluminum brackets and frames serve as connections for other rover hardware, such as the mobility system, computer, power electronics, batteries, and stereo camera. The hips of each of the four legs connect to the bottom of the chassis and to the hip of the leg on the opposite side of the rover to provide a structurally rigid connection. The hip has two

degrees of freedom in pitch (rotation about the horizontal axis) and yaw (rotation about the vertical axis) that are driven by electrical motors and worm gears. The leg has two sections, each 0.40 m in length, connected at the knee. The knee is driven by a lead screw that operates at a higher efficiency than the worm gears on the hip joints. The ends of each leg have a foot that can pivot to match the angle between the shin and the ground and contain a switch that provides feedback to the rover so that it can determine when contact with the ground is made. Four wheels are mounted below the hip yaw joints, which provide steering when in wheeled locomotion mode. MoRETA's rear wheels provide drive power, while the front two wheels are unpowered and provide encoder feedback.

6.1.2 Avionics

The avionics subsystem of the rover is responsible for powering and controlling the rover. The power system is designed to power the rover for 30 minutes of operation from lithium polymer batteries capable of proving up to 445 Wh of electrical energy through the rover's 22.2 V bus. The rover can also be run from a power supply for testing in the lab. The control system is responsible for closing the loop between the higher level autonomy software and the mechanical actuation of the rover. This is done with a main computer and five printed circuit boards (PCB). One PCB contains the power subsystem, as well as a gyroscope and two-axis inclinometer to provide the rover with orientation feedback. The other four PCBs are four identical leg modules that command all joint movements and receive feedback from optical joint angle encoders, position limit sensors, and foot touch sensors. The leg modules use RoboStix processors to send Pulse Width Modulated (PWM) signals to drive the motors. The leg modules also include safety measures in the event of high current due to events such as motor stall.

6.1.3 Autonomy

The autonomy subsystem exists as software that runs on the main computer to perform the higher level functions of the rover. Local mapping software is used to take images from a stereo camera on the front of the rover and convert the images to a height map of the surrounding terrain [Wheeler 07]. This map is used by foot placement planning

software that determines acceptable foot placement locations given the desired direction of motion and the stability constraints of the rover [Kulling 07]. The direction of travel of the rover is inputted by the user via a wireless joystick connected to the rover main computer. In the future, global mapping software could be added to MoRETA to allow it to navigate autonomously. The final piece of autonomy software is the locomotion module. The locomotion module converts the foot state plan into a control plan that achieves the desired foot placements. This control plan is used to command the leg modules and to check feedback from each joint to be sure that commanded motions are actually being achieved. Figure 6-2 shows the flow of information through the different autonomy modules just described, as well as through the avionics and mechanical subsystems.

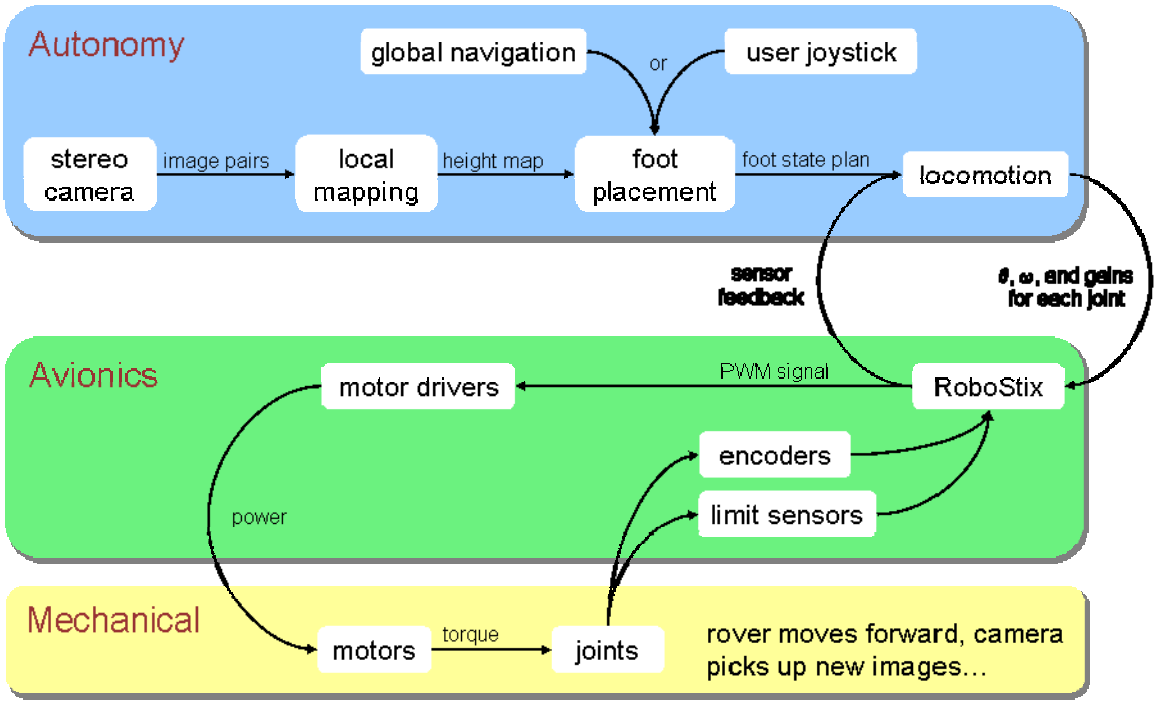

Figure 6-2: Concept of Operations for MoRETA

6.2 Application of MoRETA to Mobility Models

Designing, building, and testing the MoRETA rover has provided valuable experience that has assisted the development of the legged and hybrid mobility models. Some of these lessons have been qualitative, and simply have contributed to understanding the

design process of hybrid mobility rovers. Other lessons have provided quantitative relationships between key design parameters or test data that can be directly compared to models. The lessons learned relevant to mobility modeling will be discussed for the mechanical, avionics, and autonomy subsystems.

6.2.1 Mechanical

The mechanical design of MoRETA differs from a hybrid mobility rover that would be sent to Mars in that it is a prototype and a testbed, yet there are several aspects of the design that are still applicable. First and foremost, MoRETA provides a sense of scale between the various dimensions of a legged or hybrid rover. In the wheeled version of MSE, the user simply inputs the wheel diameter and a majority of the remaining rover dimensions are determined from the wheel diameter. In the legged and hybrid rover models, the rover dimensions are determined based on the leg length. Scaling relationships relative to the leg length are used to determine the rover width, rover length, rover height, and clearance (see Section 7.1.2). The warm electronics box is also constrained to fit within dimensions that scale based on the leg length. The surface area of solar panels that the rover is able to carry depends on the dimensions of the rover, and therefore also scales to the leg length. In the wheeled mobility model, the panoramic camera mast and instrument arm scale to the wheel diameter. MoRETA does not have a mast or arm, so the ratio of MoRETA's leg length to wheel diameter (0.80 m to 0.25 m) is used along with the original wheel diameter relationship to determine the size of these appendages. Measuring these dimensions and ratios on MoRETA provides another data point that can be used to develop the parametric relationships used in the MSE mobility models.

Another useful aspect of MoRETA's mechanical design has been experience gained from working with electric motors and gearing on each of the leg joints. MoRETA was originally prototyped with Maxon motors, and is now built with less expensive DeWalt power drill electric motors. Individual motor testing was done with each type of motor, and the DeWalt power drill motors have been tested while operating all of the rover joints on the full prototype. Even though they are no longer being used by MoRETA, Maxon motors have been used to create the mobility models in MSE because

they have very complete data sheets [Maxon 07] and have Mars flight heritage from the MER rovers. The MoRETA rover incorporates planetary gears, worm gears, and a lead screw, all of which have different efficiencies and benefits. Based on experience with this variety of gears, it was decided that using planetary gears for MSE mobility models was appropriate. Planetary gears have Mars flight heritage on the MER rovers and tend to have higher efficiency than worm gears.

Finally, the fully assembled MoRETA rover and select components have been weighed to determine the total rover mass and mobility system mass. The mass of the mobility systems is further broken down into the mass of the leg structure and the mass of the actuators. The outputs of the legged mobility model are benchmarked against this MoRETA data and the limited data available on other legged and hybrid rovers. These mass comparisons are discussed in more detail in Chapter 8.

6.2.2 Avionics

Developing MoRETA's avionics subsystem has provided a qualitative sense of the complexity involved in controlling a legged rover. Quantitatively, the avionics subsystem has been useful in studying the power required to actuate the legs with electric motors. The leg module PCBs on each of the four legs are designed to send telemetry data back to the rover's main computer to be logged. These data logs include information such as angle measurements from encoders and current draw for each motor. This data is used by the MoRETA team to test and debug the rover, and is also useful when modeling mobility because the power draw can be determined for various rover motions. Power draw is calculated by multiplying the current draw by the voltage of the power supply (22 V).

Figure 6-3 and Figure 6-4 show joint angle in encoder tics (1000 tics is one revolution) and current in amps for each of the three leg joints during unloaded and loaded leg testing, respectively. The load used for the loaded test was the rover's own weight under Earth's gravity, approximately 546 N total or 136 N per leg if the load is shared evenly between legs. Neglecting current spikes, Figure 6-3 shows current draw on the order of amps, up to roughly 10 amps, which corresponds to a power draw of up to 220 W during unloaded motion of one leg. Again neglecting current spikes, Figure 6-4

shows current draw on the order tens of amps, up to 40 amps, which corresponds to a power draw of up to 880 W during loaded motion of one leg. It is important to note that in this case, the power supply running the rover could only provide 40 amps. If a bigger power supply or batteries were used, the current draw would likely be higher. The power estimates from these tests can be compared to the output of the legged mobility model. Differences will exist because the legged mobility model walks with a different gait than the MoRETA rover and uses different motors. Nevertheless, it is interesting to compare test data to the model's power prediction to check that the estimates are reasonable. These estimates are presented in Chapter 8 after the legged model is discussed.

6.2.3 Autonomy

The autonomy subsystem of MoRETA is useful for studying the computational complexity of legged locomotion. The computation time required to plan walking motions is relevant to the MSE model because the average velocity of the rover (as opposed to the raw velocity) is dependent on how long the rover must stop and think between each walking cycle. In this context, the walking cycle is similar to the driving cycle discussed in Section 3.2.1 and refers to the rover moving forward half a body length. Only qualitative observations of the computational expense of executing locomotion software have been made. When run on the rover's 1.83 GHz Intel Core Duo

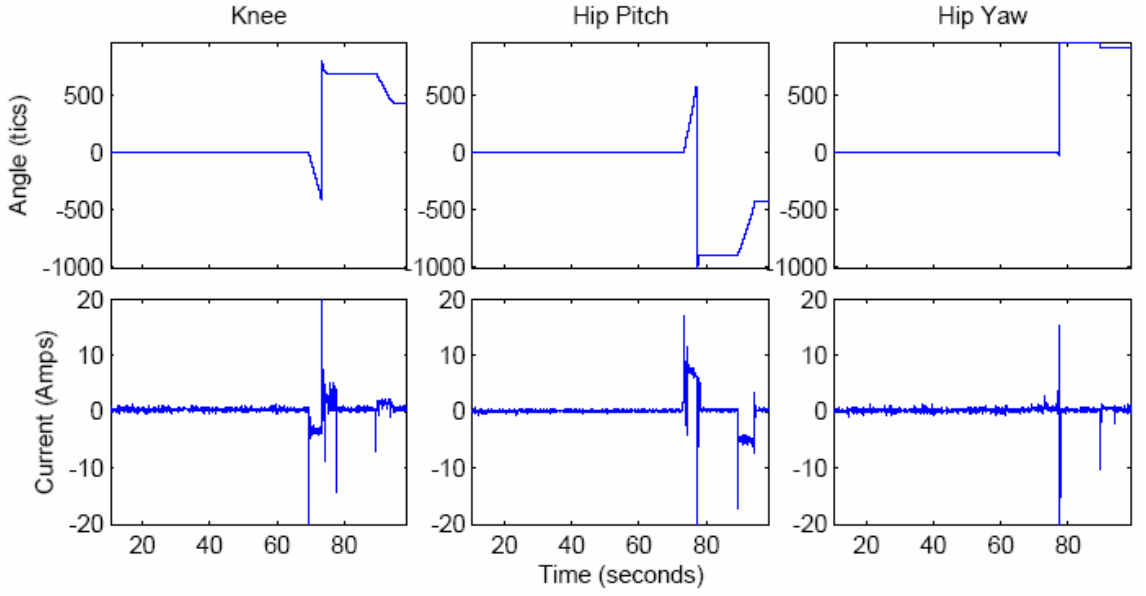

Figure 6-3: Joint Angles and Current Draws during Unloaded Movement

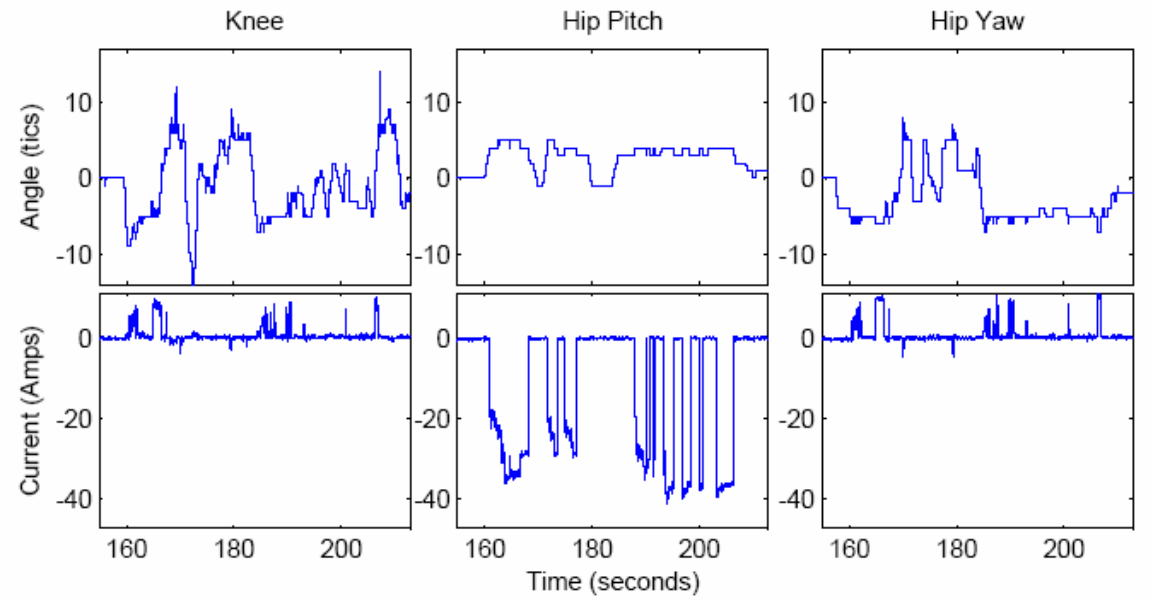

Figure 6-4: Joint Angles and Current Draws during Loaded Movement

processor in conjunction with the rest of the rover's software (excluding stereo mapping software), the locomotion software is able to run in real time. It is assumed that the computer on a Mars rover will be less powerful than MoRETA's computer, so 10 seconds per walking cycle is allotted for computation associated with walking locomotion.

The autonomy software includes a dynamic model of the rover that is used to plan the motions of the rover. The model can also be used to simulate rover motions and provide theoretical predictions for joint torque, joint speed, and other similar parameters. Comparing the output of the MoRETA dynamic model to the MSE dynamic model would provide a form of benchmarking. Figures 6-5, 6-6, and 6-7 show simulated joint torques for a walking gait. The plots are shown for one repeating period of the walking gait. This means that each leg takes one step, resulting in a total forward movement of the center of mass of the rover by one step length. This data is compared to the MSE dynamic model's output in Chapter 8.

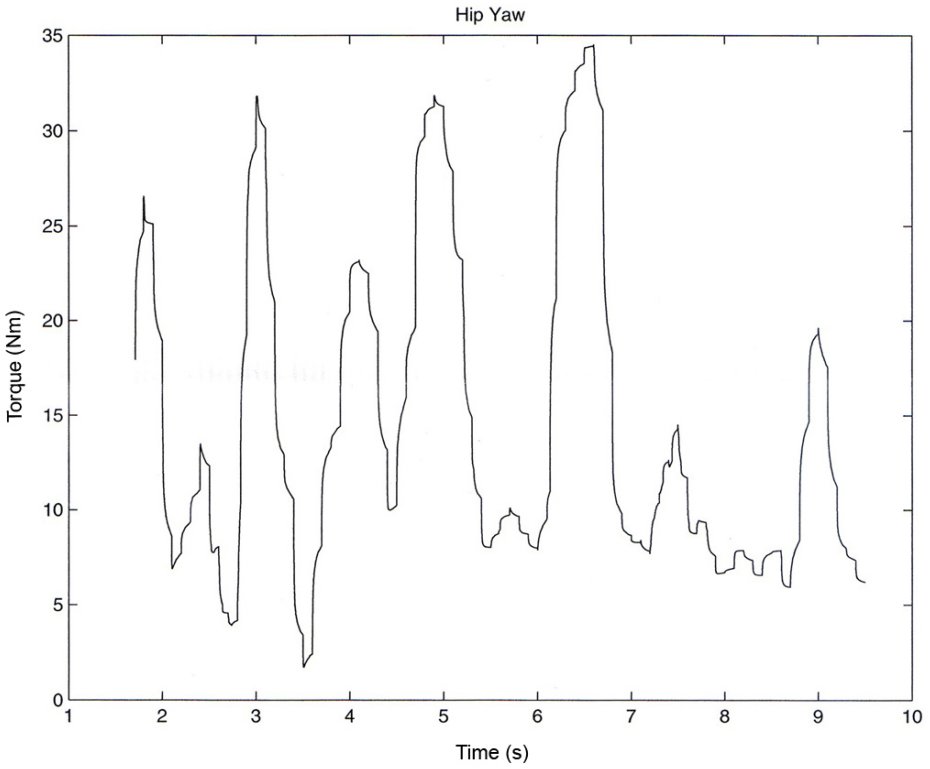

Figure 6-5: Simulated Torque over Time for the Hip Yaw Joint

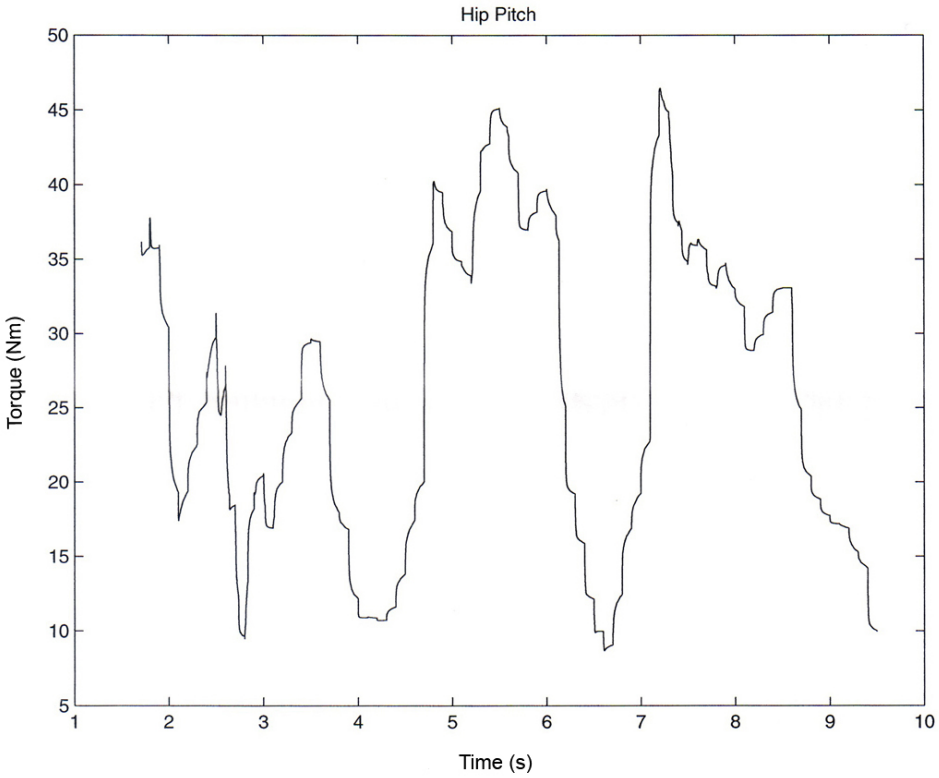

Figure 6-6: Simulated Torque over Time for the Hip Pitch Joint

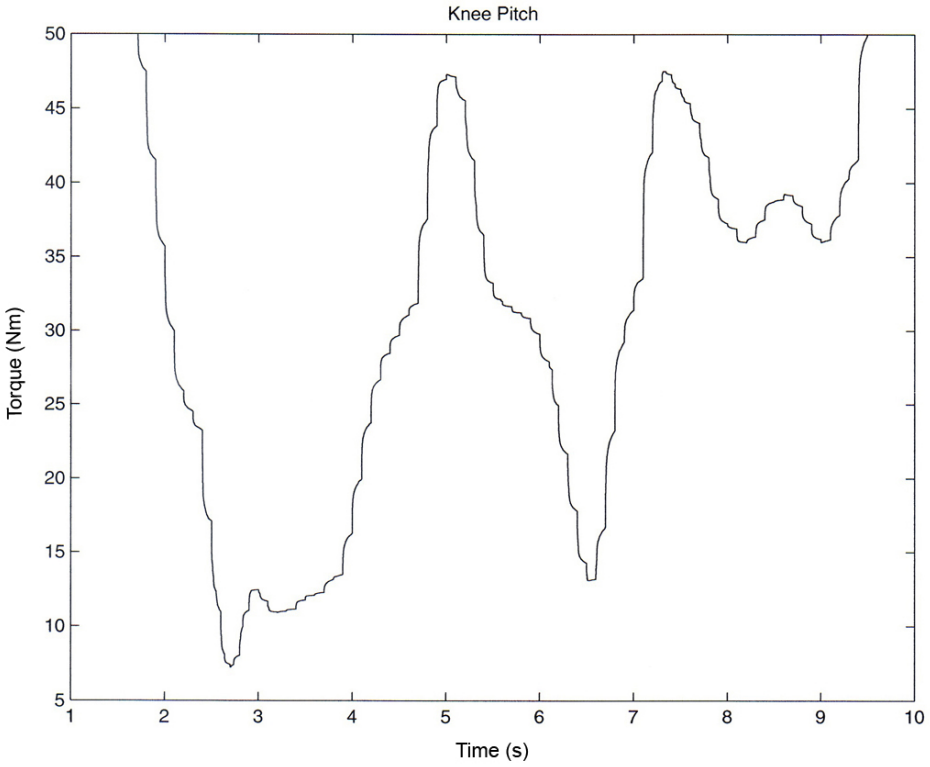

Figure 6-7: Simulated Torque over Time for the Knee Pitch Joint

6.3 Summary

A design overview of the MoRETA legged and wheeled hybrid rover has been presented with emphasis on the aspects that provide lessons relevant to modeling mobility systems. The usefulness of each of MoRETA's subsystems to mobility modeling was described, and will be mentioned again as the details of the mobility models are presented. Comparisons between MoRETA design parameters, test output, and simulation output are also discussed in more detail in Chapter 8 after the mobility models are described in Chapter 7.

Chapter 7

Modeling Wheeled, Legged, and Hybrid Mobility

Given the motivation to model additional forms of mobility in MSE provided in Chapter 5, and the knowledge gained working with the MoRETA rover described in Chapter 6, the implementation of these mobility models will be discussed. The implementation of four-wheeled, eight-wheeled, legged, and hybrid mobility models are described in detail. Keep in mind that these models must fit into the existing flow of information within MSE presented in Chapter 2. The actual models of wheeled, legged, and hybrid mobility exist within the *mobility.m* script, but many other changes were made in MSE to allow the user to specify the design parameters relevant to legged and hybrid mobility and to maintain the seamless flow of information between modules of code. These broader changes to MSE will also be described.

7.1 Model Descriptions

The wheeled, legged, and hybrid mobility models are part of the *mobility.m* script. The user can toggle each type of mobility on or off in the design vector. Depending on the user specified mobility type, different sections of the script are executed. There is very little overlap between the wheeled and legged mobility models. The hybrid mobility model draws from many elements of the wheeled and legged models and will be discussed last.

7.1.1 Wheeled Mobility

The user specified design variable inputs to the wheeled mobility model are the number of wheels and the wheel diameter. The number of wheels input must be only four, six, or eight. As with any other design vector input, the user may input multiple values and MSE will output unique designs for each value (for example six and eight). Any wheel diameter may be specified, but a majority of the rovers modeled by MSE have wheels between 0.13 m and ~0.50 m. The six-wheeled mobility model is described in Section 3.1 and in previous publications [Lamamy 04].

The wheeled mobility model described in Section 3.1 remains essentially unchanged for four and eight-wheeled rovers. The total wheeled mass scales with the number of wheels, so four-wheeled rovers tend to be lighter and eight-wheeled rovers tend to be heavier. Since the number of total wheels changes, the number of driving and steering wheels changes. It is assumed that a four-wheeled rover uses all four wheels to drive and all four wheels to steer. Similarly, it is assumed that an eight-wheeled rover uses all eight wheels to drive and all eight wheels to steer. The number of driving wheels affects the mobility system mass because each driving wheel requires actuation with an electric motor. The number of steering wheels affects the mobility system mass because each steering wheel requires actuation with an electric motor.

The suspension system must also be changed if four or eight wheels are used. The four and eight-wheeled suspension systems are modeled as combinations of different pieces of the six-wheeled rocker bogie suspension system. Figure 7-1 shows the four-wheeled rocker suspension, six-wheeled rocker bogie suspension, and eight-wheeled double rocker suspension [Lindemann 06]. The element numbers in Figure 7-1 indicate which and how many of the rocker bogie sections are used to model four and eight wheel suspension systems. The wheeled mobility model simply adjusts the amount of material needed to build the suspension system depending on the geometry.

Finally, the mass supportable by the rover is determined as a function of the number of wheels. The more wheels there are, the greater the surface area the weight of the rover is spread over, and the lower the ground pressure. This means that four-wheeled rover designs are more likely to be invalid due to the Martian soil being unable to support the rover. Eight-wheeled designs are more likely to be valid for a rover of

equivalent mass. The remainder of the wheeled mobility model is equivalent to the six-wheeled model.

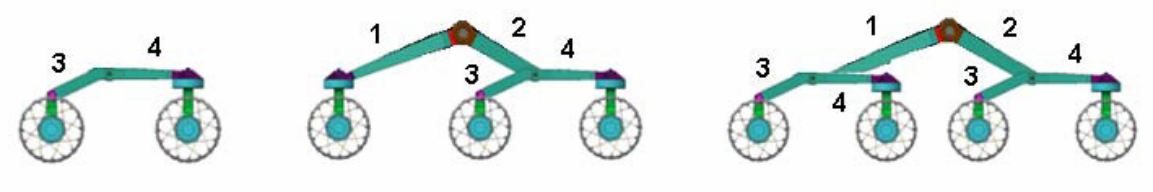

Figure 7-1: One Side of Four, Six, and Eight-Wheeled Suspension Systems with Bold Numbers Indicating Rocker Bogie Element Numbers

7.1.2 Legged Mobility

The user specified design variable inputs to the legged mobility model are the number of legs, leg length, and numbers of degrees of freedom per leg. The number of legs input should be only four, six, or eight legs. Any leg length can be specified, but it is anticipated that the user will be most interested in leg lengths on the order of tens of cm to a couple meters. The degrees of freedom per leg should be at least two and no greater than six. As described in more detail below, the power estimation for walking assumes only two degrees of freedom per leg. The degrees of freedom per leg parameter only directly influences the mass of the mobility system.

First, the dimensions of the rover are determined based on the leg length. This is done using scaling relationships derived from existing legged robots of rectangular body shape. Equations 7-1, 7-2, and 7-3 show the relationships used to determine rover size.

$$rover\_length = 1.71 \times leg\_length \quad 7\text{-}1$$

$$rover\_width = 0.38 \times rover\_length \quad 7\text{-}2$$

$$rover\_height = 1.5 \times leg\_length \quad 7\text{-}3$$

A majority of the remaining legged mobility code runs within a loop to determine the raw velocity of the rover, and is responsible for a majority of the computation time required to design a legged rover. The raw velocity is initially assigned to be zero and is iteratively increased until the capabilities of the leg motors are exceeded. For each raw velocity, the step speed and time required to step is determined. The step speed, or speed of an individual foot taking a step, is determined by Equation 7-4,

$$step\_speed = v\_raw \times n\_legs \quad 7\text{-}4$$

where v_raw is the raw velocity in m/s and n_legs is the number of legs as specified by the user in the design vector. It is assumed that only one leg is lifted and moved at a time and that one leg is always stepping. The time required to take each step can then be determined using Equation 7-5,

$$t\_step = \frac{d\_step}{step\_speed} \tag{7-5}$$

where d_step is the step length, which is assumed to be equal to the leg length. A step length of one leg length corresponds to the leg moving 60 degrees about the hip joint each step.

Leg Mass

Leg mass is estimated by calling the *leg_model.m* function from within the mobility code. The inputs to *leg_model.m* are the load on each leg, leg_length, t_step, and degrees of freedom per leg. The load on each leg is determined by

$$load = \frac{m\_suspended \times g\_mars}{1/2 \times n\_legs} \tag{7-6}$$

where m_suspended is the mass of the rover excluding the mobility system and g_mars is the acceleration of gravity on the surface of Mars. The denominator is half the number of legs because it is assumed that at least half of the rover's legs are supporting the rover's weight. The load on each leg is used to calculate the required motor torque using

$$t\_req = load \times \frac{leg\_length}{2} \tag{7-7}$$

This torque corresponds to a worst case loading condition on a leg with two sections when one joint must counteract the entire load on the leg.

Next, the gearing is designed from parametric relationships. The gear ratio at a joint is assumed to scale with the joint torque requirement, similar to the design of the ATHLETE rover. Equation 7-8 shows the scaling relationship between joint torque and gear ratio,

$$gear\_ratio = 8.4983 \times t\_req \tag{7-8}$$

Figure 7-2 shows the curve fit to ATHELE data used to derive this equation [Wilcox 06]. The quality of the curve fit is good, but the parametric relation could be improved in the

future by gathering data from a larger number of sources. The gear efficiency is determined as a function of gear ratio, also determined from a curve fit. Equation 7-9 shows the equation used to calculate gear efficiency and Figure 7-3 shows the curve fit developed after surveying a wide variety of gears by Christine Edwards [Wahab 06].

$$\eta_{gear} = \frac{92.577 - 5.8575 \times \ln(gear\_ratio)}{100} \qquad 7\text{-}9$$

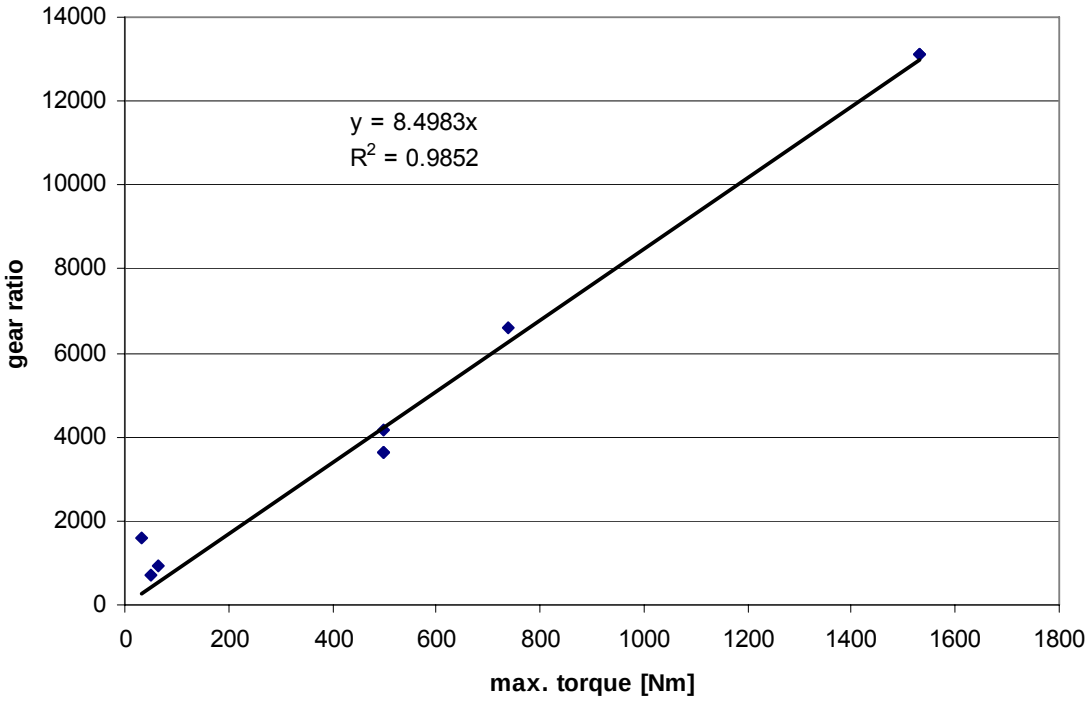

Figure 7-2: Maximum Joint Torque versus Gear Ratio for ATHLETE Joints

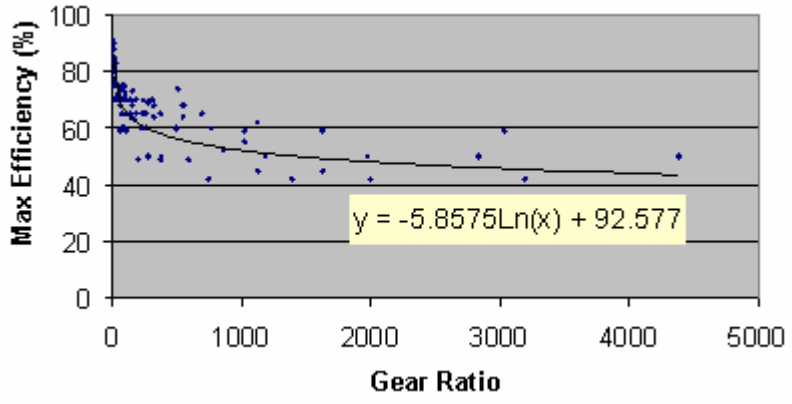

Figure 7-3: Gear Ratio versus Maximum Gear Efficiency

After the gearing is calculated, the joint and motor rotation speeds can be found. The joint rotation speed in rpm is estimated, again assuming a 60 degree rotation at the hip.

$$omega\_joint\_rpm = \frac{\pi/3}{t\_step} \times \frac{60}{2\pi} \tag{7-10}$$

Finally, the motor speed in rpm can be estimated using

$$omega\_motor\_rpm = \frac{omega\_joint\_rpm \times gear\_ratio}{\eta_{gear}} \tag{7-11}$$

and the motor load can be calculated in mNm using

$$M = \frac{t\_req \times 1000}{gear\_ratio \times \eta_{gear}} \tag{7-12}$$

The next step in designing the leg is selecting a motor to actuate the joints. It is assumed that all joints on the rover use the same gearing and motors. In reality, the joints closer to the foot tend to be smaller, so MSE's assumptions lead to a conservative over estimation of mass. Motor selection in this case means that key motor parameters describing the behavior of the motor are selected. Table 7-1 shows a list of key motor parameters. The MSE user isn't typically concerned with details such as the specific motors used, so each of these parameters is calculated from a parametric model based on the motor load, M. Equations 7-13 through 7-18 show relationships used to calculate motor parameters. Figure 7-4 through Figure 7-9 show the curve fits used to create these relationships.

Table 7-1: Motor Parameters

Parameter Name	Variable	Units
torque constant	kM	mNm/A
speed constant	kN	rpm/V
speed torque gradient	dndM	rpm/mNm
no-load current	Io	A
stall torque	MN	mNm
no-load speed	no	rpm

$$kM = 2.9583 \times M^{0.6203} \tag{7-13}$$

$$kN = 3225.2 \times M^{-0.6201} \tag{7-14}$$

$$dndM = 5623.6 \times M^{-1.5394} \tag{7-15}$$

$$Io = \frac{\left(0.1616 \times M^{2} + 51.637 \times M\right) \times 1000}{kM} \qquad 7\text{-}16$$

$$MN = 2.1977 \times M^{1.3739} \qquad 7\text{-}17$$

$$no = 1.3468 \times \left(MN \times dndM\right)^{0.9637} \qquad 7\text{-}18$$

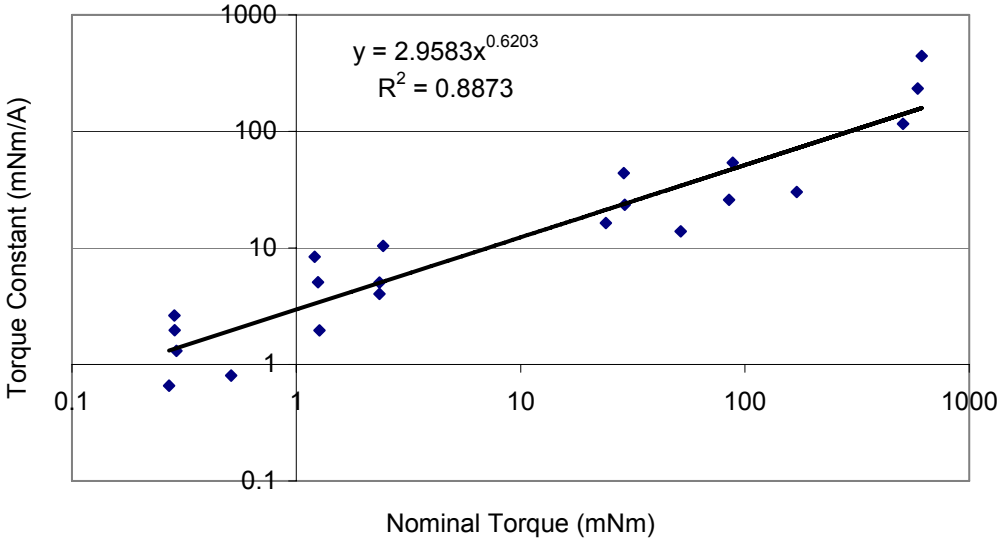

Figure 7-4: Torque Constant versus Nominal Torque for Maxon RE Series Motors

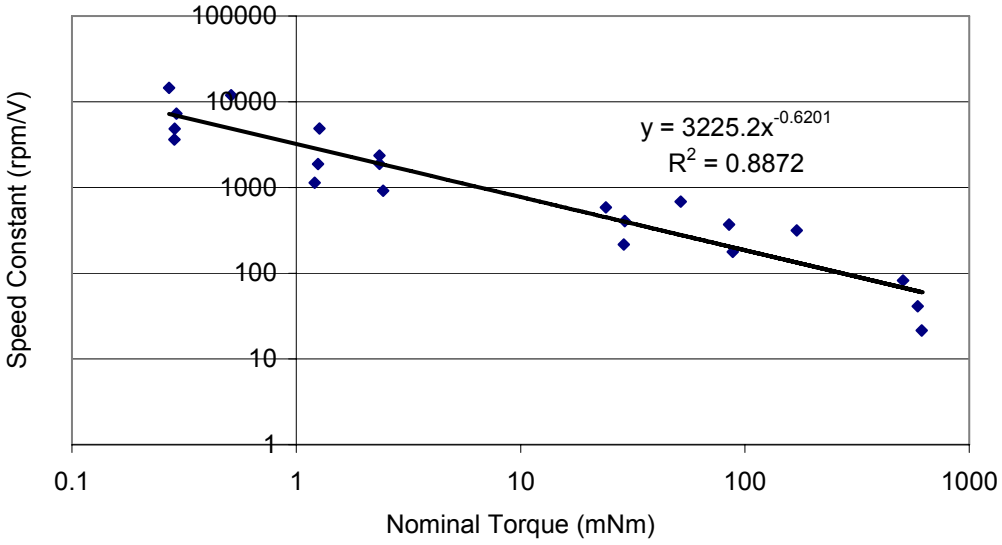

Figure 7-5: Speed Constant versus Nominal Torque for Maxon RE Series Motors

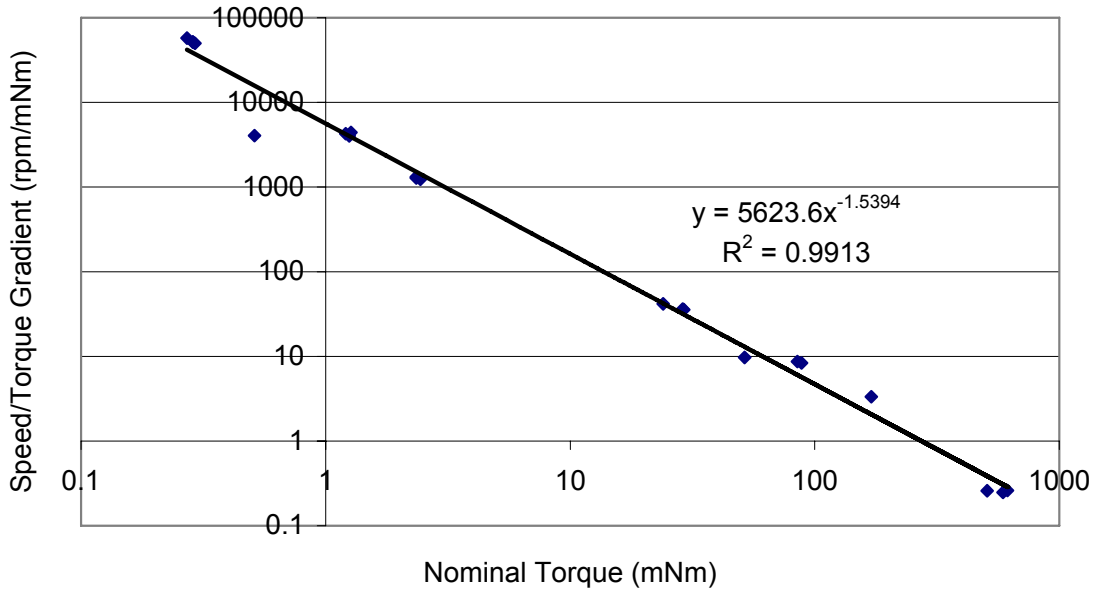

Figure 7-6: Speed Torque Gradient versus Nominal Torque for Maxon RE Series Motors

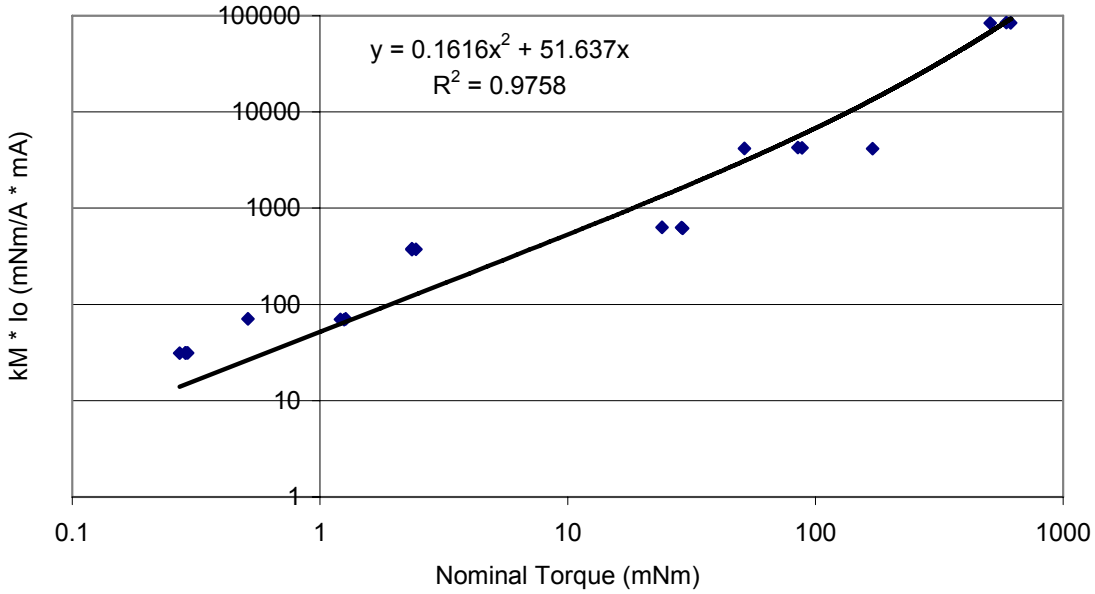

Figure 7-7: Internal Friction Torque versus Nominal Torque for Maxon RE Series Motors

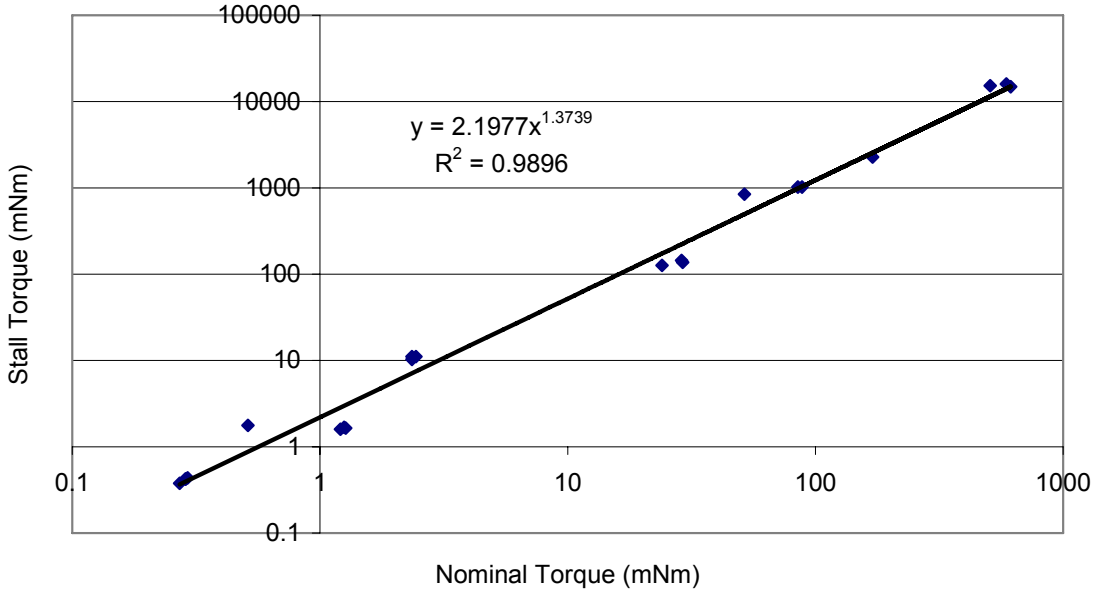

Figure 7-8: Stall Torque versus Nominal Torque for Maxon RE Series Motors

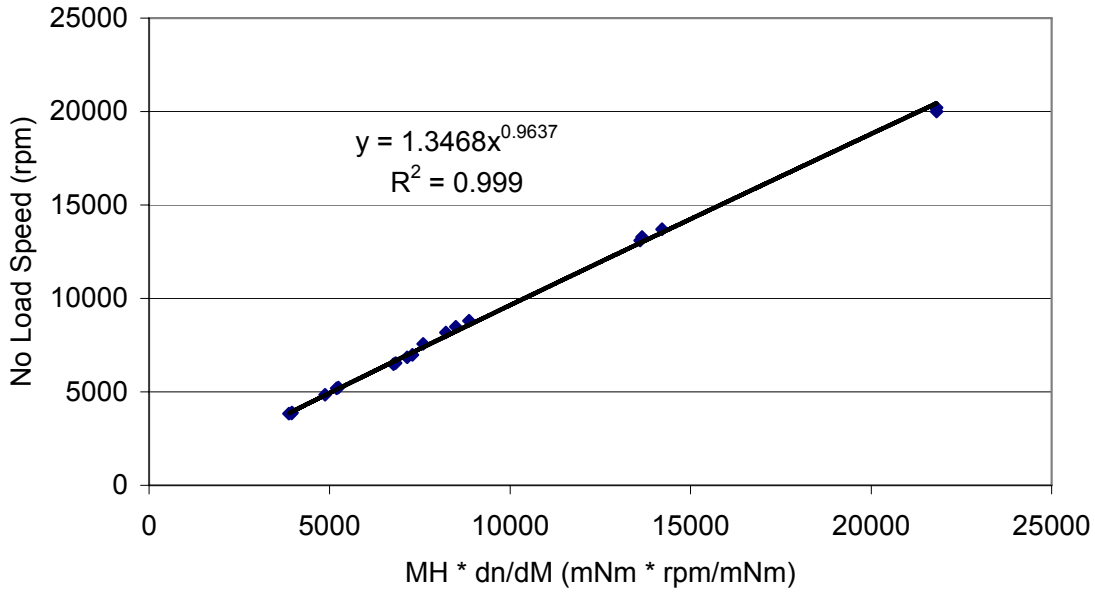

Figure 7-9: No Load Speed versus Stall Torque * Speed Torque Gradient for Maxon RE Series Motors

Once the motor parameters are determined, the power required to move the motor load, M, at the motor speed, n, calculated in Equation 7-11 can be used to estimate the

electrical power requirement. The equations used to calculate electrical power are discussed below when the methodology for power estimation is described. This power estimate is only an initial power estimate used to determine the mass of the motors needed to actuate the leg. The individual motor mass is estimated from the electrical power using Equation 3-1. The motor parameters are stored in a data structure so that the same motors can be used by the dynamic model that estimates walking power.

Motor mass is only a fraction of the total leg mass. Another significant contributor to leg mass is the material that makes up the actual mechanical structure of the leg. Each leg is assumed to be constructed of titanium beams of constant hollow square cross section. The thickness of the square tube is defined to be 0.15 times the width of the tube. The parameters that define the geometric ratios of the beam cross section can be modified in the code. Titanium was chosen for its high strength and for its flight heritage on the MER rover suspension system. Assuming that the leg has two segments, the worst case bending moment on one leg segment, approximated as a cantilevered beam, is found using

$$M_{\max} = load \times \frac{length}{2} + t\_req \tag{7-19}$$

This bending moment causes a maximum stress of

$$\sigma_{\max} = \frac{6M_{\max}h_o}{b_o h_o^3 - b_i h_i^3} \tag{7-20}$$

where b is the base of the cross section, h is the height of the cross section, and o and i subscripts denote the inner and outer dimensions of the tube, respectively. The moment and stress calculations are done iteratively to determine the minimum sized tube that can support the load. The beam starts with zero cross section and grows 0.0001 m in each dimension per iteration until

$$\sigma_{\max} \times loading\_factor \times safety\_factor \geq \sigma_{ultimate} \tag{7-21}$$

A loading factor of three is used to account for the increased strength needed to survive dynamic loads. A safety factor of five is also used. The total volume of leg material can be calculated from the cross section of the beam and the length of the leg using

$$V_{leg\_material} = \left(b_o h_o - b_i h_i\right) \times leg\_length \tag{7-22}$$

This volume of material assumes a simple mechanical design, when in fact legs would be more mechanically complex than a hollow square tube. Additional mechanical complexity would arise from the interface between the leg and the chassis and at each joint on the leg, since joints require extra material. A factor that scales with the number of degrees of freedom of the leg is used to approximate this effect (Equation 7-23) before the mass of the leg structure is calculated (Equation 7-24).

$$joint\_factor = 1.25 + 0.25 \times DOF\_per\_leg \quad 7\text{-}23$$

$$m_{leg\_material} = V_{leg\_material} \times \rho \times joint\_factor \quad 7\text{-}24$$

In addition to motor mass and structure mass, gears, encoders, cabling, and other small components contribute to the total leg mass. Rather than model the leg down to such a low level of detail, a miscellaneous mass that scales with the total mass of the leg is included.

$$m_{misc} = 0.25 \times \left(m_{leg\_material} + m_{motor} \times DOF\_per\_leg \right) \quad 7\text{-}25$$

The total leg mass can then be calculated.

$$m_{leg} = m_{leg\_material} + m_{motor} \times DOF\_per\_leg + m_{misc} \quad 7\text{-}26$$

The find the total mass of the mobility system, the mass of one leg must be multiplied by the number of legs.

Walking Power

Once the mass of the leg is determined, the power required to walk for each raw velocity can be calculated. This code is still within the loop of iteratively increasing raw velocity until motor capabilities are exceeded. Power estimation is done using a dynamic walking rover model originally developed as a 16.851 course project by Adam Wahab and Christine Edwards; their final report can be found in the appendix [Wahab 06]. Inputs to the power model are collected in the *powerinputs* data structure. Inputs include the motor and gear parameters calculated within the *leg_model.m* function, number of legs, acceleration due to gravity, rover dimensions, raw velocity, leg length, body mass, leg segment mass, and foot mass. For the power model, it is assumed that the leg has only two segments, and that they are of equal length and mass. The mass of the foot is

assumed to be zero for legged mobility, but is non-zero for hybrid rovers to account for the wheel mass on the end of the leg.

These inputs are passed to the *leg_dynamic_power_model.m* function in MATLAB. The *leg_dynamic_power_model.m* calls several other functions that must be present for the model to work properly: *legMech.m*, *motRMS.m*, *motTorque.m*, *motStats.m*, and *maxLstep.m*. The model calculates the trajectories of the feet and hips for a walking gate, and then solves the inverse kinematics problem to determine the states of each joint at each time step. The forces and torques on each joint are also computed for each time step. These outputs can be used to determine the mechanical power at each joint. A more detailed description of the model can be found in a paper written by Adam Wahab and Christine Edwards in the Appendix.

The outputs of the mechanical aspect of the model are passed to an electrical motor model, since electrical power, not mechanical power, is needed to determine the power required to walk. The power required to actuate each joint at each time step is calculated in *motTorque.m*. To find the electrical power required, first the load on the motor in mNm is determined.

$$M = \frac{torque \times 1000}{gear\_ratio \times \eta_{gear}} + kM \times Io \qquad 7\text{-}27$$

where torque is the output from the mechanical model and the product of kM and Io represents the internal friction torque from the motor. The speed of the motor in rpm is also calculated from the mechanical model outputs.

$$n = gear\_ratio \times |psid| \times \frac{60}{2\pi} \qquad 7\text{-}28$$

where psid is in radians per second. From the motor load and motor speed, the current draw in amps can be calculated using the motor torque constant.

$$I = \frac{M}{kM} \qquad 7\text{-}29$$

Next, the equivalent no load motor speed is calculated from the actual motor speed and load. This concept is illustrated in Figure 7-10 and described by equation 7-30.

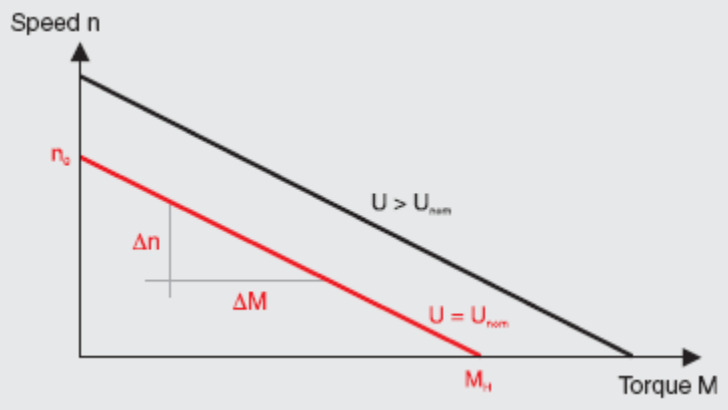

Figure 7-10: Two Contours of Constant Voltage on a Motor Speed versus Torque Plot [Maxon 07]

$$n_o = n + \frac{\Delta n}{\Delta M} M \qquad 7\text{-}30$$

The equivalent no load speed is then used to calculate the voltage at which the motor is operating.

$$U = \frac{n_o}{kN} \qquad 7\text{-}31$$

The product of current and voltage gives the power required in Watts for the given time step and motor.

$$P_e = U \times I \qquad 7\text{-}32$$

The energy consumption in Joules is calculated from the electrical power and time step.

$$E = P_e \times \Delta t \qquad 7\text{-}33$$

These calculations are done for all motors at each time step over a total period equal to the time it takes the rover to complete one full gait. The electrical and mechanical power over time can be plotted by uncommenting code at the end of the *leg_dynamic_power_model.m* script. These plots are useful when developing, debugging, and benchmarking the model, but provide more than the required level of detail when the model is run within MSE. The electrical power over the gait is averaged and outputted to MSE to determine the walking power.

Motor Efficiency

Motor inefficiencies are already accounted for when calculating electrical power from Equations 7-27 through 7-32, but it is interesting to examine motor efficiency explicitly. Instantaneous motor efficiency is the useful mechanical power divided by the electrical power required to run the motor. Mechanical power used to overcome internal motor friction is subtracted from the total mechanical power in the numerator of Equation 7-34.

$$\eta_{motor} = \frac{\frac{\pi}{30000}(M - kM \times Io) \times n}{U \times I} \qquad 7\text{-}34$$

To check these equations and illustrate the relationship between efficiency and motor operating conditions, efficiencies were calculated for a range of motor loads and speeds for motors on an approximately MER-sized walking rover. The blue efficiency curve shown in Figure 7-11 indicates that for a fixed voltage, maximum efficiency occurs at a small fraction of the motor's stall torque.

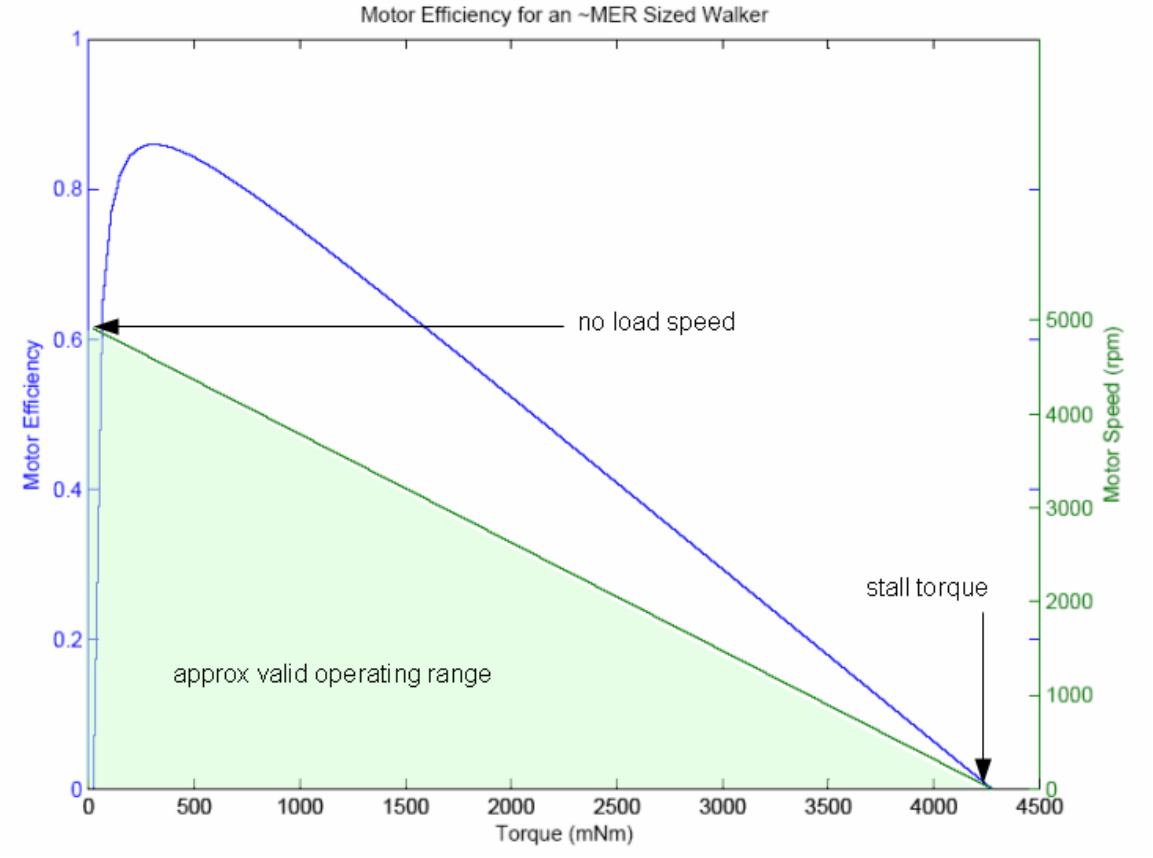

Figure 7-11: Motor Efficiency for a Range of Motor Torques and Speeds

Raw Velocity

The code described in the preceding sections used to calculate the mass and power of legged mobility requires that the raw velocity be specified as an input. Rather than burden the MSE user with specifying a speed, the model determines the speed at which the rover can walk. The legged mobility model begins by assuming that the raw velocity is zero m/s and that the design is valid. The raw velocity is iteratively increased by a step size adjustable within the mobility code. Figure 7-12 shows the raw velocity increasing by increments of 0.001 m/s, but to reduce computation time the step size is increased to 0.005 m/s in the actual mobility code.

For each velocity, the motor load and motor speed calculated in Equation 7-27 and Equation 7-28 are used to determine if the motors are capable of moving the rover at the currently iterated speed. The capabilities of the motor are defined by the no load speed and the stall torque, represented by the green shaded in region of Figure 7-11. The validity check occurs within the *motTorque.m* script. If the inequality in Equation 7-35 is false, then a validity flag is defined to be invalid and the velocity iteration ceases.

$$no - \frac{no}{MN} \times M < n \qquad 7\text{-}35$$

As raw velocity increases, the average motor efficiency increases (see Figure 7-12). This may seem counterintuitive, but is correct because as the raw velocity increases, the motors on average run and higher speeds. Figure 7-13 shows the increase in no load speed calculated by Equation 7-30 as raw velocity is increased. For the example show here, the maximum no load speed is about 4900 rpm, thus on average the no load speed is up to only 20% the maximum value. Figure 7-14 reveals the penalty of operating the motor at no load speeds significantly below their capability. This inefficiency is unavoidable in the model, because even when the average no load speed is very low, the instantaneous no load speed can exceed the motor capabilities at some point during the gait.

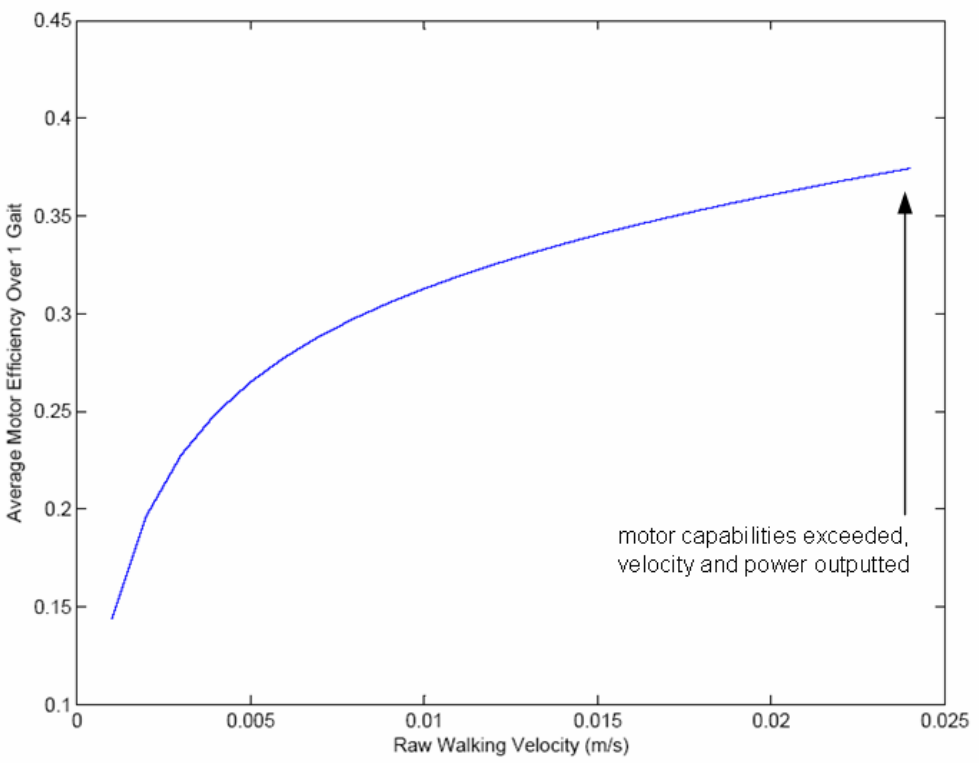

Figure 7-12: Average Motor Efficiency versus Raw Velocity for a MER-Sized Walker

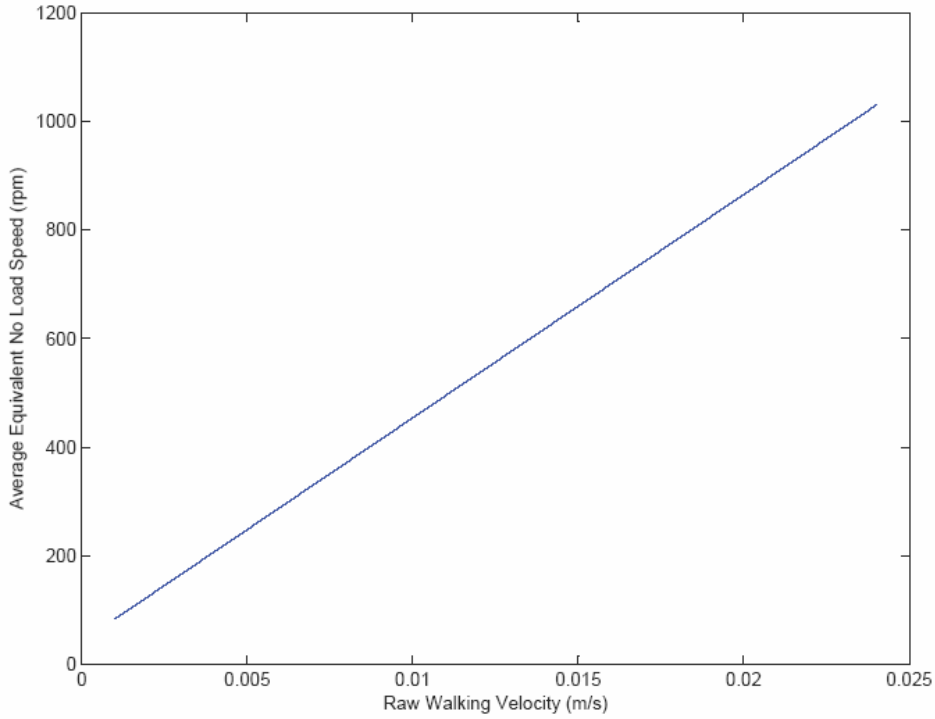

Figure 7-13: Average No Load Speed (Equation 7-30) versus Raw Velocity for a MER-Sized Walker

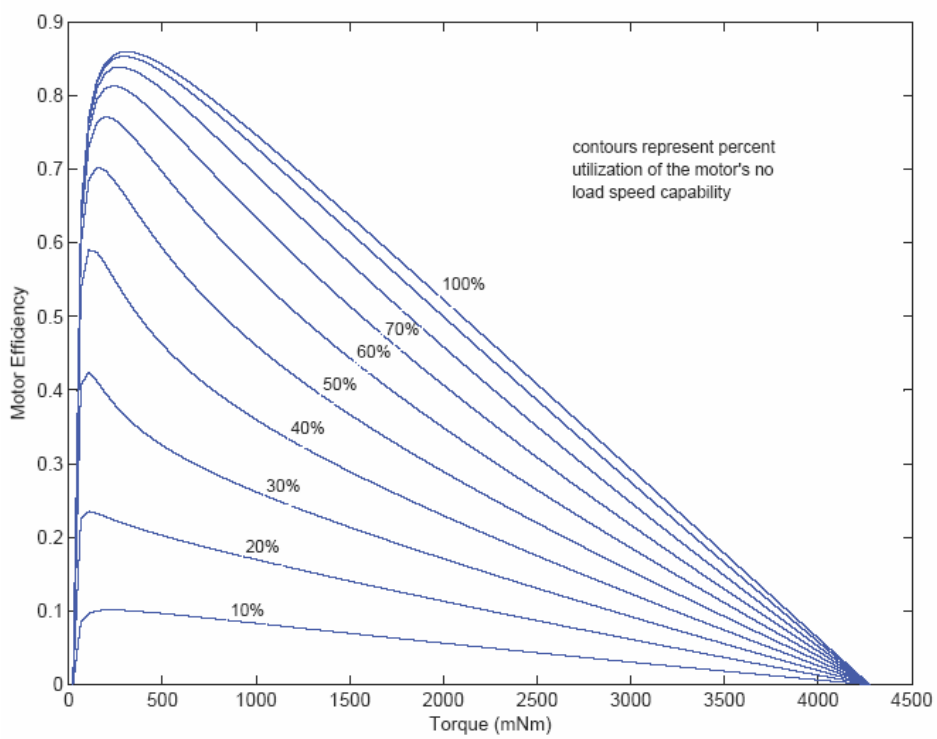

Figure 7-14: Motor Efficiency versus Torque across Different No Load Speeds for a MER-Sized Walker

Once the raw velocity iterations are completed, the *mobility.m* script outputs the size, mass, power, raw velocity, and other parameters to the mobility data structure.

7.1.3 Hybrid Mobility

The user specified design variable inputs to the hybrid mobility model are all the wheeled mobility model inputs and all of the legged mobility model inputs. Essentially the entire wheeled model and entire legged model are run when designing a hybrid rover, with the exception of the wheeled mobility suspension and differential code. When sizing the rover, legged scaling relationships are used rather than wheel scaling relationships. The sizing relationships for a wheeled rover assume a rocker bogie suspension system and are therefore not appropriate for a hybrid rover with wheels on the end of legs. Figure 7-15 shows the elements of the wheeled and legged mobility models used to create the hybrid mobility model.

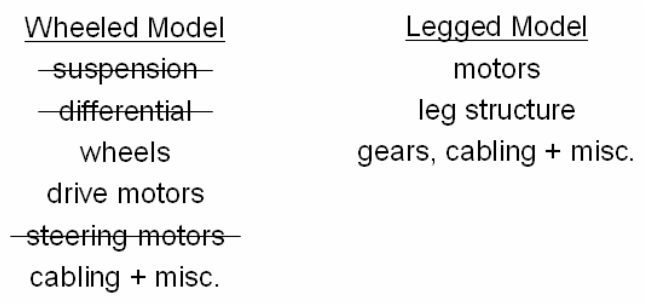

Figure 7-15: Wheeled and Legged Model Components used to Model Hybrid Mobility

As with the wheeled and legged mobility models, the outputs of the hybrid mobility model are stored in the mobility data structure.

7.2 Integration into MSE

Expanding the mobility modeling capabilities of MSE primarily involved changing the *mobility.m* script, but additional changes had to be made to accommodate the modifications. These changes were necessary to allow the user to specify new design vector inputs and to work around the assumption of wheeled mobility inherent throughout MSE. The following scripts were modified: *rover_init.m*, *environment.m*, *arm_jal.m*, *mast.m*, *structure.m*, *master.m*, *utility.m*, and *design_gui.m*. Each of these changes will be described briefly.

The design vector graphical user interface had to be modified to allow legged and hybrid mobility parameters to be specified. The new design vector graphical user interface is shown in Figure 7-16. It is shorter and wider than the old version to create room for the new inputs without causing the window to be too tall to fit on the screen. Three check boxes were added to allow the user to specify which of the three forms of mobility are to be modeled. Below each type of mobility's check box there are input fields for the user specified input parameters. Hybrid mobility does not have its own set of unique input parameters, because it uses the inputs to both the wheeled and legged mobility models.

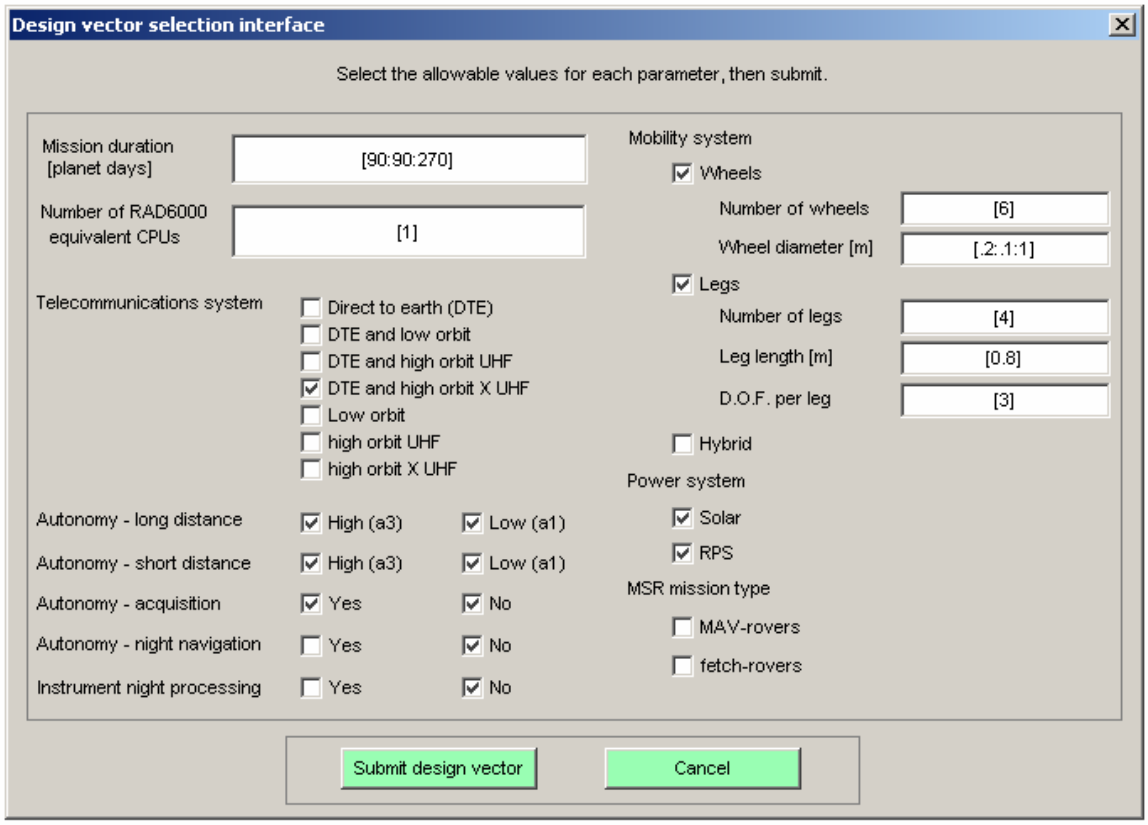

Figure 7-16: Updated Design Vector Graphical User Interface

Adding design variables changes the way that the full factorial search over all possible combinations of inputs must be done in the *master.m* script. For loops are used to vary each parameter over its range, and then the code for each of the various rover subsystems is run within all of the for loops. The inner section of this code that is run within all of the for loops was removed and saved as the *subsystems.m* script. This makes no difference when the code is executed, but makes the *master.m* script much cleaner. A different set of for loops had to be created for each of the three mobility types, because each has different design vector inputs. Within each set of for loops the *subsystems.m* script is called.

Most of the scripts changed are subsystem functions called by the *subsystems.m* script. The *rover_init.m* script creates an initial estimate of rover size and raw velocity. For legged and hybrid mobility, rover size is determined the same way that it is determined in the mobility code. Since raw velocity is unknown for legged rovers when *rover_init.m* is executed, the wheeled raw velocity rule is used for equivalently sized

wheels. This is done by assuming that the leg is equivalent to a wheel 0.25/0.80 in size, the wheel diameter to leg length relationship observed on MoRETA.

The *environment.m* script calculates the clearance of the rover. As with the wheeled mobility model, the legged and hybrid mobility models have a clearance that is some fraction of the leg length. The clearance is defined to be 0.675 times the leg length, which is equivalent to LittleDog's clearance to leg length ratio. The *subsystems.m* script had to be modified to base the initial guess for solar array area on leg length rather than wheel diameter. The *arm_jal.m* and *mast.m* scripts were changed so that the arm and mast scale with leg length instead of wheel diameter for legged and hybrid rovers. The *structure.m* script was changed so that the dimensions, aspect ratio, and surface area of the warm electronics box scale with leg length. Finally, the *utility.m* script had to be changed due to the addition of new design variables.

7.3 Summary

The additional forms of mobility added to the MSE tool are four-wheeled, eight-wheeled, legged, and hybrid mobility. The models for each of these types of mobility were described in detail. Finally, the challenges of integrating these models into MSE and the necessary adaptations to code were summarized.

Chapter 8

Mobility Model Benchmarking and Trade Studies

The wheeled, legged, and hybrid mobility models developed and integrated into MSE will be useful for developing and evaluating mission concepts for the next generation of robotic Mars explorers. To begin to examine the utility of the functionality added to MSE, benchmarking of mobility model outputs against independent models and existing rovers is done. Initial model outputs are also examined to compare the benefits of different forms of mobility.

8.1 Benchmarking

Two types of benchmarking are done with the new mobility models incorporated into MSE. First, the outputs of selected sections of code are benchmarked. For example, the outputs of the dynamic walking model used to estimate power consumption can be compared to MoRETA data. Second, the final outputs of the mobility code can be compared to existing rover systems. The second form of benchmarking is particularly useful for checking the accuracy of the mass estimation.

8.1.1 Dynamic Walking Model

The dynamic walking model is described in Section 7.1.2 and in the Appendix [Wahab 06]. This model is a very versatile tool that can output anything from video of the simulated walking rover to plots of joint positions over time. The torque on each joint can be compared to the MoRETA model's estimates of torque shown in Figures 6-5

through 6-7. Given inputs representative of the MoRETA rover (Table 8-1), the hip torque for one walking gait can be plotted, as seen in Figure 8-1. There are two lines on the plot because some legs are supporting the weight of the rover for the first half of the gait, then stepping during the second half of the gait and visa versa. Figure 8-1 can be compared to Figure 6-5 and Figure 6-6 to judge the similarity of predictions made by the MSE model and the MoRETA model. For this particular comparison, Earth gravity was used in MSE instead of Mars gravity. It is reassuring that the torque predicted by both models is similar. MSE predicts hip torques between 22 Nm and 55 Nm, while MoRETA predicts hip torques between 2 Nm and 46 Nm. The variation of torque over time and the exact torque values do not match, because MoRETA and MSE assume different types of walking motion. MoRETA also assumes two degrees of freedom at the hip, while the MSE model assumes only one degree of freedom at the hip.

Table 8-1: MSE Inputs used to Simulate the MoRETA Rover

Input	MoRETA Value
m_suspended	50 kg
leg_length	0.80 m
n_legs	4
DOF	3

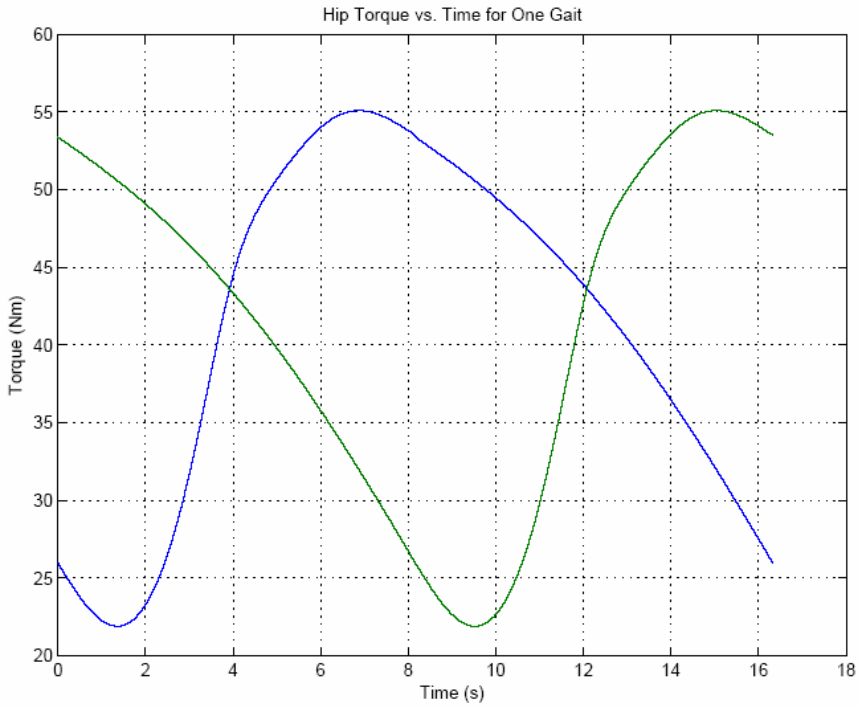

Figure 8-1: Hip Torque versus Time for a Simulated MoRETA Rover in MSE

Figure 8-2 shows the knee joint torque over time as predicted by the MSE model. The MSE output can be compared to the knee torque output predicted by MoRETA shown in Figure 6-7. Again, the torque predictions are of the same order of magnitude. MSE predicts knee torques between 25 Nm and 33 Nm, while MoRETA predicts knee torques between 7 Nm and 50 Nm. As with the hip joint, the variation of torque over time and the exact torque values don't match, because MoRETA and MSE assume different types of walking motion.

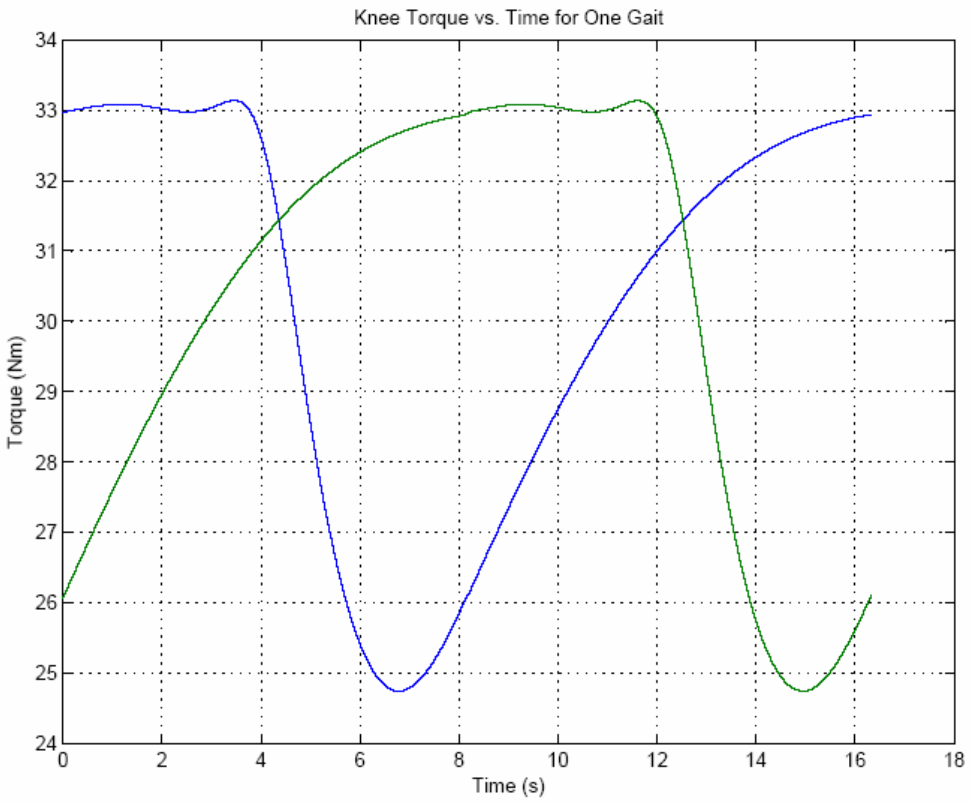

Figure 8-2: Knee Torque versus Time for a Simulated MoRETA Rover in MSE

These comparisons of joint torque provide confidence that the MSE mobility model's predictions are reasonable. In the future, it would be interesting to compare both MoRETA and MSE model predictions to actual data logged from the MoRETA hardware while walking.

The dynamic walking model can also output power and efficiency over the period of one gait. Figure 8-3 shows the modeled electrical and mechanical power over time for a MoRETA rover simulated by MSE. Unfortunately, as of this writing MoRETA has not

been able to complete a full walking gait, so comparable data is unavailable. The closest MoRETA data available for comparison is power data recorded during leg testing described in Section 6.2.2. During testing, a power draw of 880 W was recorded while the MoRETA rover was making small adjustments to leg position under its full weight. This measured power is far higher than the 15 to 60 W predicted by the MSE model. This discrepancy should not cause alarm, because the conditions that caused 880 W of power draw are very different than MSE's simulated walking motion. During the MoRETA test, the legs were in a position near the worst case loading with the knee at a right angle and the thigh horizontal. The motors during the MoRETA load test were essentially stalled and providing very little motion. Once more MoRETA testing occurs, it will be more relevant to compare power draw during a walking motion, rather than the limited load testing completed. It is also worth noting again that MoRETA uses DeWalt power drill motors that tend to have higher power consumption than the Maxon motors used to develop the MSE model.

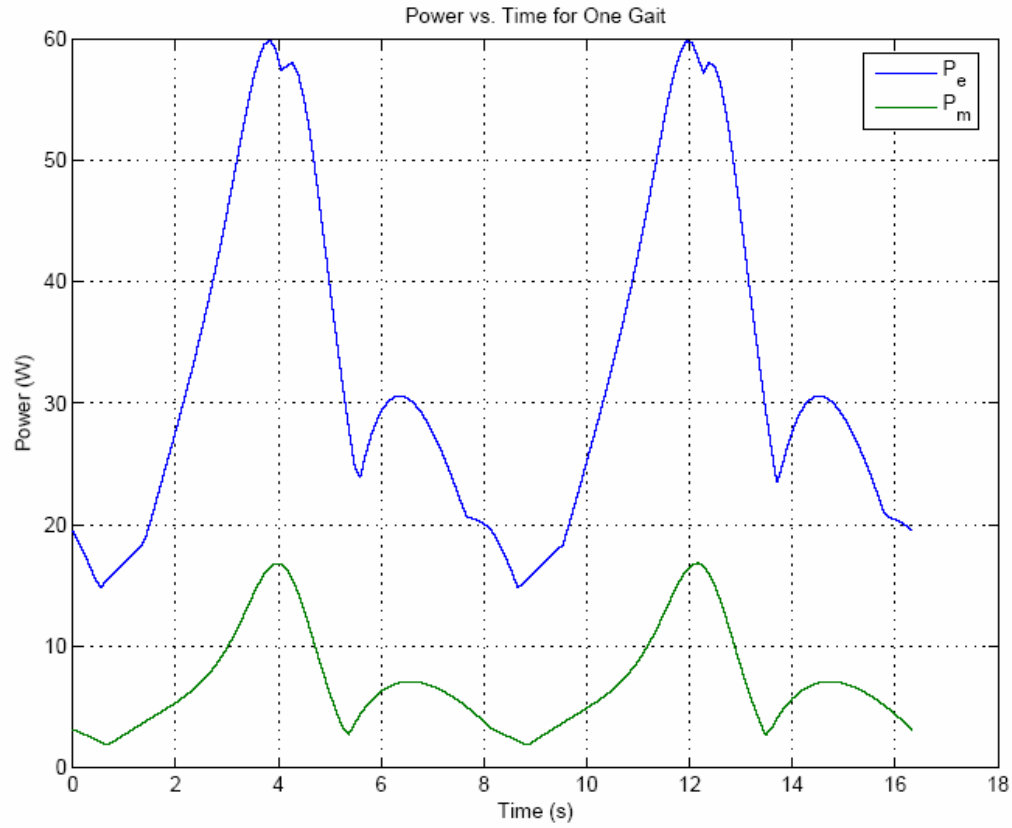

Figure 8-3: Electrical and Mechanical Power over Time Simulated by MSE

Even though there is no testing data available from MoRETA that shows efficiency over a walking gait, the simulated efficiency is shown in Figure 8-4 in case the testing data becomes available in the future. There are two lines for each of the hip and knee motor efficiency, because some legs support the weight of the rover for the first half of the gait and step during the second half and visa versa. The red line, which varies between 12% and 29% efficiency includes all of the motor and gear inefficiencies, and is calculated by dividing the mechanical power by the electrical power at each time step. In other words, it is the lower green line divided by the upper blue line in Figure 8-3.

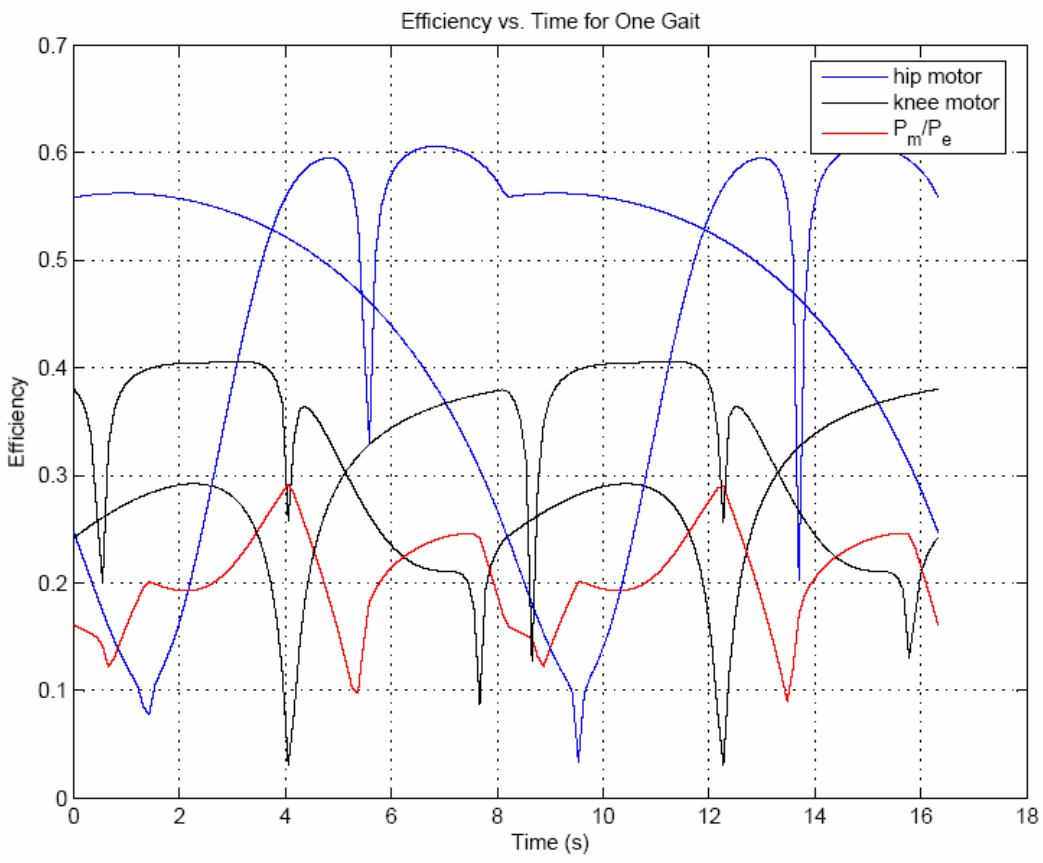

Figure 8-4: Efficiency versus Time for a Simulated MoRETA Rover in MSE

The comparisons presented show that the walking model in MSE is reasonable. If more testing data becomes available in the future as MoRETA begins to walk, a closer comparison should be made between the simulated and test outputs. Performing this type of benchmarking reveals the true benefit of using a hardware testbed to develop a

software model. Without a testbed locally available, such detailed data from a walking rover would be very difficult to obtain.

8.1.2 Mobility Model

Benchmarking the outputs of the dynamic walking model is valuable, but it is also very important to compare the final outputs of the MSE mobility model to existing robotic systems. This type of benchmarking allows the accuracy of the size, mass, power, and raw speed models to be checked. Three rovers were selected for benchmarking based on the availability of data and specifications describing each rover. Rovers that did not share some of the same underlying assumptions as MSE were not considered. For example, rovers with articulated bodies, dynamic walking capability, and other significantly different forms were not considered. The LittleDog, MoRETA, and ATHLETE rovers are simulated in MSE and the outputs are compared to the available data on these existing systems. Descriptions of these three rovers can be found in Chapter 5. Table 8-2 shows the inputs used to simulate each of the three rovers and compares the expected outputs to the simulated outputs. Earth gravity is assumed in the MSE model, since the vehicles used for benchmarking operate on Earth.

Table 8-2: Comparison of MSE Model Output to LittleDog, MoRETA, and ATHLETE

		LittleDog		MoRETA		ATHLETE	
Inputs	Suspended mass [kg]	2.24		50		248	
	Leg length [m]	0.178		0.8		1.786	
	# legs	4		4		6	
	D.O.F.	3		3		6	
		Actual	**MSE**	**Actual**	**MSE**	**Actual**	**MSE**
Outputs	Body length [m]	0.30	0.30	1.04	1.37	-	3.05
	Body width [m]	0.12	0.12	0.53	0.52	-	1.16
	Mass of motors [kg]	?	2.24	5.1	7.2	?	43
	Mass of structure [kg]	?	0.13	13.4	12.7	?	221
	Mass other [kg]	?	0.77	4.5	4.96	?	66.0
	Total legged mobility mass [kg]	0.76	3.84	23	24.8	399	330
	Average walking power [W]	<60	349.02	?	32.5	?	115
	Raw velocity [m/s]	?	0.8	?	0.049	?	0.014

The MSE output does relatively well at predicting the MoRETA and ATHLETE designs, but does not predict the LittleDog design well. A detailed breakdown of the leg

mass was unavailable for the LittleDog rover, but the modeled total leg mass is about five times the actual leg mass. The walking power is also significantly greater than the actual required walking power. Examining the mass breakdown of MSE's model of the LittleDog leg reveals that the excess mass is due to the motors being too large. This is consistent with the very high raw velocity of 0.8 m/s, which causes the walking power to be very high. Note that this disparity does not necessarily mean that the legged model is wrong, but rather that if LittleDog could walk at 0.8 m/s, it would have to be five times its actual mass and require over 5 times the power to walk. The solution to this problem would be to place an upper bound on the walking speed of smaller robots. This would prevent the code from increasing the motor size and causing the rover to walk very fast when the designer does not desire such speed. Typical rovers studied with the MSE tool have masses of at least 180 kg (approximately MER-sized), so this issue would not arise during typical use of the tool. However, the MSE user should exercise caution if the tool is used to design very small robots.

MoRETA is the rover with the most actual data available since it is physically located at MIT. MoRETA is also the rover that shows the best correlation between actual and modeled mass. The modeled mobility mass is off by less than 2 kg. The motor mass and miscellaneous mass are slightly too heavy and the leg structure mass is slightly too light. The estimates for walking power and walking speed appear to be reasonable, but there is no testing data that can be directly compared to these estimates.

ATHLETE has relatively little data available describing its design. Only the geometry, leg mass, and body mass were provided by Brian Wilcox of JPL [Heverly 06]. The size of ATHLETE cannot be directly compared to the MSE model output because ATHLETE is hexagonal, rather than rectangular. The total mobility mass is about 70 kg lighter than the actual ATHLETE mobility mass. Without more specific ATHLETE design information, it is difficult to determine which aspect of the model is causing this discrepancy. Since the MoRETA leg structure mass is underestimated, it is probable that the leg structure mass for ATHLETE is also underestimated. As was the case for MoRETA, the estimates for walking power and walking speed appear to be reasonable, but there is no testing data that can be directly compared to these estimates.

Benchmarking the MSE mobility model against three existing rovers has shown that mass estimation is within 20% of actual values except for small robots, such as LittleDog. As the MSE hybrid mobility models are used, continuing effort should be put into gathering additional data to validate the models. The ability to continually benchmark and adapt the MSE tool to rover design practices is one of its strengths.

8.2 Comparison of Mobility Systems on Extreme Terrain

The addition of legged and hybrid mobility to MSE was partially motivated by the assumption that legged rovers are more efficient on extreme terrain and wheeled rovers are more efficient on smooth, flat terrain. It is also assumed that legged rovers can walk up stepper terrain than wheeled rovers. The mobility modeling capabilities of the MSE tool will be applied to test these assumptions. Two types of extreme terrain will be considered: rocky terrain and steep terrain.

8.2.1 Rocky Terrain

The MSE tool already has the ability to model flat terrain of varying rock density [Lamamy 04]. The modeling capabilities of MSE are used to quantitatively examine the performance of wheeled and legged locomotion as a function of rock density. The user is able to specify a percentage rock density in the science vector graphical user interface. Based on the clearance of the rover and the rock density, the mean free path of the rover is determined. The traverse model assumes that each time the rover encounters a rock that it cannot drive or walk over, the rover must drive or walk around the obstacle. This extra driving distance around each obstacle causes the actual odometry of the rover to be greater than the straight line distance covered during the traverse. Vehicles with greater clearance tend to have odometry closer to the straight line distance, and vehicles with low clearance have higher odometry to cover an equivalent straight line distance. Legged rovers tend to have higher clearances than wheeled rovers, and therefore can cover more straight line distance per sol on rocky terrain.

To make these comparisons in MSE, MSL-like rovers were simulated with varying wheel diameters and leg lengths. Only six-wheeled and six-legged rovers were considered for this comparison. Figure 8-5 shows the straight line traverse capability per

sol for rovers of different mass and terrains of different rock density. When the rock density is 0%, the straight line path is equal to the odometry because there are no obstacles to avoid. As rock density increases, the odometry per sol remains the same, but the straight line distance traversed decreases. This is because for higher rock densities, more odometry is used to navigate around obstacles instead of move directly toward the next site. The red and black contours in Figure 8-5 represent legged and wheeled rovers, respectively, and rock densities between 0% and 20% in increments of 5%. Note that the wheeled rover contours have more spread than the legged rover contours, indicating that variation in rock density has a greater affect on the performance of wheeled rovers than legged rovers.

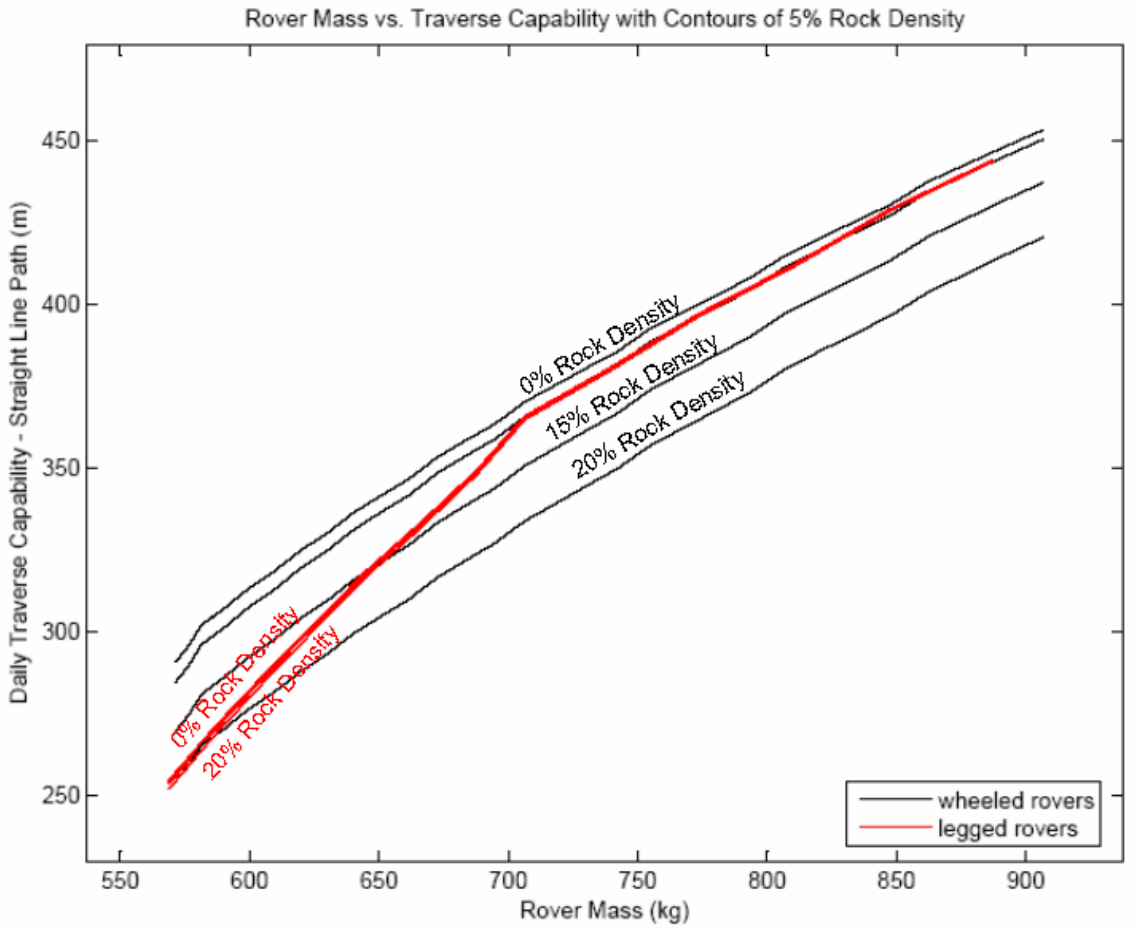

Figure 8-5: Rover Mass versus Traverse Capability for Rock Densities between 0% and 20%

Figure 8-5 can be used to determine the benefit of using wheeled versus legged mobility by examining contours of equivalent rock density. For example, the 0% rock density contour for wheels is always above the 0% rock density contour for legs; indicating that wheeled rovers are always able to traverse further than legged rovers on flat and level terrain. Examining the 20% rock density contours reveals that a legged rover is almost always able to traverse further than a wheeled rover, since the legged rover has a greater clearance and has to navigate around fewer rocks. The conditions at which legs become better than wheels depends on both rover mass and rock density, but generally speaking legged rovers are superior on rockier terrains, especially for longer legs (hence heavier rovers).

Another way to compare wheeled and legged mobility is using the specific resistance metric. Specific resistance is unitless and defined as

$$SR = \frac{P_{total}}{m_{total} g_{mars} v_{equivalent}} \tag{8-1}$$

where P_{total} is the total average power output of the rover's power subsystem, m_{total} is the mass of the rover, g_{mars} is the acceleration due to gravity on the surface of Mars, and $v_{equivalent}$ is

$$v_{equivalent} = \frac{straight\ line\ distance}{t_{traverse}} \tag{8-2}$$

Equation 8-2 represents the equivalent speed of the rover over the straight line path. The specific resistance is a measure of power required per useful movement of rover weight. Specific resistance is also a measure of the energy required to move the weight of the rover some distance. Moving the rover with a minimal amount of energy is desirable, so lower specific resistance is better.

Figure 8-6 shows the specific resistance as defined in Equation 8-1 for rovers of different mass and terrains of different rock density. The red and black contours in Figure 8-6 represent legged and wheeled rovers, respectively, and rock densities between 0% and 20% in increments of 5%. Note that the wheeled rover contours have more spread than the legged rover contours, indicating that variation in rock density has a greater affect on the performance of wheeled rovers than legged rovers. The 0% rock density contour for wheels is always above the 0% rock density contour for legs,

indicating that wheeled rovers have lower specific resistance than legged rovers on flat and level terrain. This is consistent with the conclusion that wheeled rovers can traverse farther on non rocky terrain, because they are more efficient. Also consistent with the results using the daily traverse metric, legs have lower specific resistance than wheels in most cases when the rock density is 20%. The conditions at which legs become better than wheels depends on both rover mass and rock density, but generally speaking legged rovers are superior on rockier terrains, especially for longer legs (hence heavier rovers).

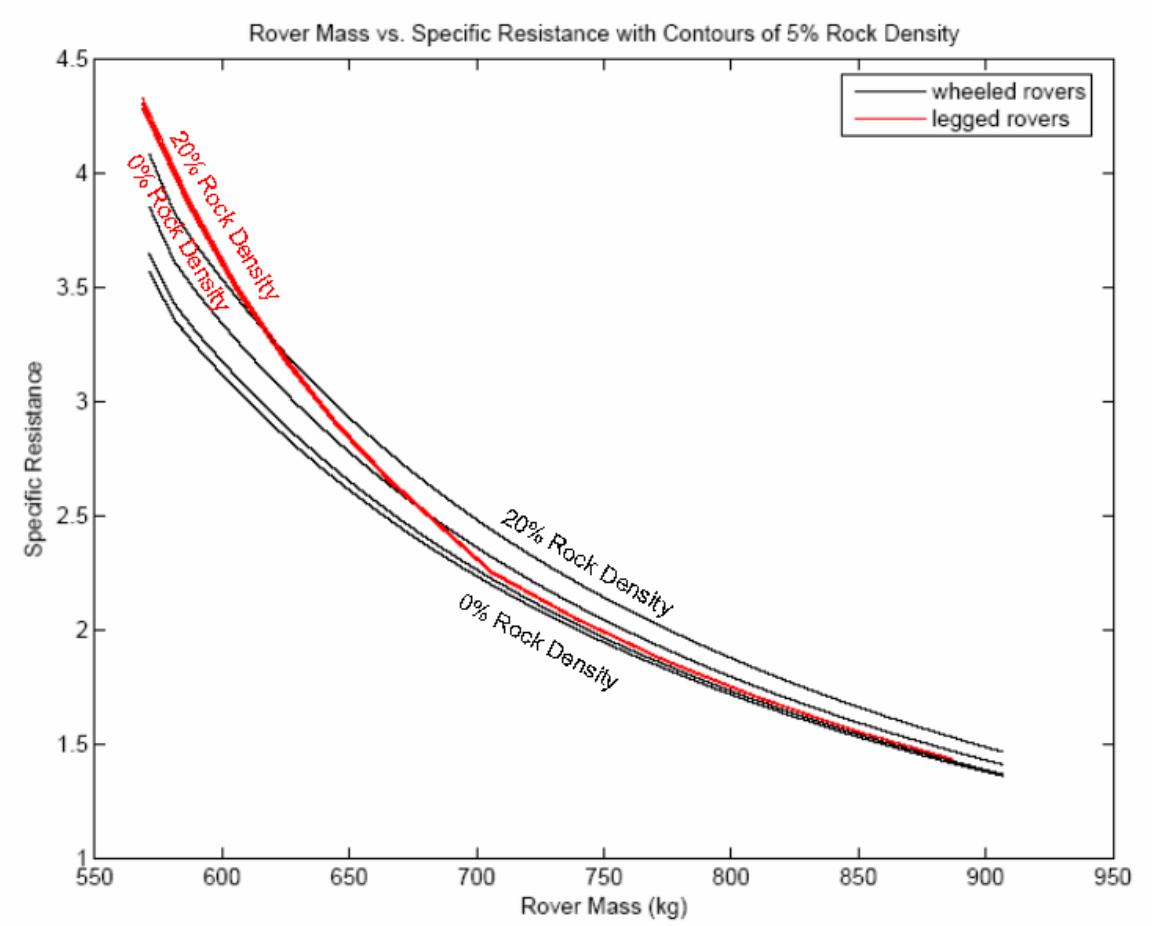

Figure 8-6: Rover Mass versus Specific Resistance for Rock Densities between 0% and 20%

8.2.2 Steep Terrain

The framework for comparing rovers on rocky terrain was already present in MSE, but slopes have not been considered in MSE prior to this study. Rather than reworking the MSE tool to model sloped terrain, the maximum accessible slope is calculated after the

rover is designed by MSE. The downside of this approach is that the energy required to traverse on sloped terrain instead of flat terrain is not modeled. This is not a significant drawback for missions on terrain similar to the Opportunity rover, where a vast majority of the driving is on flat terrain. The ability to walk up slopes is only relevant for short distances near science sites, thus treating the maximum incline as a rover operational parameter is appropriate. For missions on terrain with consistent slope, it would be more accurate to fully integrate slope modeling into MSE in the future.

Several assumptions are made when determining the maximum slope a legged rover can traverse. It is assumed that the feet have sufficient friction with the surface to not slip significantly. Therefore, it is assumed that the maximum traversable slope is determined by the geometry of the rover and when it would tip over. Tipping occurs when the projection of the center of gravity of the rover is outside the area enclosed by the supporting feet. In practice, some margin is kept on this static stability constraint. The geometry is approximated as shown in Figure 8-7. The dashed line represents the centerline of the rover. If the rover is walking straight up a slope, to the right, then the projection of the center of gravity will be back toward the rear legs, as shown in Figure 8-7. For this study, the stability margin is the fraction of the dashed line that the center of gravity is not allowed to fall on during operations. For example, a stability margin of 0.5 means that the projection of the center of gravity is only allowed to fall along half of the dashed line. Figure 8-8 shows the maximum traversable slope as a function of stability margin. The stability margin used on a rover would likely depend on the amount of risk rover operators are willing to tolerate, but even with a stability margin of 0.5, a legged rover is able to climb a 60 degree slope. This performance would double the slope climbing capabilities of the MER rovers.

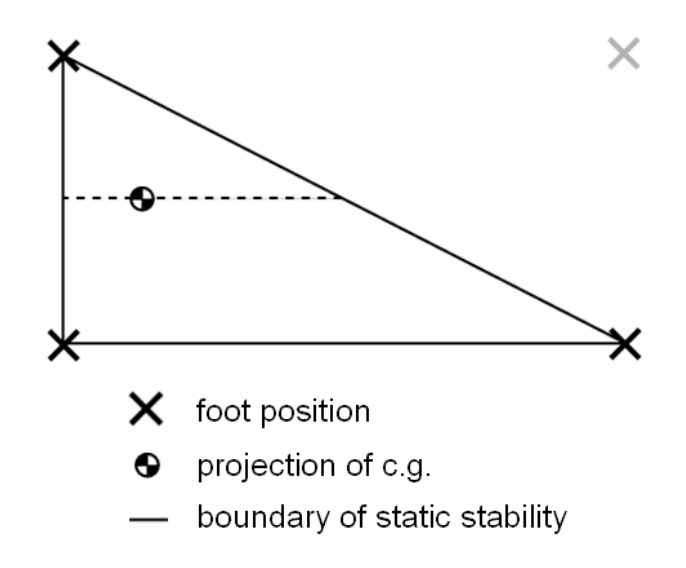

Figure 8-7: Illustration of Geometric Stability Constraint

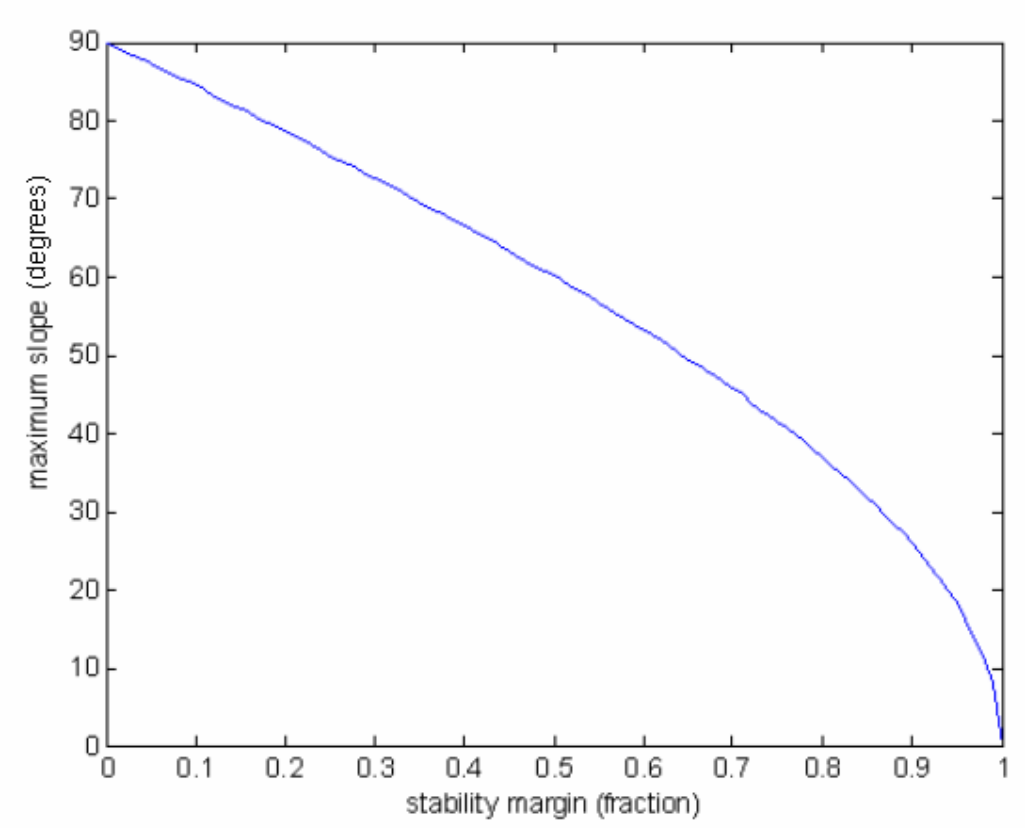

Figure 8-8: Maximum Slope Capability of a Walking Rover assuming varying Stability Margins

8.3 Summary

The mobility models added to MSE have been benchmarked and initial evaluation of the benefits of legged mobility has been done. Benchmarking was done on the dynamic walking model used to estimate power draw by comparing outputs to MoRETA testing and simulation. The mobility code as a whole was benchmarked against data from LittleDog, MoRETA, and ATHLETE. Results show that mobility model outputs are reasonable, with the exception of very small robots. Initial trade space exploration was done for MSL-like rovers to compare the daily traverse capability and specific resistance of wheeled and legged rovers of various sizes. Results indicate that wheeled mobility is better on terrains with low rock density, and legs are better on terrains with high rock density. A geometric stability argument was presented to show that legged rovers can climb steeper slopes than wheeled rovers.

Chapter 9

Conclusions

This chapter provides a summary of the material presented and highlights major contributions to the field. Recommendations for future work developing, refining, and applying the MSE tool and its enhanced mobility modeling capabilities are discussed.

9.1 Thesis Summary

This thesis describes the development of wheeled, legged, and hybrid mobility models and their value to planetary surface exploration, specifically Mars. First, the MSE tool is introduced. MSE is a systems engineering tool that allows rover designers to rapidly create large trade spaces to do mission architecture studies early in the project lifecycle. An example of such a trade study is the trade off between rover size and EDL system accuracy for a MSR fetch rover. The results of this study show the dependence of entry mass on the mission duration, wheel size, and power system of the fetch rover. To establish confidence in trade study results, the wheeled mobility version of MSE is described and validated. Both the exploration model and hardware model are validated against MER and other rovers.

After wheeled mobility is discussed, a survey of alternative forms of mobility is given. Particular emphasis is placed on MoRETA, the hybrid rover developed at MIT, and how developing MoRETA has helped mobility modeling. The MSE tool is written in MATLAB in a modular fashion, allowing the mobility code to be modified to model these new forms of mobility without requiring complete redesign of the tool. The details of the four-wheeled, eight-wheeled, legged, and hybrid mobility models are given. The modifications to the MSE tool as a whole are also summarized. Just as the wheeled mobility model was validated, the legged and hybrid mobility models are compared to

other simulation outputs and existing robotic systems. Initial application of the enhanced MSE tool has confirmed that wheeled mobility is superior to legged mobility on flat and level terrain. Legged mobility is better on terrain with higher rock density or steeper slopes.

9.2 Contributions

The worked described in this thesis makes several important contributions to the academic and rover development communities. First, a powerful tool is delivered that is able to model rover systems with wheeled, legged, and hybrid mobility. The wheeled mobility model is very well refined, and has been and will continue to be used to analyze future Mars rover missions. The legged and hybrid mobility modeling capabilities of MSE have the same potential to help architect future rover missions. These modeling capabilities could be used by engineers at JPL to do early trade space exploration for the Astrobiology Field Laboratory (AFL), the next Mars rover mission on the horizon. Using a tool like MSE in the proposal phase or early conceptual design phases of a mission allows the top level architecture decisions to be based on sound reasoning and analysis, potential saving headaches and cost during later stages of a rover mission.

The survey of wheeled, legged, and hybrid robotic systems gathers existing information about these systems and collects them into one reference. This, along with the more detailed description of the MoRETA rover, could be of use to other researchers looking to familiarize themselves with robots featuring hybrid mobility systems. The modeling approach could also be of use to anyone trying to develop a rover modeling tool with similar capabilities.

Finally, some specific recommendations can be made through the application of the MSE tool that contribute to the design of future rover missions. It was shown that the lowest mass system that can be sent to Mars to retrieve a sample cache and return it to Earth uses a small fetch rover with solar power and 19 cm diameter wheels. This solution requires roughly seven months to fetch the sample cache. If less time is available, then heavier systems with either larger rovers or more accurate landing systems should be proposed. The modeling tool developed to study the MSR mission could also

be of use to future mission planners looking to perform other MSR related architecture studies.

The MSE tool was also applied to sample wheeled and legged rover designs to examine the relative merit of the different forms of mobility. By comparing the daily traverse capability and specific resistance of legged and wheeled rovers on terrains of varying rock density, the conditions under which each form of mobility are preferable are discovered. Wheeled rovers are superior on terrains with low rock density, and legged rovers are superior on terrains with high rock densities. It was also shown how legged rovers can remain statically stable on steeper slopes than wheeled rovers. These general conclusions contribute to the understanding of different forms of mobility, but the true power of the MSE tool will be revealed when used to perform early mission architecture analysis for a future Mars rover.

9.3 Future Work

The original wheeled mobility version of MSE has existed for years. The tool constantly undergoes validation whenever new data becomes available, refinement whenever a model can be improved, and application whenever anyone has a rover mission design question needing to be answered. These activities will continue for the wheeled, legged, and hybrid mobility models in MSE. The legged and hybrid models in particular will likely be validated and refined as more information becomes available. Hopefully, MSE will be applied to the AFL mission and many others after it to demonstrate its capabilities.

References

[16.89 03] S. Chiesi, B. Cohanim, E. Fong, K. Galabova, I. Garrick-Bethell, M. Hilstad, E. Hines, J. Lamamy, J. Marquez, T. Mikaelian, R. Nilchiani, C. Roberts, J. Wertz, B. Willhite, *Rapid Modeling of Mars Robotic Explorers*, 16.89 Design Document, MIT, Spring 2003.

[BDI 06] *LittleDog Robot 1.0 User Guide*, Boston Dynamics, 2006.

[BDI 07] Boston Dynamics Website, http://www.bostondynamics.com/, accessed 2007.

[Bekker 56] M. Bekker, *Theory of Land Locomotion: The Mechanics of Vehicle Mobility*, The University of Michigan Press, Ann Arbor, 1956.

[Bekker 69] M. Bekker, *Introduction to Terrain Vehicle Systems. Part I: The Terrain. Part II: The Vehicle*, The University of Michigan Press, Ann Arbor, 1969.

[Besseron 05] G. Besseron, C. Grand, F. Ben Amar, F. Plumet, P. Bidaud, *Stability of an Hybrid Wheeled-Legged Robot*, 8th International Conference on Climbing and Walking Robots (CLAWAR 2005), 2005.

[Biesiadecki 05] J. Biesiadecki, M. Maimone, *The Mars Exploration Rover Surface Mobilty Flight Software: Driving Ambition*, IEEE Aerospace Conference, 2005.

[Braun 05] R. Braun, R. Manning, *Mars Exploration Entry, Descent and Landing Challenges*, IEEEAC paper #0076, 2005.

[Coso 07] A. Coso, C. Tortora, eds., *Modular Rover for Extreme Terrain Access Design Document*, 16.83x Space Systems Product Development, MIT, 2007.

[Deen 04] B. Deen, D. Alexander, *Rover Motion Counter Master File*, JPL Module ID SIS-SCI013-MER, 2004.

[Ellery 05] A. Ellery, *Environment-robot Interaction-the Basis for Mobility in Planetary Micro-Rovers*, Robotics and Autonomous Systems 51, pp. 29-39, 2005.

[Heverly 06] M. Heverly, J. Matthews, *Some ATHLETE Kinematic and Mass Data*, personal communication, 2006.

[Kennedy 05] B. Kennedy, A. Okon, H. Aghazaian, M. Garrett, T. Huntsberger, L. Magnone, M. Robinson, J. Townsend, *The Lemur II-Class Robots for Inspection and Maintenance of Orbital Stricture: A System Description*, 8th International Conference on Climbing and Walking Robots (CLAWAR 2005), 2005.

[Kennedy 05] B. Kennedy, A. Okon, H. Aghazaian, M. Badescu, X. Bao, Y. Bar-Cohen, Z. Chang, B. Dabiri, M. Garrett, L. Magnone, S. Sherrit, *LEMER IIb: a Robotic System for Steep Terrain Access*, 8th International Conference on Climbing and Walking Robots (CLAWAR 2005), 2005.

[Kulling 07] K.C. Kulling, K. Voelbel, and C. M. Wilcox, *A Foot Placement Planning Algorithm for a Walking Quadruped Rover*, submitted to AIAA 2007 Infotech@Aerospace Conference, Rohnert Park, CA, 2007.

[Lamamy 04] J.A. Lamamy, *Enhancing the Science Return of Mars Missions via Sample Preparation, Robotic Surface Exploration and in Orbit Fuel Production*, M.S. Thesis, Massachusetts Institute of Technology, June 2004.

[Lamamy 06] J.A. Lamamy, D.W. Miller, *Designing the Next Generation of Rovers through a Mid-Rover Analysis*, 9th ESA Workshop on Advanced Space Technologies for Robotics and Automation (ASTRA 2006), 2006.

[Lamamy 07] J.A. Lamamy, *Methods and Tools for the Formulation, Evaluation and Optimization of Rover Mission Concepts*, Ph.D. Thesis, Massachusetts Institute of Technology, June 2007.

[Lamamy 07] J.A. Lamamy, S. McCloskey, D.W. Miller, *The Mars Surface Exploration Rover Modeling Tool*, to be published, 2007.

[Lindemann 05] R. Lindemann, C. Voorhees, *Mars Exploration Rover Mobility Assembly Design, Test, and Performance*, 2005 IEEE Confrence on Systems, Man, and Cybernetics, 2005.

[Lindemann 06] R. Lindemann, D. Bickler, B. Harrington, G. Ortiz, C. Voorhees, *Mars Exploration Rover Mobility Development*, IEEE Robotics & Automation Magazine, 2006.

[Lindemann 06] R. Lindemann, Personal communication regarding wheeled mobility, 2006.

[Mattingly 05] R. Mattingly, *The Many Faces of the Mars Sample Return Mission Architecture*, 27th Annual AAS Guidance and Control Conference, 2005.

[Maxon 07] *Key information on – Maxon DC motor and Maxon EC motor*, available at: http://www.maxonmotorusa.com/dc_motor.asp, accessed 2007.

[Maxon 07] *RE Series Motor Data Sheets*, available at: http://www.maxonmotorusa.com/dc_motor.asp, accessed 2007.

[MERAN 06] MER Analyst's Notebook, http://anserver1.eprsl.wustl.edu/, accessed 2006.

[MER 07] Mars Exploration Rover Mission, http://marsrovers.nasa.gov/home/, accessed 2007.

[MPF 99] Mars Pathfinder Home, http://mpfwww.jpl.nasa.gov/MPF/index1.html, accessed 2007.

[Patel 04] N. Patel, G. Scott, A. Ellery, *Application of Bekker Theory for Planetary Exploration through Wheeled, Tracked and Legged Vehicle Locomotion*, AIAA Space 2004 Conference and Exhibit, 2004.

[Steltzner 06] A. Steltzner, D. Kipp, A. Chen, D. Burkhart, C. Guernsey, G. Mendeck, R. Mitcheltree, R. Powell, T. Rivellini, M.S. Martin, D. Way, *Mars Science Laboratory Entry, Descent, and Landing System*, IEEEAC paper #1497, 2006.

[Wahab 06] A. Wahab, C. Edwards, *Parametric Walking Model for Hybrid Rover Design*, MIT 16.851 Satellite Engineering, fall 2006.

[Volpe 07] R. Volpe. *JPL Robotics: Home Page*, http://www-robotics.jpl.nasa.gov/, accessed 2007.

[Wertz 03] J. Wertz, W. Larson, eds., *Space Mission Analysis and Design 3rd Edition*, Microcosm Press, El Segundo, California, 2003.

[Wheeler 07] D. Wheeler, *Local Mapping from Stereo Vision*, submitted to AIAA InfoTech@Aerospace 2007 Conference, Rohnert Park, CA, 2007.

[Wilcox 06] B. Wilcox, Personal communication regarding ATHLETE, 2006.

[Wolf 06] A. Wolf, J. Tooley, S. Ploen, M. Ivanov, B. Acikmese, K. Gromov, *Performance Trades for Mars Pinpoint Landing*, IEEEAC paper #1661, 2006.

Appendix

Parametric walking model for hybrid rover design

Adam J. Wahab, Christine Edwards
December 11, 2006

ABSTRACT

A parametric walking model has been created for performing trade studies in the spirit of developing rovers with hybrid locomotion capable of accessing extreme terrain. This model consists of three parts: a motion planner, a mechanical subsystem model, and an electrical subsystem model. The current implementation simulates a hexapod configuration capable of walking with a stable tripod gait pattern and has been used for trade studies in which the parameters describing the gait, rover configuration, and motor design were varied and compared using a set of performance metrics. The results show that there are several parameters, including but not limited to forward velocity, gear reduction ratios and leg mass that may be optimized for each presented metric.

Keywords: hybrid, rover, parametric, model, legged, locomotion, performance, simulation, walking

1. INTRODUCTION

In January of 2004, the Spirit and Opportunity rovers successfully landed on Earth's neighboring planet, beginning the longest Mars exploration mission in humankind's history thus far. This Mars Exploration Rover (MER) mission has been immensely successful, with discoveries of scientific consequence and a lifespan that exceeded expectation. However, the mobility of the rovers is limited. The rovers were unable to reach some potentially significant rock outcroppings, because the steep and rocky terrain was more extreme than what the rovers were designed for. Also, one of the rovers became stuck for days as its wheels lost traction in when traversing a patch of fine sand. To improve rover capability for future exploration missions, the following question must be asked: Is there another rover mobility design that can access extreme terrain while remaining power efficient?

This study aims to help answer this question. A hybrid rover that utilizes both wheels and legs can potentially access extreme terrain more efficiently than a convention rover design equipped with large wheels. To investigate this possibility, the following mission motivates this project:

Mission Statement

To pursue the improvement of rover capability for accessing extreme terrain and enable trade studies of hybrid rover subsystem designs by developing a parametric model of legged rover locomotion. To compare the walking mode of hybrid systems with conventional wheeled locomotion using power and mobility performance metrics.

A parametric model of a walking rover has been developed using MATLAB™ for conducting trade studies. The model's subsystems are capable of analyzing different design options. For example, the leg mass and length can be varied and the motor joint specifications may be altered to quantify the impact of parameter changes on rover performance. Section 2 describes parametric model in greater detail, and Section 3 discusses several results that were produced using model.

2. METHODOLOGY

2.1. Approach (CE)

The rover model is decomposed into mechanical and electromechanical components. It is based on the assumption of an ideal control system that moves the legs and body precisely to the desired placement. Because of this, no controller subsystem model is needed to operate this virtual rover. Figure 2.1 illustrates how the model fundamentally works.

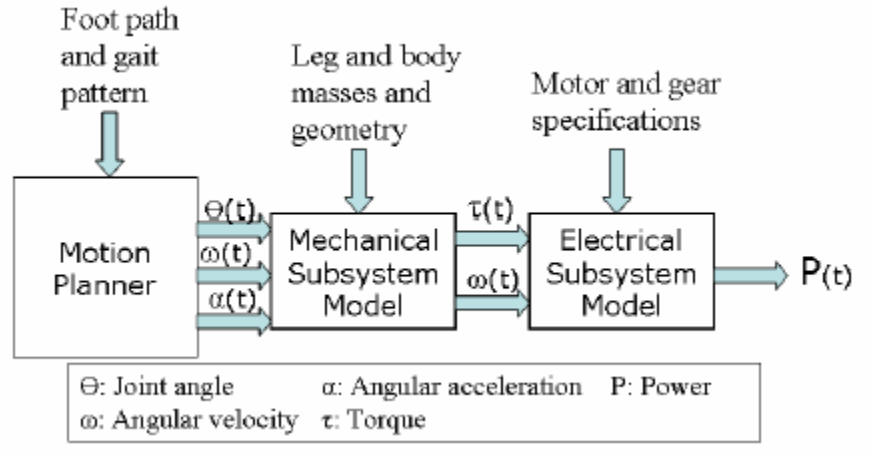

Figure 2.1 Rover subsystem models and interactions.

Given a desired foot path and gait pattern, the motion planner computes the desired angular velocity and acceleration for each joint. Kinematics are used to obtain dynamics of a lossless mechanical system. These idealized torques and angular velocities are then used as inputs for the electrical model, which includes gear and motor efficiency losses. Then, the electrical model estimates the power needed for that movement given the motor and gear specifications. The mechanical and electrical subsystems are described in greater detail in Sections 2.3 and 2.4.

2.2. Simplifications (AW)

A number of simplifications and assumptions were implemented to constrain the modeling and simulation tasks to manageable levels, some of which are listed here.

1. Joints are frictionless single degree of freedom revolutes allowing leg motion in the x-y plane.

2. Actuators are non-backdriveable electric motors fitted with gear heads. The motors have zero starting torque and no-load speeds that vary linearly with voltage.
3. The leg links are thin, rigid bodies with finite lumped masses located at a user defined position along their spans.
4. The body is a rigid and represented by a plane joining all of the leg hip joints, with a lumped mass located at its center. Body motion is constrained to translation in the x-z plane at a constant rate Vf.
5. The ground is a rigid body of infinite mass represented by a flat surface with zero gradient.
6. Wheel-motor assemblies are finite lumped masses located at the foot of each leg. No slipping occurs at the foot-ground interface.
7. Ambient conditions are neglected; only the Martian gravitational field is considered.
8. Computing time for terrain analysis and motion planning are not modeled.

2.3. Mechanical Subsystem (AW)

The coded mechanical model combines the motion planning with the inverse kinematics, and closed form dynamics solvers. The motion planning coordinates the timing of leg movements and describes the foot and hip trajectories through time. The positions, velocities and accelerations of the feet and hips are provided as input for the inverse kinematics solver, which determines the joints' angular positions, velocities, and accelerations. The solved kinematics are then used to determine the computed forces and torques seen by each joint actuator. The product of the each joint's computed torque and angular velocity results in the instantaneous mechanical power, P_{mech}, which does not account for any losses or inefficiencies.

Design vectors were defined for three walker size classes representative of Sojourner, MER, and MSL rover geometries. The mass parameters for each walker were assigned values intended to reflect the added bulk of mechanical legs over traditional wheels. That is to say, the mass of six legs for a MER-sized walker is considerably greater than the mass of MER's wheeled mobility system. The code also enforces certain

parameter relationships to avoid simulating any physically implausible designs (e.g. selecting a body height greater than leg length would prevent the feet from touching the ground). The details of the base configurations and parameter ranges used to define the variant may be found in the appendix.

H_b	Body height	[m]
L_b	Body length	[m]
W_b	Body width (not shown)	[m]
S_p	Step pitch	[m]
F_c	Peak foot clearance	[m]
L_{ij}	Length of link j on leg i	[m]
τ_{ij}	Torque at joint j on leg i	[N m]
m_{ij}	Mass of link j on leg i	[kg]
r_{ij}	Distance from joint j to link j's c.g.	[m]
m_b	Mass of body	[kg]
m_{if}	Mass of foot on leg i	[kg]
(x_{iF},y_{iF})	Position of leg i's foot	[m]
(x_{iH},y_{iH})	Position of leg i's hip	[m]
(x_{iK},y_{iK})	Position of leg i's knee	[m]
θ_{ij}	Angular position of link j on leg i	[rad]
L_s	Step length	[m]
V_f	Forward speed	[m/s]
g	Gravitational acceleration	[m/s^2]

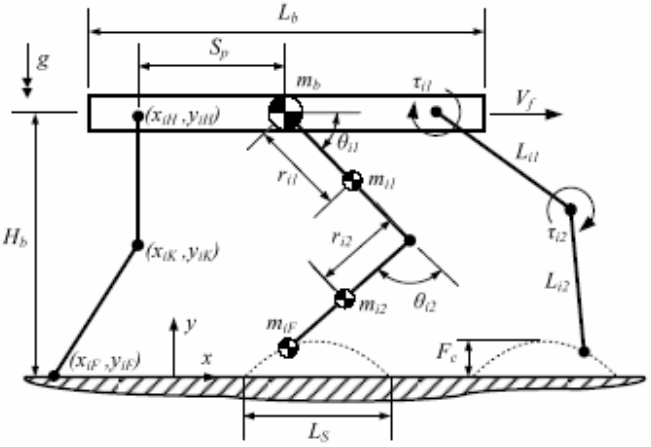

Figure 2.2 Key parameters used to describe the mechanical model.

2.4. Electrical Subsystem (CE)

The electrical model reads in the joint torques and rotation rates from the mechanical model and the motor and gear specifications from the user. A series of calculations (Figure 2.3) determined the electrical power required for the desired mechanical movement.

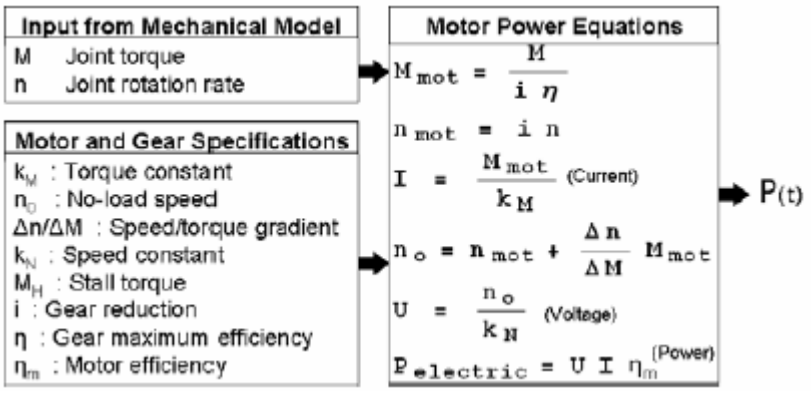

Figure 2.3 Relationships used in electrical subsystem.

After looping through a database of Maxon™ motors, the electrical model indicated that a motor with the lowest speed/torque gradient requires the least electrical power to drive the mechanical walking motion. The newer Maxon™ EC 45 required less power than the other Maxon™ motors due to their rather low speed/torque gradient.

As expected, it was also seen that the gear efficiency decreases with increasing gear ratio. Using the specification from a database of Maxon™ planetary gears, the following empirical relation was determined:

$$\eta \approx -5.8575 \ln(i) + 92.577 \quad (2.1)$$

where η is gear efficiency and i is the gear reduction ratio.

Using this relation, the electrical subsystem shows that there is an optimum gear ratio for each joint in a given rover configuration. Figure 2.4 shows a power efficiency curve resulting simulating the rover model with a series of different hip-joint gear ratios. When the gear ratio is less than the optimum, the power performance declines because of motor characteristics. At gear ratios greater than the optimum, the power performance declines due to decreasing gear efficiency. For every base configuration that was tested, each joint's optimum gear ratio was found and assigned to that configuration.

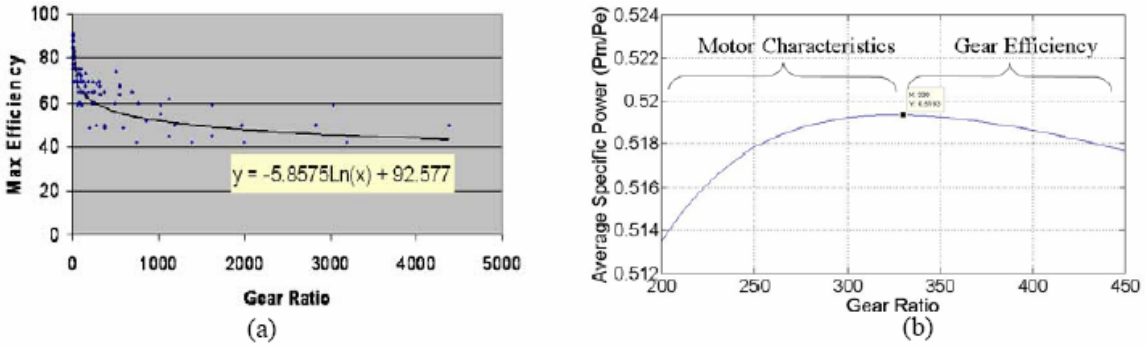

Figure 2.4 (a) Scatter data used to develop empirical relation for gear efficiency; (b) Power efficiency of actuator over a range of gear ratios.

2.5. Energetics (AW)

As stated earlier, the primary focus of this study is to examine how various aspects of a walking rover's configuration impact the energy consumed for locomotion. In order to compare the energetic performances of different configurations, the specific resistance and specific power metrics were applied to single- and dual-axis trades in which one

parameter from the input design vector was varied over a range, while the rest of the parameters were held constant.

2.5.1. Specific Resistance (AW)

Specific resistance ε is often used as metric for vehicle energetic efficiency based on the notion that a mass moving horizontally at constant speed is not performing any mechanical work. One may consider ε to be a measure of the resistance to motion offered by the medium in which the motion occurs [12]. Since a vehicle's power output is used in defining ε, the aforementioned resistance will include external effects (e.g. aerodynamic drag, terrain conditions) as well as internal ones (e.g. transmission losses). The original metric was defined in 1950 by Gabrielli and von Karman using a vehicle's maximum speed,

$$\varepsilon = \frac{\overline{\mathbf{P}}(v_{\max})}{mgv_{\max}} \tag{2.2}$$

where m is the total vehicle mass, g is the gravitational acceleration, and v is the vehicle's speed in the direction of motion. is the vehicle's average power output. A more general form, which is a function of speed, is used in this study and may be expressed as,

$$\varepsilon(v) = \frac{\overline{\mathbf{P}}(v)}{mgv} \tag{2.3}$$

$\overline{\mathbf{P}}(v)$ is the average power consumed while advancing at velocity v over time period T (one cycle period for the walking rover). The most efficient rover configuration minimizes the specific resistance.

2.5.2. Specific Power Ratio (AW)

The specific power ratio is defined herein as the instantaneous mechanical power over the instantaneous electrical power at time t,

$$\eta_{sp}(t) = \frac{\mathbf{P}_m(t)}{\mathbf{P}_e(t)} \tag{2.4}$$

where the numerator and denominator are the mechanical and electrical power, respectively. A rover with ideal actuators would exhibit a unity specific power ratio,

however since losses in the gears and motors are modeled, the electrical power required for a given motion is always greater than the mechanical power. To compare the specific power ratios of a number of designs, each variant's average ratio was computed using the following,

$$\overline{\eta}_{sp} = \frac{1}{N}\sum_{i=1}^{N}\frac{\mathbf{P}_m(t)}{\mathbf{P}_e(t)} \tag{2.5}$$

where N is the number of discrete time steps during in a simulation of one walking cycle. The most efficient combination of gears and motors will maximize the specific power ratio.

2.6. Stability (AW)

Walking machines often suffer from poor stability, especially when traversing uneven terrain or traveling at high speeds. Since this study was limited to low speed walking with a tripod gait on flat terrain, static stability did not arise as a concern, however its consideration is mentioned here for completeness. For a walker to exhibit static stability, the projection of its center of mass (C.o.M) onto the ground in the direction of gravity must lie within the boundaries of the polygon, or support pattern, formed by connecting the ground contacts of its supporting legs. The stability margin S_m is the shortest distance from vertical ground projection of the C.o.M. to the boundaries of the support pattern. The longitudinal stability margin S_L is the shorter of the front and rear stability margins ($S_{L,f}$ and $S_{L,r}$) and the gait stability margin S is the minimum S_L over an entire cycle of locomotion. A gait is statically stable if $S \geq 0$ for $t \in [0,T]$. The modeled calculated all of the aforementioned stability values for each simulation.

3. RESULTS

3.1. Time Series of One Configuration (CE)

This section discusses some of the results from simulations of the baseline walker configurations. Figure 3.1 shows frames from a visualization of the 'MER' walker. Note that the projected center of mass remains inside the stability triangle formed by the supporting legs. The rover's legs appear long, however this was done to allow a wide

range of body heights and step lengths to be tested for constant leg length.

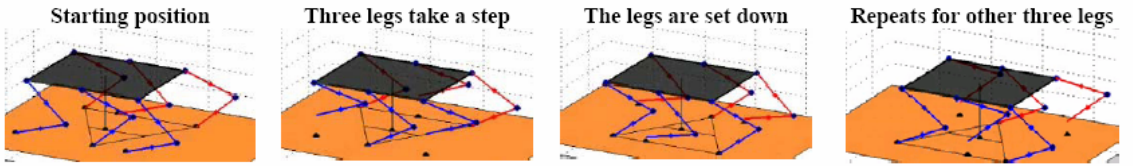

Figure 3.1 Key frames from a sample rover animation sequence.

The following series of plots (Figure 3.2) show the power required by configuration throughout the locomotive cycle shown above. From t=0~4 seconds, three legs lift, swing forward, and touch down, which causes two power peaks. From t=4~8 seconds, the other three legs perform the same motion, resulting in another two power peaks. Note how the electrical power does not directly scale with the mechanical power. This is due to some nonlinear qualities of the motor model.

The 'MER' walker base configuration consumed a peak electrical power of 36W, with an average of 25W. The Sojourner Walker's peak power was 2.2W, and the MSL Walker's peak power was 460W. These values are underestimated due to some model limitations.

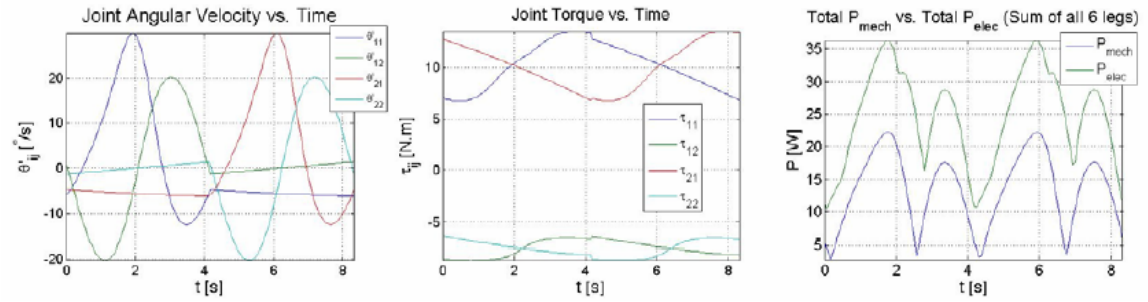

Figure 3.2 Sample time series plots of angular velocity, mechanical torque, and absolute power consumption.

All three of the plots in Figure 3.2 are related. The total mechanical power is computed as the absolute value of the product of joint angular velocity and joint torque summed over all joints on all legs. The electrical power is calculated in the electrical model, using the raw angular velocity and torque values. The absolute value is then

taken of the raw electrical power, which is then summed for all joints on all legs. These relations are illustrated in Figure 3.3.

Figure 3.3 Differentiating mechanical power from electrical power.

3.2. Single Axis Trades (AW)

Both single- and dual-axis trade studies were performed for each of the three base configurations. Since all three base configurations produced results with similar characteristics, the discussion of the results will focus on general trends using the 'MER' walker base design's numerical results as a means of quantitative support.

A single-axis trade of each base configuration was performed over a range of forward velocities, holding the rest of the design vectors constant. Both specific resistance and specific power were evaluated at each speed considered. The results for the individual metrics are considered below.

3.2.1. Specific Resistance (AW)

For the case of the specific resistance (Figure 3.4), it can be seen that an operating range exists within the first two velocity decades where the specific power remains relatively constant. As the forward speed increases beyond the "operating bandwidth's" apparent "corner velocity", the specific resistance increases dramatically. This illustrates a significant increase in power to achieve the required leg motions at elevated speeds.

The mechanical power is responsible the aforementioned "operating bandwidth" shape and the related "corner velocity". The electrical power introduces a non-uniform offset from the mechanical specific resistance that increases at extremely low and high forward speeds, where the joint actuators are no longer functioning in their intended design regimes. Additionally, the electrical specific resistance reaches a minimum, signifying an optimal forward speed may be found based on this metric.

The walker model's results tend to respect the trends shown by the other vehicles plotted. Wheeled vehicles are more efficient at higher speeds, so they lie in the lower right of the plot. Rovers and walkers are designed to operate at low speeds, the latter of

which are relatively power hungry, so one can see why they sit in the left hand side of the plot. Although the Sojourner, MER, and MSL Mars rovers are wheeled vehicles, their specific resistance values fall in the walkers' performance regime. This may be due, in part, to their design for robustness, and scientific payload, rather than for speed and transportation efficiency. Humans benefit from evolution and have adapted to be fairly efficient at moderate speeds, as seen by their position near middle of the plot. It bears mentioning that the data for vehicles other than the modeled results has been adjusted to roughly reflect performance in Martian gravity.

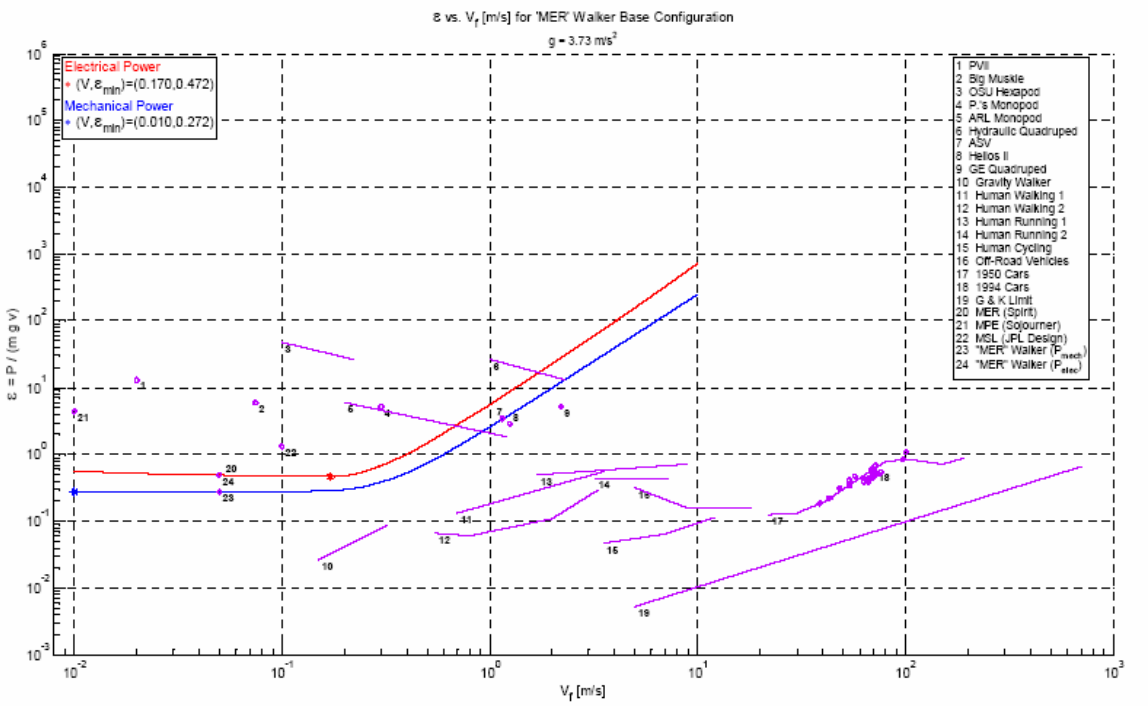

Figure 3.4 Specific resistance using electrical and mechanical power of 'MER' base configuration over a range of speeds. Other vehicles [12] are shown in purple. MER, Sojourner, and MSL points computed from data found in [14].

3.2.2. Specific Power Ratio (AW)

The specific power ratio metric produced results which supported those of the specific resistance study. A clear maximum for the metric can be seen in Figure 3.5 at a forward speed that is slightly higher than the design speed. This difference is likely due to the fact that the instantaneous values of the ratio were averaged over each variant's locomotive cycle in order to produce a single value of the metric at each speed tested. As

the speed deviates from the peak performance value, the metric decreases illustrating how the actuators are no longer functioning under their optimal design conditions and require more and more electrical power to achieve the required mechanical motions.

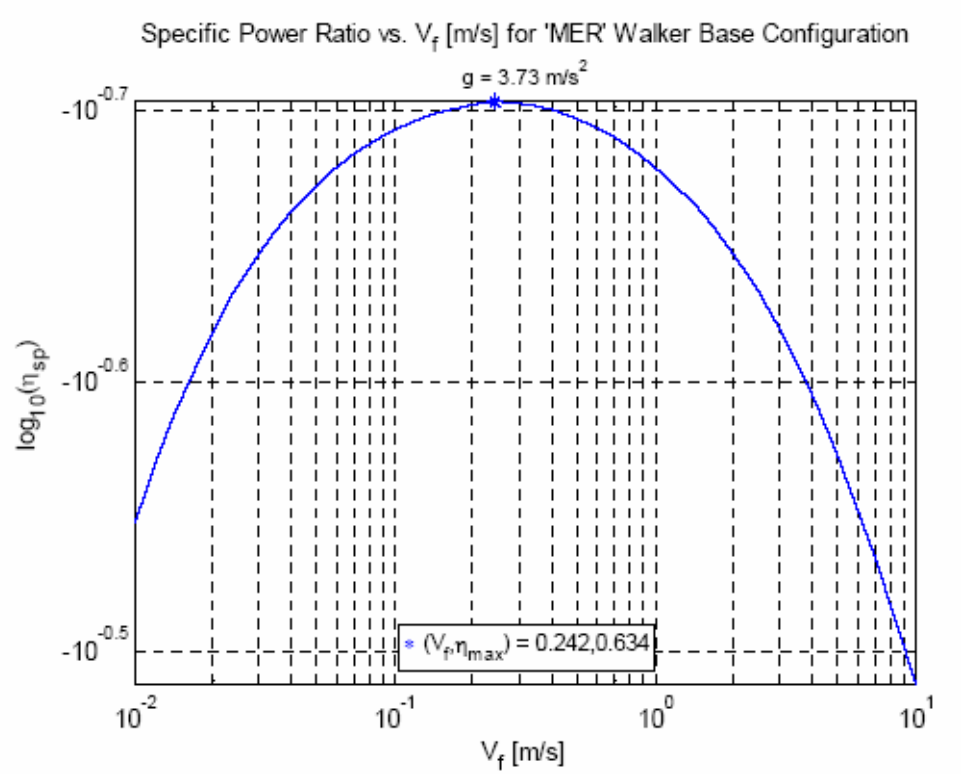

Figure 3.5 Specific power ratio of 'MER' base configuration over a range of forward speeds.

3.3. Dual-Axis Trades (AW)

A number of dual-axis trades were performed using both performance metrics, however only a small sample of the results will be considered here.

3.3.1. Specific Power Ratio (AW)

The contour plot seen on the left of Figure 3.6 depicts the specific power ratio of the 'MER' configuration over a range of forwards speeds and link masses. This may be considered as an extrusion of the specific power ratio plot shown earlier. As the mass of the links (and thus to total leg mass) is increased, the metric-optimal forward speed varies little, but the design's operating reason narrows. At all speeds, it can be seen that lightest legs would improve the performance as determined by the specific power ratio.

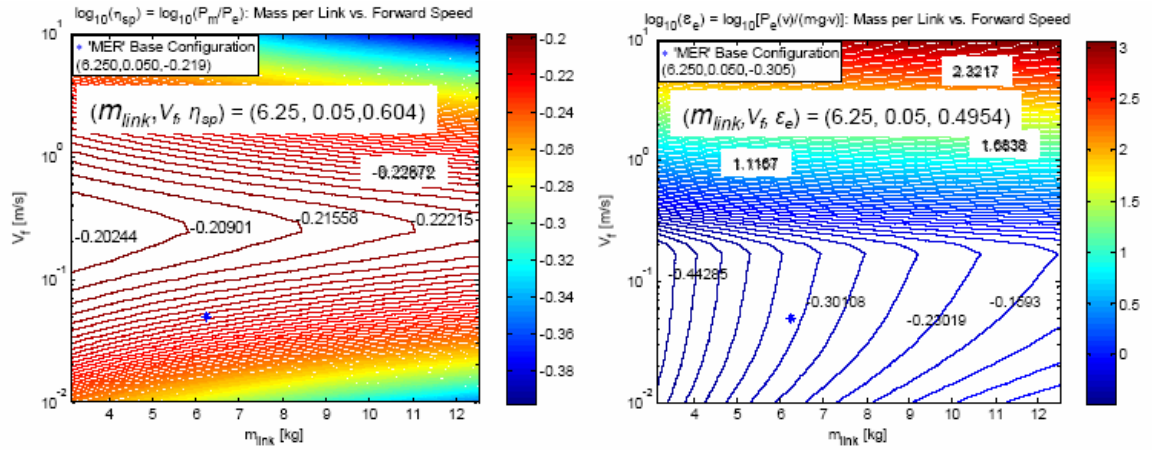

Figure 3.6 Two-axis trade results for 'MER' base configuration. Specific power ratio (left) and electrical specific resistance (right) for ranges of forward speeds and link masses.

3.3.2. Specific Resistance (AW)

The right hand side of Figure 3.6 is a contour plot of the electrical specific resistance metric of the same link mass and velocity ranges. This plot may also be seen as an extrusion of the metric's single-axis trade results. As the forward speed is increased for a given leg mass, a steep gradient of decreasing performance begins near the middle of the velocity range and continues up the plot. This would suggest that a wider operating range is available using this metric, albeit at lower rates of speed than for the specific power ratio. Furthermore, for a given forward speed, the performance at higher does not seem to vary much with increasing leg mass, while a more apparent decrease in performance may be seen at speeds in the operating range.

4. SUMMARY AND CONCLUSIONS

In this project, the mission to compare walking mobility with conventional wheeled mobility for rovers was achieved. The specific resistances of MER, MSL, and Sojourner were compared with those of similarly sized walkers. The results show that the rover model estimates walking performance that is equal to or slightly better than that of similarly sized wheeled vehicles. In reality, it is known that legged rovers similar to those modeled would draw more power than wheeled rovers while operating on flat terrain.

The performance overestimates are likely due to several deficiencies of the model. For example, the friction losses in the model are limited to motor and gear inefficiency. Another limitation is that motor dynamics are not modeled. The motor would see additional torque while ramping up, which would increase its power draw. Other system dynamics would appear if compliance in the body, legs, and ground were modeled, all of which would serve as energy sinks. Additionally, an actual rover design team may have reasons not to choose the most efficient motor or gear ratio. When a motor with a speed/torque ratio higher than that of the Maxon™ EC 45 is used in the walker models, the performance declines noticeably, and the electrical specific resistance becomes worse than that of Sojourner, MER, and MSL.

Even with the performance overestimate, the model shows very useful trade-study results. Single- and dual-axis trades show that there are several parameters that may be optimized, including forward velocity, individual joint gear reduction ratios, and leg mass.

In the future, this model could be adapted to simulate operation on rough terrain, estimating the required power consumption to negotiate rocks and inclines. Furthermore, the model's limitations and estimates of energy losses could be refined for a closer approximation of actual power requirements.

5. REFERENCES

1. M.F. Silva, J.A.T. Machado, A.M. Lopes, Performance Analysis of Multi-Legged Systems, Proc. IEEE International Conference on Robotics & Automation, Washington DC, May 1992, pp. 2234-2239.
2. S.L. Chiu, Kinematic Characterization of Manipulators: An Approach to Defining Optimality, IEEE, 1988, pp. 828-832.
3. T.A. Guardabrazo, P. Gonzalez de Santos, Building and energetic model to evaluate and optimize power consumption in walking robots, The Industrial Robot, 2004, Vol. 31, No. 2, pp. 201-208.
4. M.F. Silva, J.A.T. Machado, A.M. Lopes, J.K. Tar, Gait Selection for Quadruped and Hexapod Walking Systems, IEEE, 2004, pp. 217-222.
5. S.M. Song, K.J. Waldron, Machines that Walk: The Adaptive Suspension Vehicle, MIT Press, 1989.

6. J.J. Craig, Introduction to Robotics: Mechanics & Control, Addison-Wesley, Reading, MA, 1986.
7. M.Y. Al-Zaydi, S.H.M. Amin, Simulation Kinematics Model of A Multi-Legged Mobile Robot, ICAR '97, Monterey, CA, July 7-9, 1997, pp. 89-94.
8. M.Y. Al-Zaydi, S.H.M. Amin, Locomotion Simulation of A Quadruped Robot on General Level Terrain, IEEE, 1997, pp. 159-164.
9. J.X. Liu (Editor), Mobile Robots: New Research, Nova Science Publishers, Inc., 2005, pp. 291-315.
10. Roger Arno, Planetary Surface Vehicles, Human Spaceflight Mission Analysis and Design, McGraw-Hill Companies, Inc., 2000, pp.455.
11. Key information on – Maxon™ DC motor and Maxon™ EC motor, http://www.maxonmotorusa.com/technology/
12. P. Gregorio, Design, Control and Energy Minimization Strategies for the ARL Monopod, M. Eng. Thesis, M.E., McGill University, Aug. 1994.
13. J.A. Lamamy, D. Miller, Enhancing the science return of Mars missions via sample preparation, robotic surface exploration, and in orbit fuel production, M.S. Thesis, A.A., MIT, May 2004.
14. D. Miller, J. Keesee, Rapid Modeling of Mars Robotic Explorers, 16.89 Design Document, MIT, Spring 2003.

APPENDIX:

Design Vectors for Walker Base Configurations (AW)

Parameter, Variable (Base value) [Units]	'Sojourner' Walker	'MER' Walker	'MSL' Walker
Number of legs, n	6	6	6
Number of joints per leg	2	2	2
Body Length, L_b [m]	0.65	1.04	1.76
Body Width, W_b [m]	0.48	0.84	1.42
Step Pitch, S_p (=L_b/2) [m]	0.325	0.52	0.88
Foot Clearance, F_c [m]	0.13; [1e-5:3.33e-3:0.13]	0.2; [1e-5:5e-3:0.2]	0.3; [1e-5:1.5e-2:0.6]
Body Height (from ground), H_b [m]	0.3; [0.3:1.92e-3:0.375]	0.5; [0.5:3.125e-3:0.625]	1.0; [0.75:1.3e-2:1.25]
Step Length, L_S (=0.4L_b) [m]	0.26; [0.1:1.06e-2:0.5196]	0.416; [0.1:1.92e-2:0.866]	0.704; [0.1:4.2e-2:1.7]
Leg Length, L_l (=2H_b) [m]	0.6; [0.33:6.92e-3:0.6]	1.0; [0.55:1.125e-2:1]	2.0; [1.1:4.9e-2:3]
Link Length, L_{lj} (=L_l/2) [m]	0.3	0.5	1.0
Link CG Location, r_{lj} (=L_{lj}/2) [m]	0.15	0.25	0.5
Body Mass per Supporting Leg, m_b [kg]	3.5; [1.925:8.08e-2:5.075]	61.67; [33.92:1.423:89.42]	300; [165:6.92:435]
Link Mass, m_{lj} (=100D^2_{wheel}) [kg]	0.206; [0.98:7.54e-2:3.92]	1.172; [3.125:0.2404:12.5]	36; [18:1.385:72]
Foot Mass, m_{lf} [kg]	0.25	1.5	5
Forward Speed, V_f [m/s]	0.01 [1e-2:10]	0.05; [1e-2:10]	0.1 [1e-2:10]
Joint Actuator Gear Ratios, $N_{gear,hip}$, $N_{gear,knee}$	257,230; [1:3500]	308,308; [1:3500]	1200,1000; [1:3500]

Note 1: Parameter ranges used for trade studies shown in square brackets.
Note 2: Some ranges limited by robustness of inverse kinematics singularity handling.